

Analysis of Measured and Calculated Pylon Ground/Earth Resistances and Soil Resistivity

**AEMC[®] Ground Resistance Tester Model 6472
and GroundFlex[™] Adapter Model 6474**



Report prepared for Chauvin Arnoux by:



Institute of Electrical Power Systems

A-8010 GRAZ, Inffeldgasse 18

Phone: (+43 316) 873 - 7550

Fax: (+43 316) 873 - 7553

Chair: Univ.-Prof. Dr. Lothar Fickert

Project No: 2006-52

Date: 04 / 2007

Project Management:

Univ.-Prof. Dr. Lothar Fickert

Dipl.-Ing. Dr. Ernst Schmautzer

Dipl.-Ing. Walter Hipp

Research Associates:

Dipl.-Ing. Johann Frei

Dipl.-Ing. Alexander Gaun

Dipl.-Ing. Georg Rechberger

Dipl.-Ing. Werner Friedl

Herwig Breitwieser

Acknowledgment

We would like to thank Wienstrom, Steweag-Steg and Pichlerwerke for giving us the opportunity to carry out measurements at grounding systems of overhead power lines, thus enabling us to verify the results of our research.

In particular we would like to thank Mr Baumühlner from Wienstrom for his active support and for providing us with data concerning the power lines 108/7 and 108/8 in Wiener Neudorf as well as Dipl.-Ing. Schwarz and Ing. Deutsch from Steweag/Steg for informing us about the necessary details concerning the power line in Lieboch. Furthermore we would like to express our gratitude to Ing. Ziegerhofer from Pichlerwerke for helping us to get access to an unimproved meadow in the Birkfeld area where we could carry out earth measurements. A special thanks to our graduates and students for their support.

Table of Contents

1	Introduction	5
1.1	Assignment of Tasks	5
1.2	Short Description of the Earth and Resistivity Tester MODEL 6472	5
2	Ground Potential rise around Pylons.....	6
2.1	General Information	6
2.2	Calculations of Various Standard Pylons.....	7
2.2.1	110 kV Standard Power line 2x3x1 STALU 240/40	8
2.2.2	110 kV Standard Power line 2x3x2 STALU 560/50	10
2.2.3	220 kV Standard Power line 2x3x1 STALU 340/110	12
2.2.4	380 kV Standard Power line 2x3x2 STALU 680/85	14
2.3	Simulation of the interconnected Earthing System of two Standard 110 kV Pylons.....	16
2.4	Interference of Multilayered Soils with Varying Soil Resistivity	18
3	Ground Currents and Earth Wire Currents	19
3.1	General Information	19
3.2	Description of Simulation Model	19
3.3	Power line Model	21
3.4	General Observations	22
3.4.1	Method	22
3.4.2	Untransposed System - 2 Systems Active	22
3.4.3	Transposed System - 2 Systems Active	23
3.4.4	Transposed System - 2 nd System Inactive	23
3.4.5	Transposed System - 2 nd System Short-Circuited	24
3.4.6	Untransposed System - 2 nd System Inactive	24
3.4.7	Untransposed System - 2 nd System Inactive and Short-Circuited	25
3.4.8	Doubling Length of Power line by Doubling Spans and Numbers of Pylons	25
3.4.9	Results of General Observations	26
3.5	110 kV Power line Wr. Neudorf 108/7 and 108/8.....	26
3.5.1	Introduction	26
3.5.2	Transposed System – 2 Systems active	27
3.5.3	Transposed System - 2 nd System Short-Circuited	28
3.5.4	Transposed System - 2 nd System inactive.....	28
3.6	Comparison of Simulations and Measurements	29
4	Ladder Network Impedances	30
4.1	Principle	30
4.2	General Information	30
4.3	Results of the Simulations and Comparison with the Results of the Measurements	32
4.3.1	Ladder Network Impedances of Pylon 29 of Power line 108/7 and 108/8	32
4.3.2	Ladder Network Impedance of Pylon 32 of Power line 108/7 and 108/8	33

5	Comparative measurements	34
5.1	Measuring Methods and Measuring Systems	34
5.1.1	Soil Resistivity	34
5.1.2	Ladder Network Impedance	34
5.1.3	Grounding System Resistance	35
5.1.4	Relative Errors of Measuring Systems using Rogowski coils	36
5.2	Measurements in Lieboch Concerning Power line 130/7 and 130/8B.....	37
5.2.1	Soil Resistivity ρ	37
5.2.2	Grounding System Resistance R_A Determined by Active Measurement	37
5.2.3	Grounding System Resistance R_A Determined by Passive Measuring	38
5.2.4	Ladder Network Impedance	39
5.2.5	Grounding System Resistance and Ladder Network Impedance	40
5.2.6	Grounding System Resistances of Several Pylons (Active Measurement)	41
5.2.7	Grounding System Resistance of Several Pylons (Passive Measurement)	41
5.2.8	Pictures Illustrating the Measuring Setup at Pylon 40	42
5.3	Measurements in Wr. Neudorf	43
5.4	Measurements in an Unimproved Meadow.....	44
5.4.1	Measurements in Highly Conductive Soil	44
5.4.2	Measurements in Low Conductive Soil	46
6	Influences on Rogowski Coils	48
6.1	Basics	48
6.1.1	Construction	48
6.1.2	Mode of Operation	49
6.2	Current Measuring	51
6.2.1	Principle	51
6.2.2	Disturbing Interference	53
6.3	Magnetic Fields as Sources of Interference.....	55
6.3.1	Calculation of Interference Currents.....	55
6.3.2	Measurements in a Homogeneous Magnetic Field	59
6.3.3	Calculation of the Magnetic Flux Density at the Footing of a Pylon.....	61
6.3.4	Assessment of Additionally Induced Errors	62
7	Summary.....	64
8	Applied Devices	65
8.1	Measurement Devices and Sources	65
8.2	Measurement Devices	65
8.3	Current Probes	65
9	Bibliography	66

1 Introduction

1.1 Assignment of Tasks

In the autumn of 2006 Chauvin Arnoux® Inc. d.b.a AEMC® Instruments introduced a newly developed earth and resistivity tester (Model 6472), which in addition to performing ground/earth resistance and soil resistivity measurements at variable frequencies, measures ladder network impedances and resistances of grounding systems of pylons (individual legs and total) with connected earth wire in one step.

The Institute of Electrical Power Systems of the Graz University of Technology has been assigned to develop the theoretical background for measuring and evaluating ladder network impedances and grounding system resistances of overhead power lines and ground/earth wires. The second part of this task has been to compare the respective measuring systems by carrying out measurements using different measuring systems and principles.

In detail:

- Mathematical simulation and presentation of the ground potential rise around pylon ground/earth systems along an overhead power line
- Mathematical simulation in order to calculate the current which the magnetic field of power lines induces into earth wires and pylons
- Pre-calculation of currents induced into the pylon as well as into Rogowski coils (GroundFlex™ Sensors) in inhomogeneous fields
- Application of a mathematical model in order to verify results of measuring ground/earth and network ladder impedances of power lines using Rogowski coils
- Practical checking of the theoretical assumptions and assessment of interfering factors; analysis of interferences due to the magnetic field of Rogowski coils
- Mathematical simulation of pylon ground/earth impedances ranging from 40Hz to 5kHz

1.2 Short Description of the Earth and Resistivity Tester Model 6472

The Model 6472 is a ground/earth and resistivity tester with the following measuring functions:

- (1) Ground/earth resistance measuring ranging from 1mΩ to 100kΩ
- (2) 3-pole ground/earth measurements
- (3) 4-pole ground/earth measurements with/without selective earth current measurements
- (4) Soil resistivity measurements
 - Using the Wenner method
 - Using the Schlumberger method
- (5) Measurement of the Step Voltage
- (6) Measurement of ground/earth resistance using 2 current clamps
- (7) GroundFlex™ measurements
 - This particular measuring method requires the additional device Pylon box Model 6474 with four Rogowski coils (GroundFlex™ Sensors), which makes it possible to measure the ground current flowing pylon, in individual pylon legs as well as the overall resistance to ground/earth or of each pylon leg.

This study focuses on (3), (4) and (7) and compares the measurement results using the Model 6472 with results using different measurement systems as well as with the results of theoretical calculations and simulations results.

2 Ground Potential Rise around Pylons

2.1 General Information

When a current flows into a ground/earth system the potential surrounding the ground/earth system rises. In order to be able to calculate this, data concerning the physical size of the ground/earth system, the soil resistivity and the total amount of the earth current are needed.

The Institute of Electrical Power Systems of the Graz University of Technology has developed a software program which computes conductive coupling (OBEIN [10]) and which has been applied here.

This program uses potential coefficients (equation 2-1) for calculating grounding system resistances. Moreover the potential for a given current (e.g. 1000A) can be calculated for any space point P (x, y and z). Thus it is possible to calculate the potential curve along a straight line or plane.

In order to analyze multilayered soils with varying soil resistivity, the program solves various alternative configurations in a homogeneous conductive half space which extends towards infinity.

$$\varphi = k \cdot I$$

$$\begin{bmatrix} \varphi_1 \\ \vdots \\ \varphi_i \\ \vdots \\ \varphi_N \end{bmatrix} = \begin{bmatrix} k_{11} & \dots & k_{1i} & \dots & k_{1N} \\ \vdots & \ddots & \vdots & \ddots & \vdots \\ k_{i1} & \dots & k_{ii} & \dots & k_{iN} \\ \vdots & \ddots & \vdots & \ddots & \vdots \\ k_{N1} & \dots & k_{Ni} & \dots & k_{NN} \end{bmatrix} \cdot \begin{bmatrix} I_1 \\ \vdots \\ I_i \\ \vdots \\ I_N \end{bmatrix}$$

equation 2-1

- φ potential
- k potential coefficient
- I current

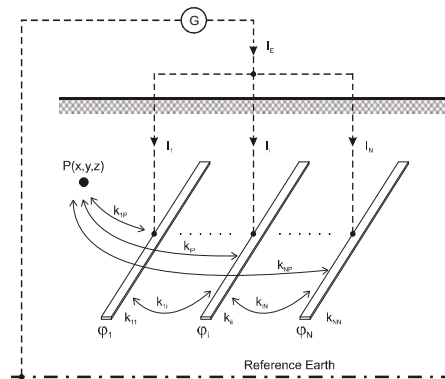


Figure 2-1: Potential Coefficients

2.2 Calculations of Various Standard Pylons

With the help of OBEIN the following ground/earths of standard power lines have been simulated:

- 110kV standard power line 1x3x1 STALU 240/40
- 110kV standard power line 1x3x2 STALU 560/50
- 220kV standard power line 2x3x1 STALU 340/110
- 380kV standard power line 2x3x2 STALU 680/85

The following parameters have been applied for all pylons:

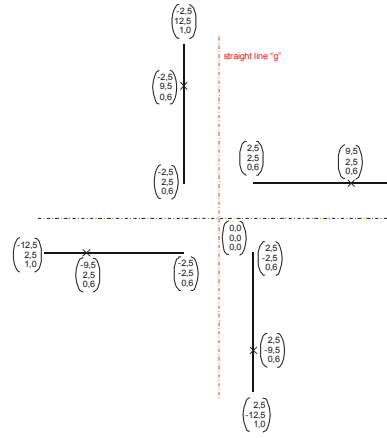
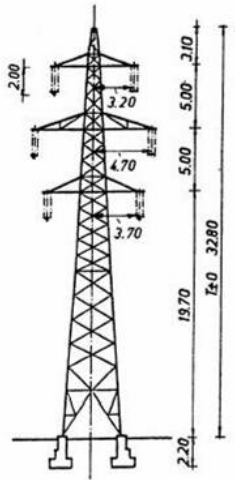
- | | |
|-------------------------------------|----------------------|
| • Soil Resistivity of top layer | 100 Ωm |
| • Soil Resistivity of deeper layers | 100 Ωm |
| • Width of top layer | 2 m |
| • Total amount of earth current | 1000 A |

The following calculations have been performed:

- Calculation of the grounding system resistance R_A and the maximum earth potential U_E with a ground/earth current of 1kA
- Simulation of the ground potential (height 0m) along a straight line g directly below the ground/earth wire
- Simulation of the step voltage at ground level (height 0m) along a straight line g directly below the earth wire
- 3D plot of the ground potential normalized by the maximum pylon potential

2.2.1 110kV Standard Power Line 2x3x1 STALU 240/40

Grounding system resistance $R_A = 4.421\Omega$
 Earth potential U_E at 1kA = 4421V



Phase configuration: 2x3x1 STALU 240/40
 1 ST III 95
 Standard span length: 300 m
 Maximum wire sag (20°C): 10 m

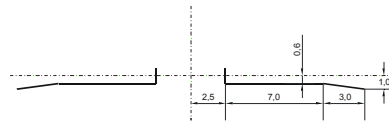


Figure 2-2:

Head of Pylon 110-kV-2x3x1 STALU 240/40

Figure 2-3:

Ground/Earth System 110-kV-2x3x1 STALU 240/40

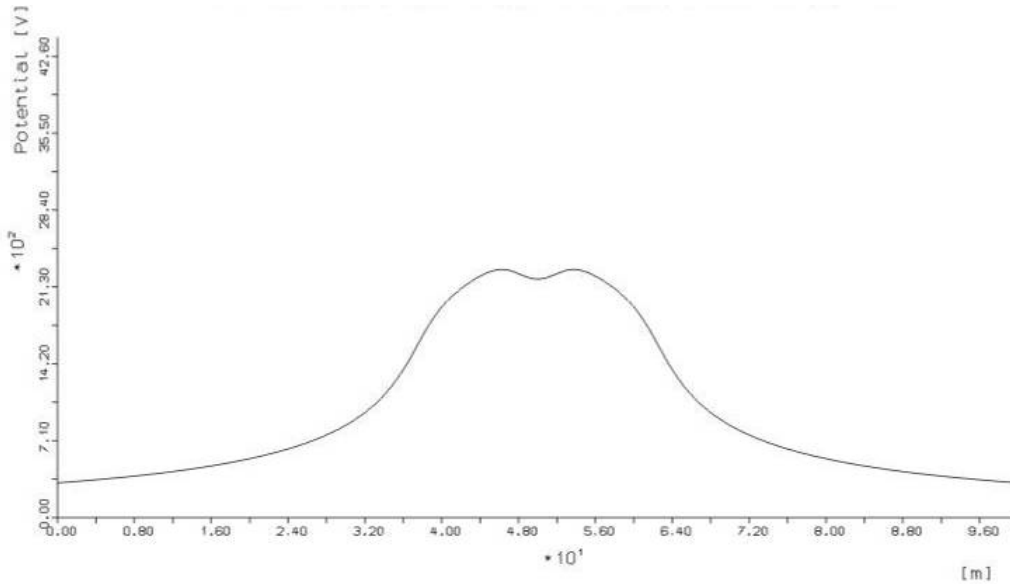


Figure 2-4: Potential Curve Along the Straight Line g 110-kV-2x3x1 STALU 240/40

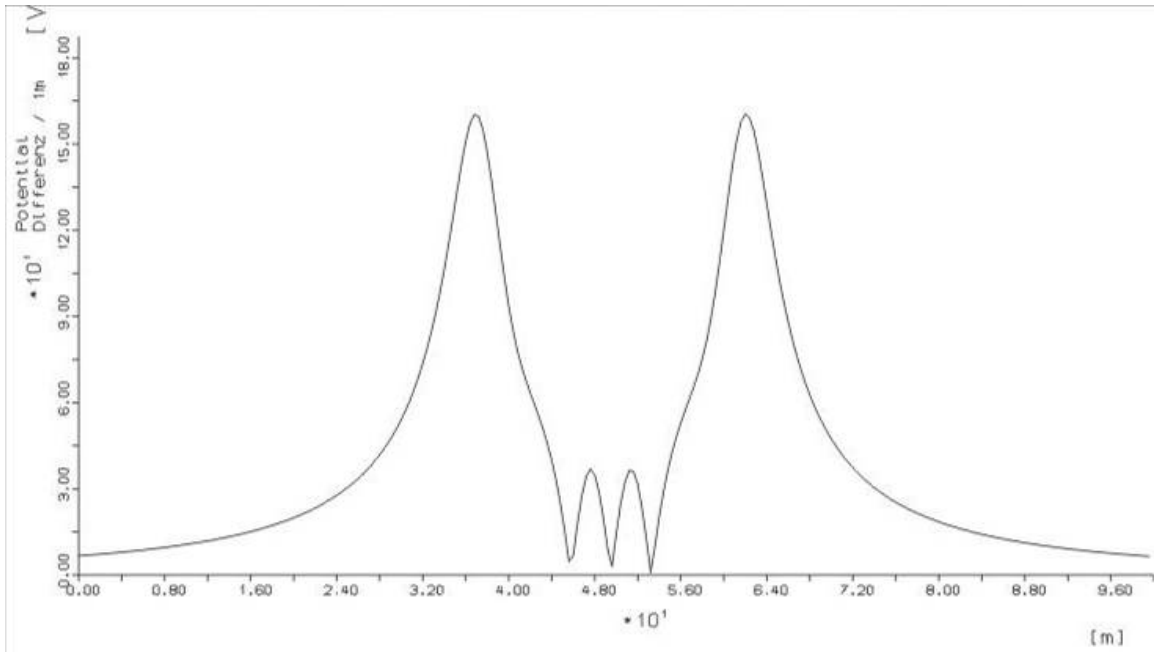


Figure 2-5: Step Voltage along the Straight Line g 110-kV-2x3x1 STALU 240/40

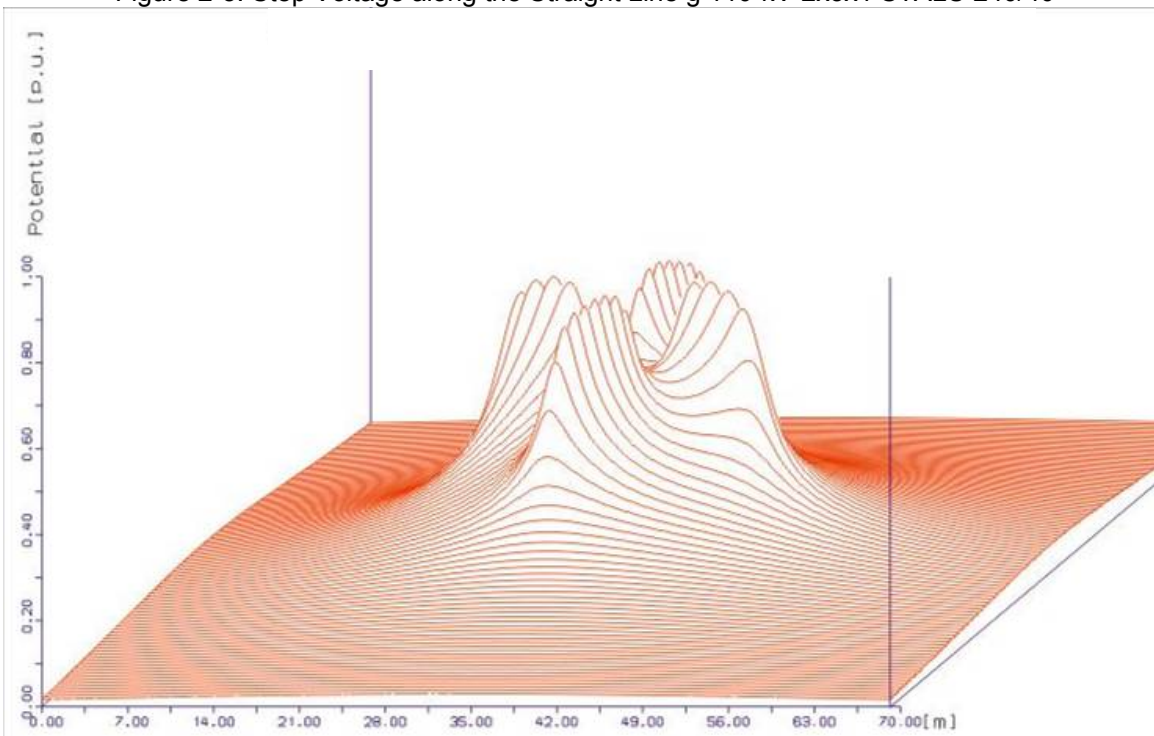
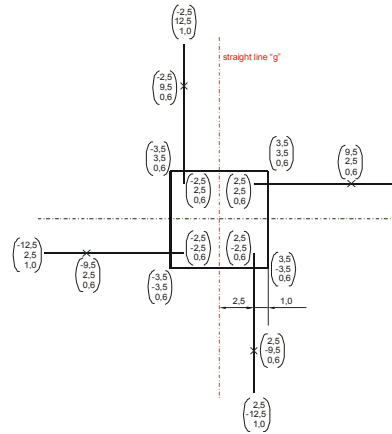
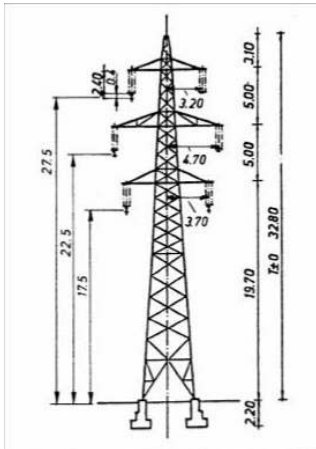


Figure 2-6: 3D Plot of Ground Potential 110-kV-2x3x1 STALU 240/40

2.2.2 110kV Standard Power Line 2x3x2 STALU 560/50

Grounding system resistance $R_A = 3.719\Omega$
 Earth potential U_E with 1kA = 3719V



Phase configuration: 2x3x2 STALU 560/50
 1 STALU 95/34
 Standard span length: 330 m
 Maximum wire sag (20°C): 9,8 m

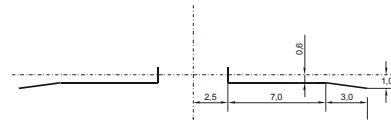


Figure 2-7:
 Head of Pylon 110-kV-2x3x2 STALU 560/50

Figure 2-8:
 Ground/Earth System 110-kV-2x3x2 STALU 560/50

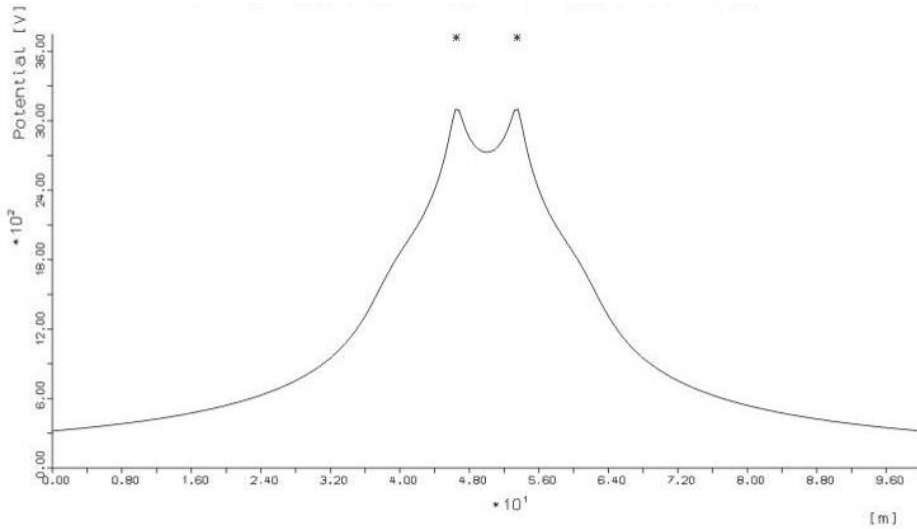


Figure 2-9: Potential Curve Along the Straight Line g 110-kV-2x3x2 STALU 560/50

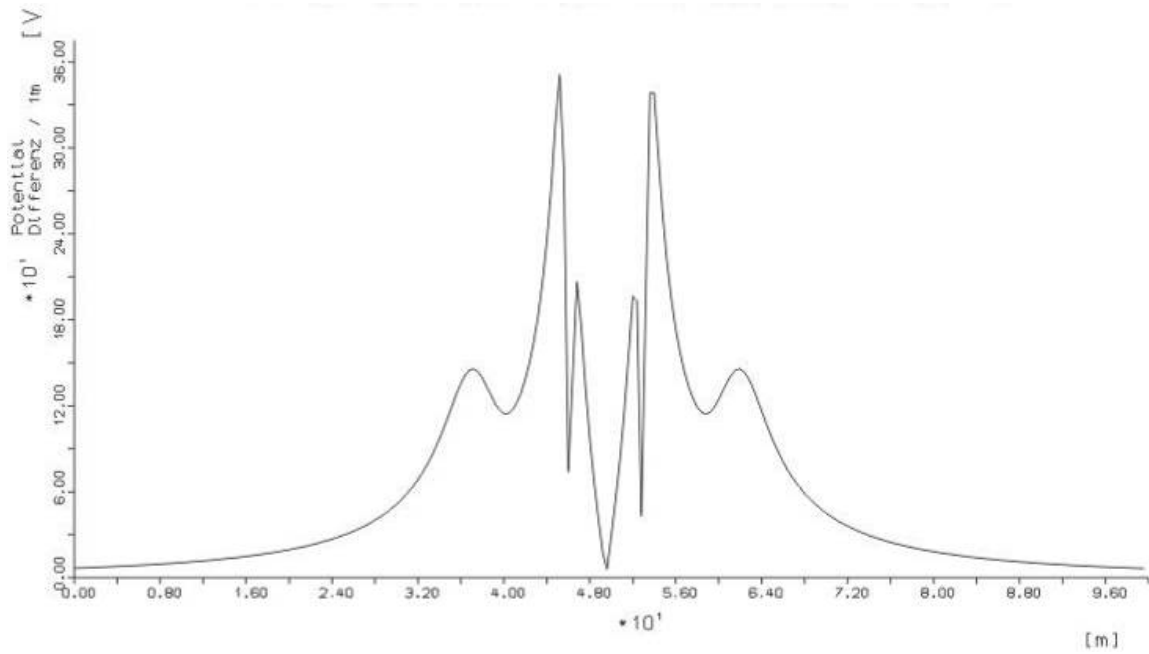


Figure 2-10: Step Voltage along the Straight Line g 110-kV-2x3x2 STALU 560/50

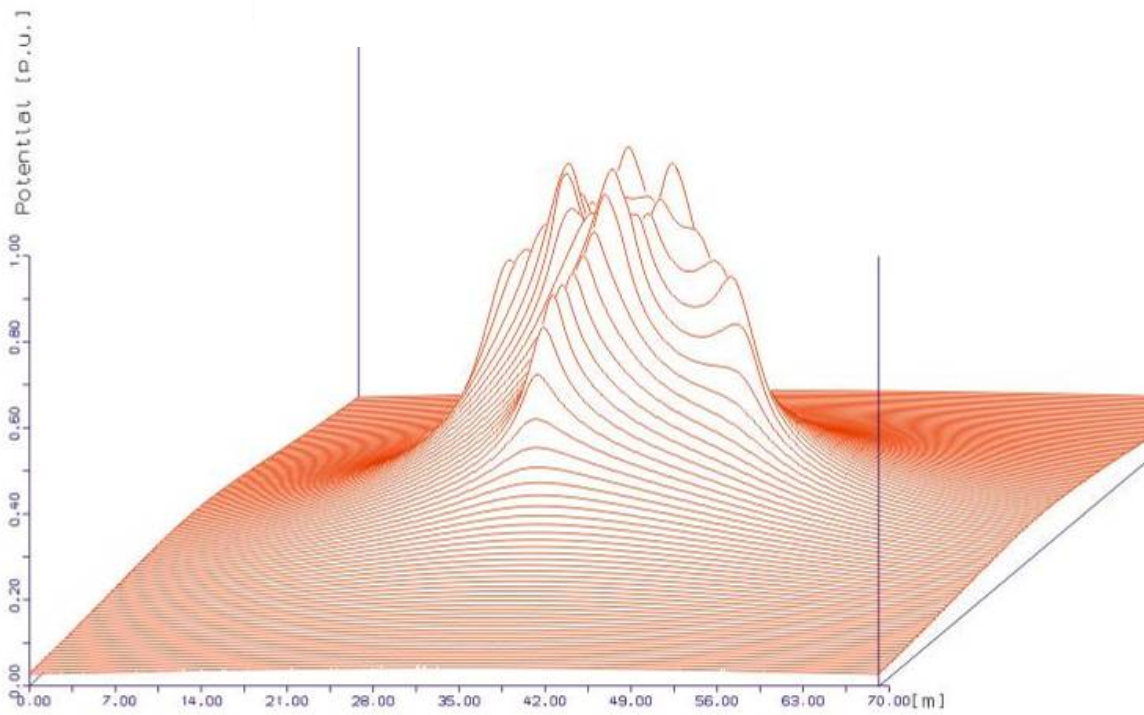
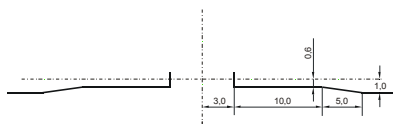
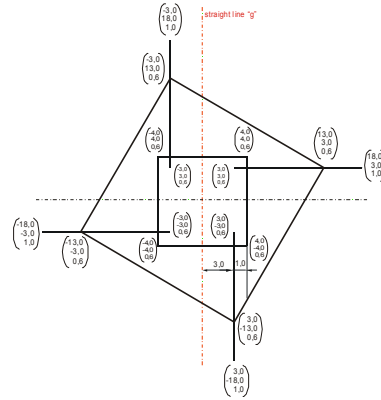
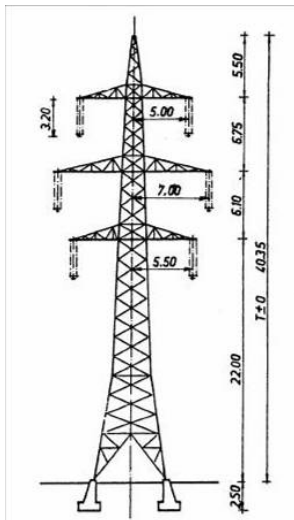


Figure 2-11: 3D Plot of Ground Potential 110-kV-2x3x2 STALU 560/50

2.2.3 220kV Standard Power Line 2x3x1 STALU 340/110

Grounding system resistance $R_A = 2.197\Omega$
 Earth potential U_E with 1kA = 2197V



Phase configuration: 2x3x1 STALU 340/110
 1 STALDR 120/42
 Standard span length: 330 m
 Maximum wire sag (20°C): 11,3 m

Figure 2-12:
 Head of Pylon 220-kV- 2x3x1 STALU 340/110

Figure 2-13:
 Ground/Earth System 220-kV 2x3x1 STALU 340/110

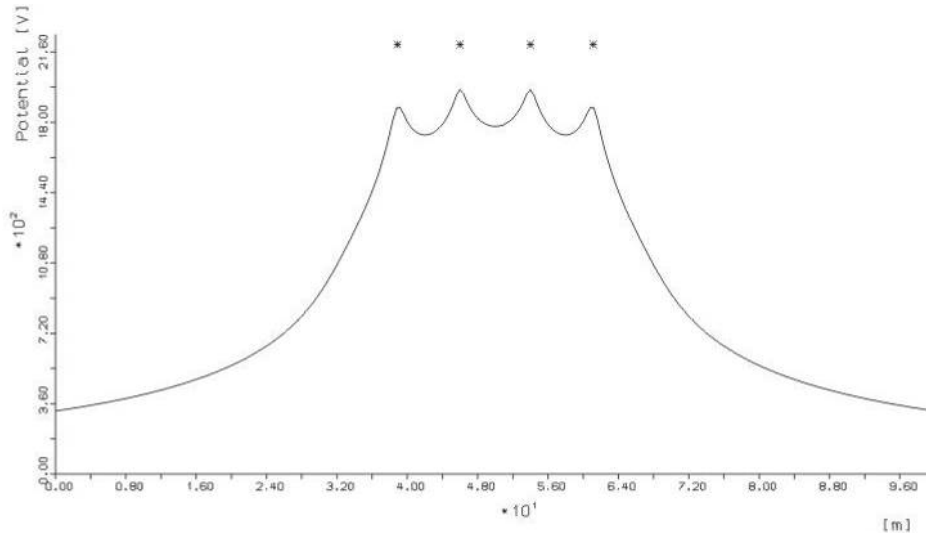


Figure 2-14: Potential Curve Along the Straight Line g 220-kV 2x3x1 STALU 340/110

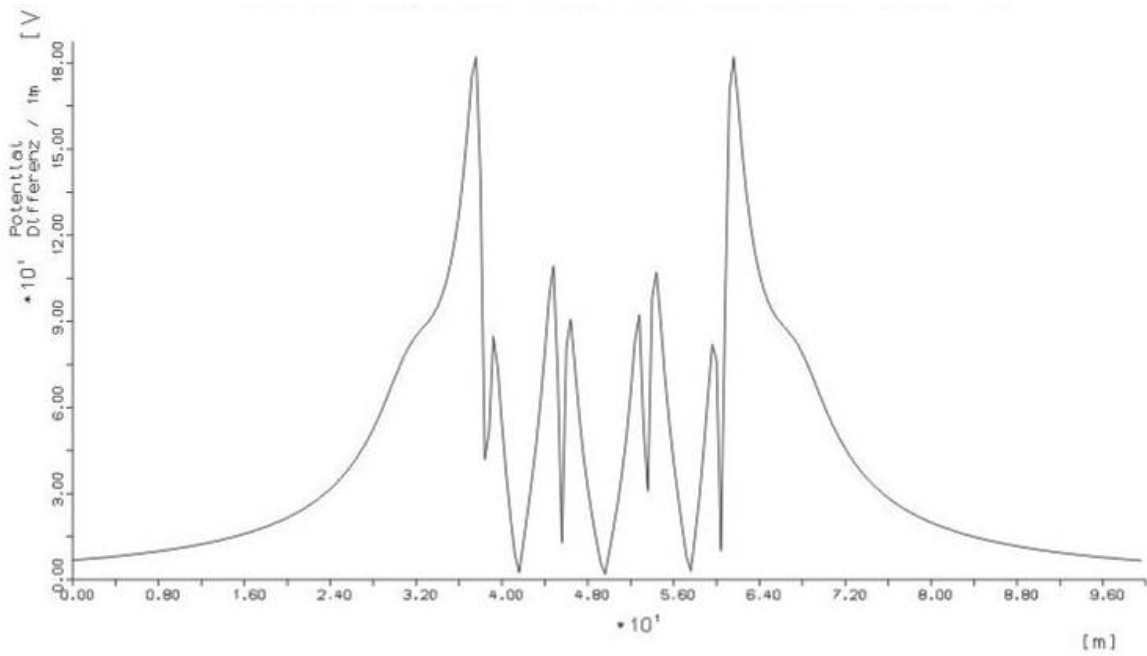


Figure 2-15: Step Voltage along the Straight Line g 220-kV 2x3x1 STALU 340/110

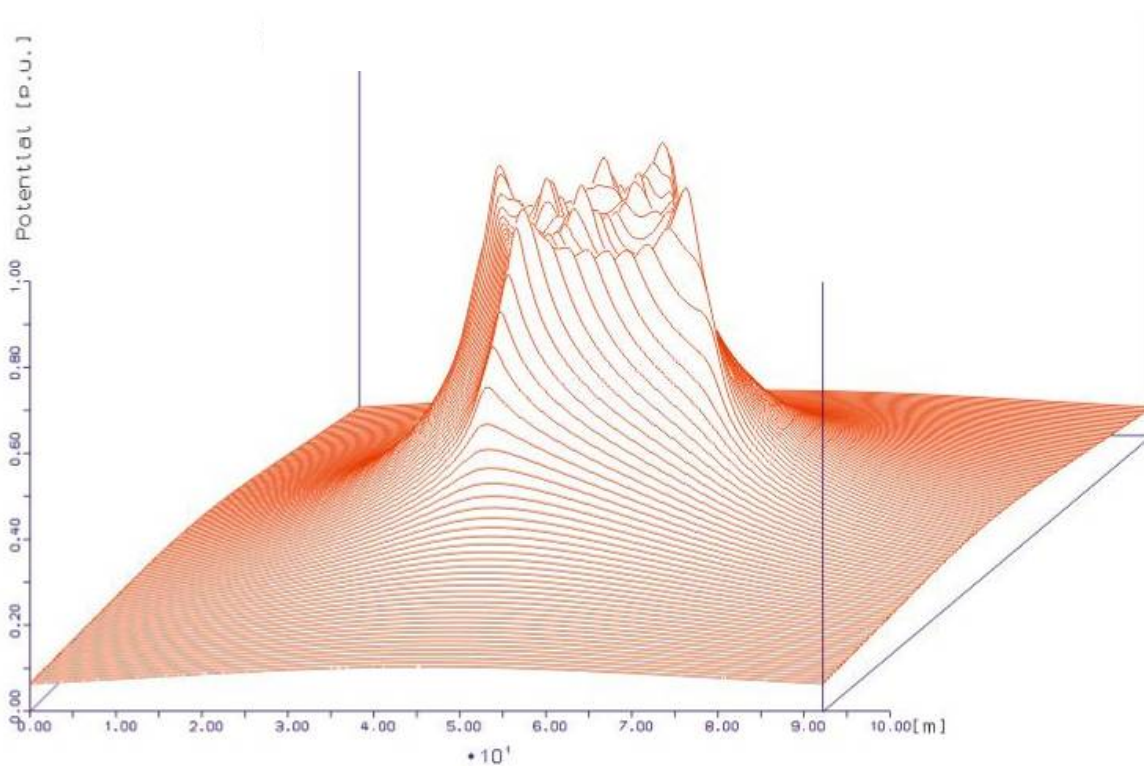
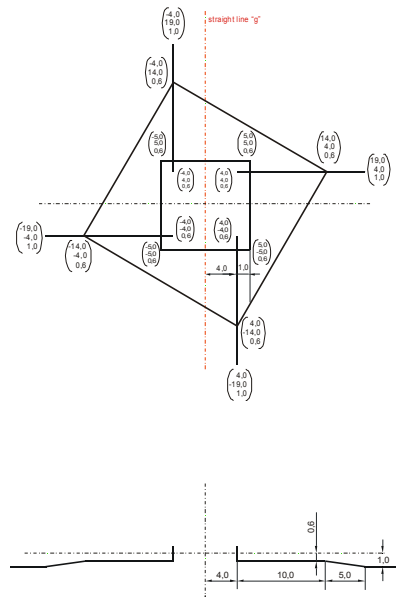
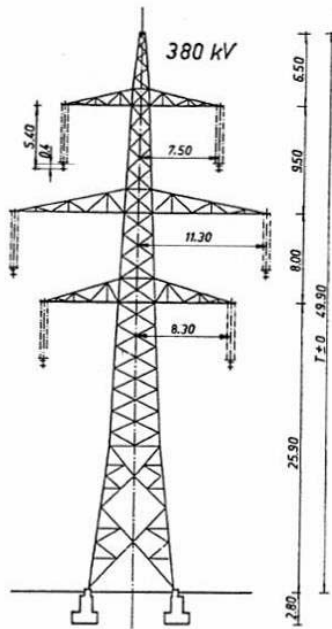


Figure 2-16: 3D Plot of Ground Potential 220-kV 2x3x1 STALU 340/110

2.2.4 380kV Standard Power Line 2x3x2 STALU 680/85

Grounding system resistance $R_A = 2.051\Omega$
 Earth potential U_E with 1kA = 2051V



Phase configuration: 2x3x2 STALU 680/85
 1 STALDR 240/40

Standard span length: 330 m

Maximum wire sag (20°C): 11,8 m

Figure 2-17:
 Head of Pylon 380-kV 2x3x2 STALU 680/85

Figure 2-18:
 Ground/Earth System 380-kV 2x3x2 STALU 680/85

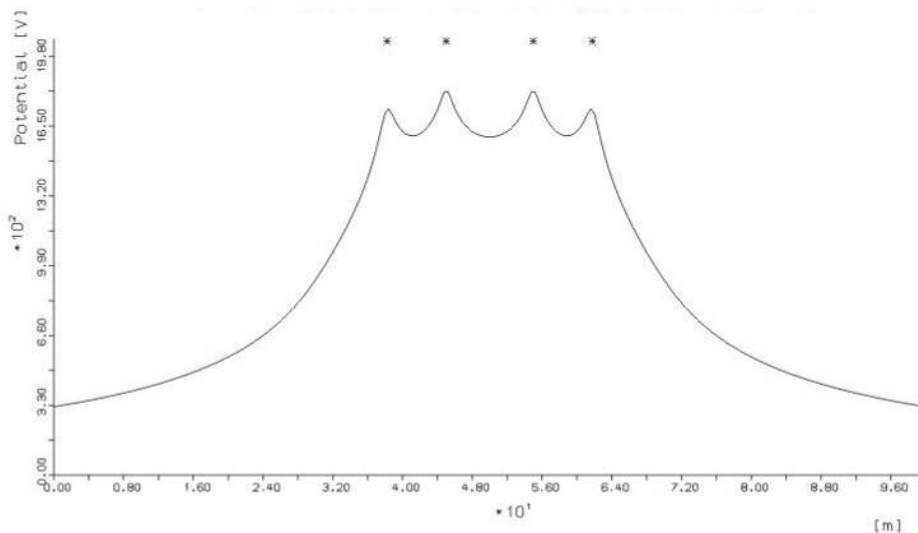


Figure 2-19: Potential Curve Along the Straight Line g 380-kV 2x3x2 STALU 680/85

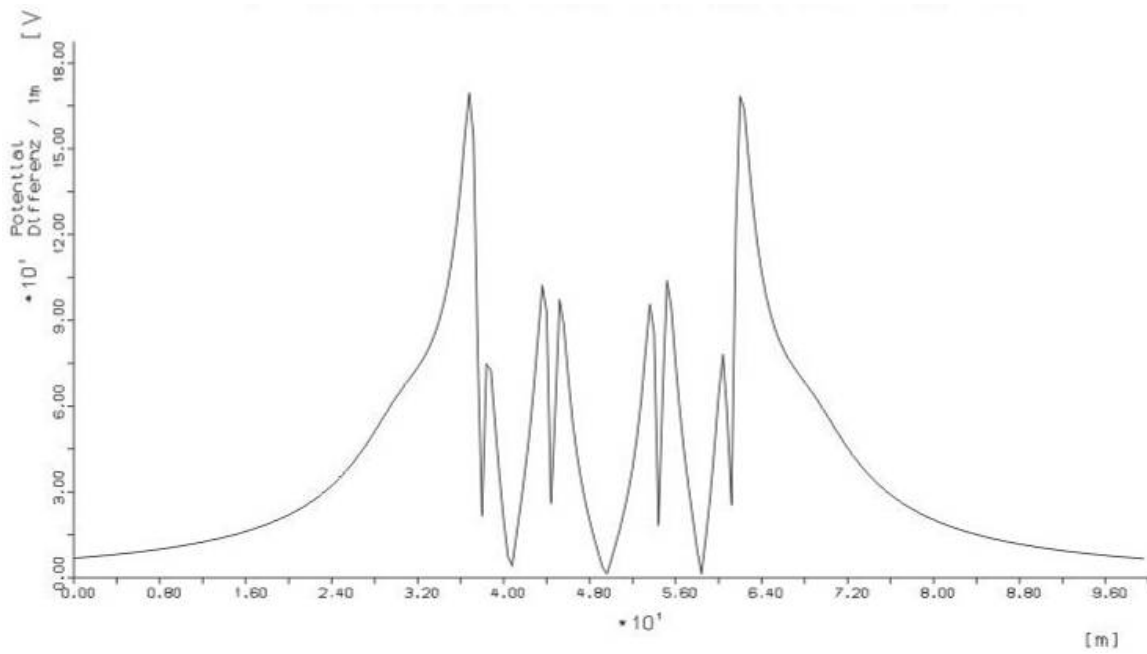


Figure 2-20: Step Voltage along the Straight Line g 380-kV 2x3x2 STALU 680/85

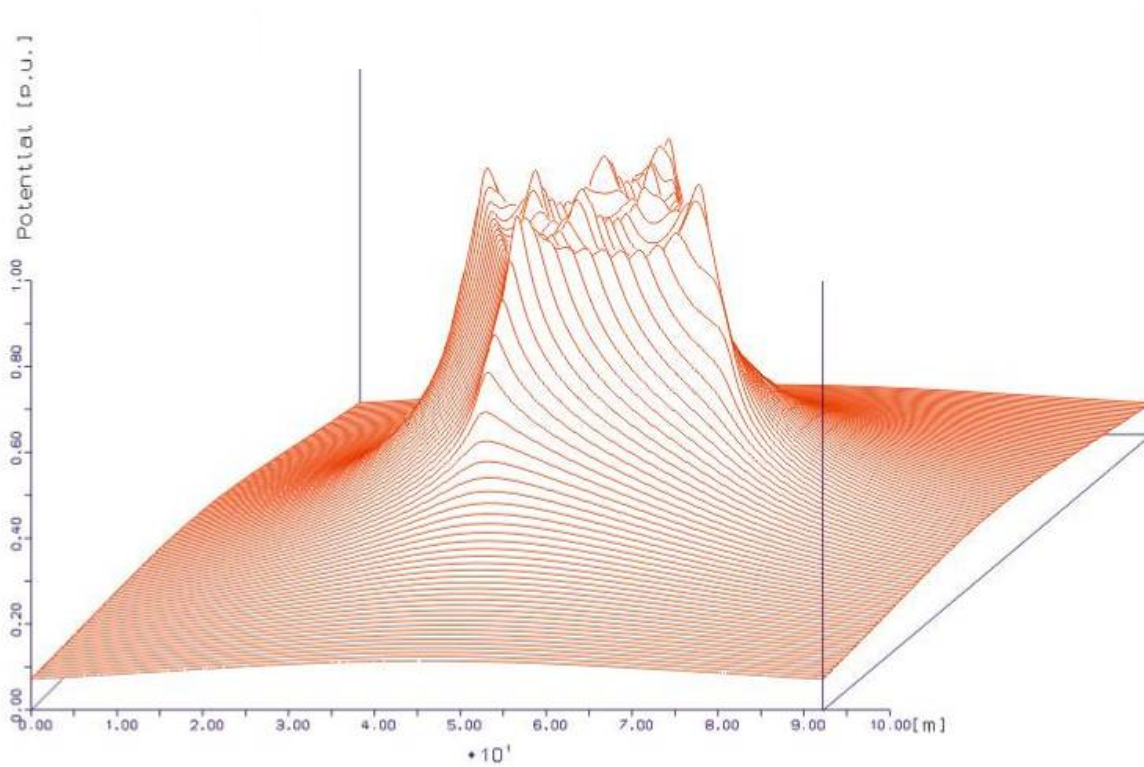


Figure 2-21: 3D Plot of Ground Potential 380-kV 2x3x2 STALU 680/85

2.3 Simulation of the Interconnected Ground/Earth System of Two Standard 110kV Pylons

In order to represent the mutual interference of two pylon ground/earths which are connected by an infinitely inductive earth wire, two of the 110kV pylons which have been dealt with in 2.2.1 have been simulated with a distance of 300m standard span length. For this simulation the same parameters have been applied as in 2.2.1.

The simulation produced the following results for the total system:

Grounding system resistance $R_A = 2.237\Omega$

The grounding system resistance is approximately half of the grounding system resistance of one single pylon. This shows that there is hardly any ohmic interference between both ground/earth systems.

Earth potential U_E with 1kA (500A per pylon) = 2237V

The potential curve along a straight line g which runs along the ground directly below the earth wire, and the 3D plot of the ground potential, respectively, show how far one has to move away from the pylon in order to get out of the ground potential rise or to reach fairly neutral earth.

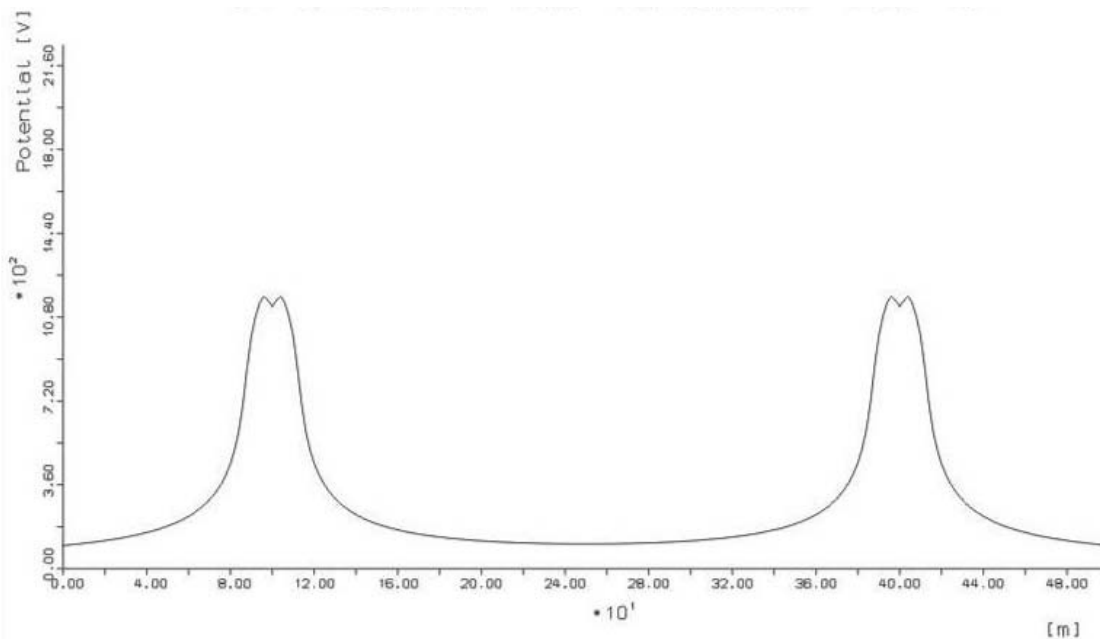


Figure 2-22: Potential Curve Along the Straight Line g between two pylons

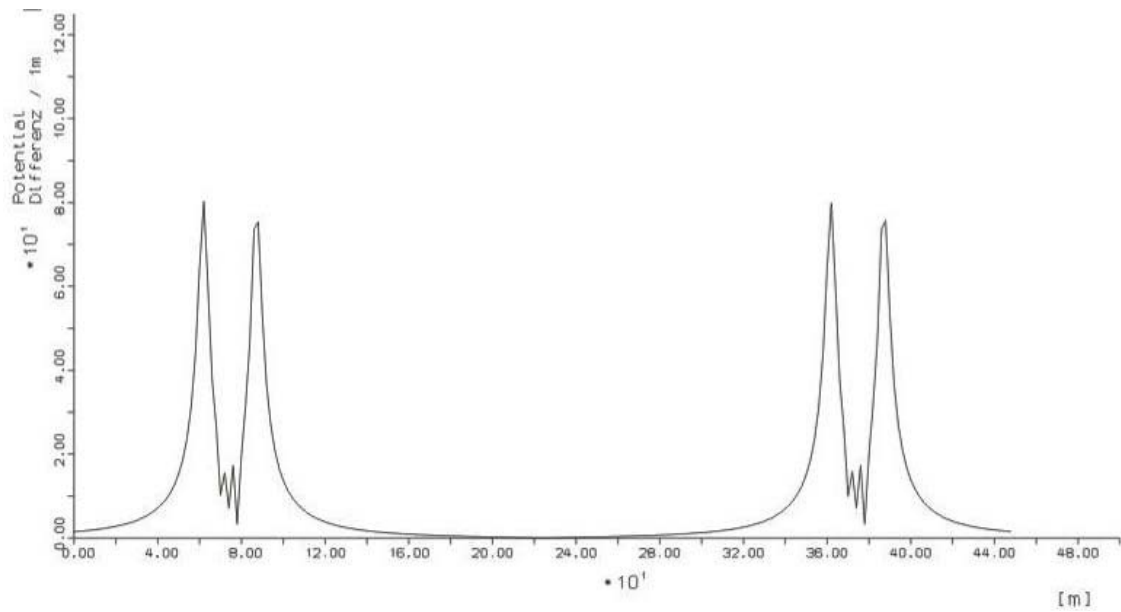


Figure 2-23: Step Voltage Along the Straight Line g between Two Pylons

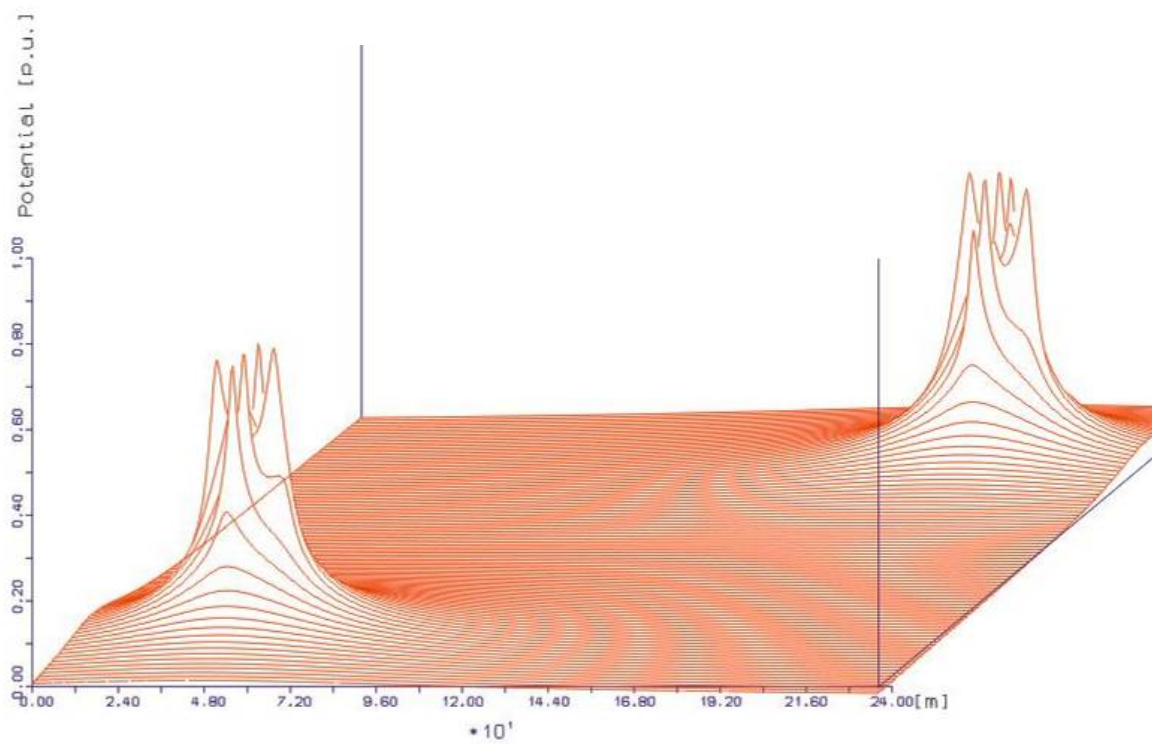


Figure 2-24: 3D Plot of Ground Potential between Two Pylons

2.4 Interference of Multilayered Soils with Varying Soil Resistivity

In order to analyze the interference of multilayered soil on the grounding system resistance, the 110kV pylon, which has been referred to in 2.2.1, has been calculated for multilayered soil.

For the top layer (2m) a soil resistivity of $100\Omega\text{m}$ and for the deeper layers a soil resistivity of $1000\Omega\text{m}$ has been assumed. This results in a ratio of $R_{A-1\text{layer}} / R_{A-2\text{layers}}$ of $4.42\Omega / 12.4\Omega$. In that case this is 2.8-fold higher than the grounding system resistance of the single layered $100\Omega\text{m}$ soil. In Figure 2-25 and Figure 2-26 the potential curve for an earth current of 1000A is shown with regard to the soil conditions mentioned above.

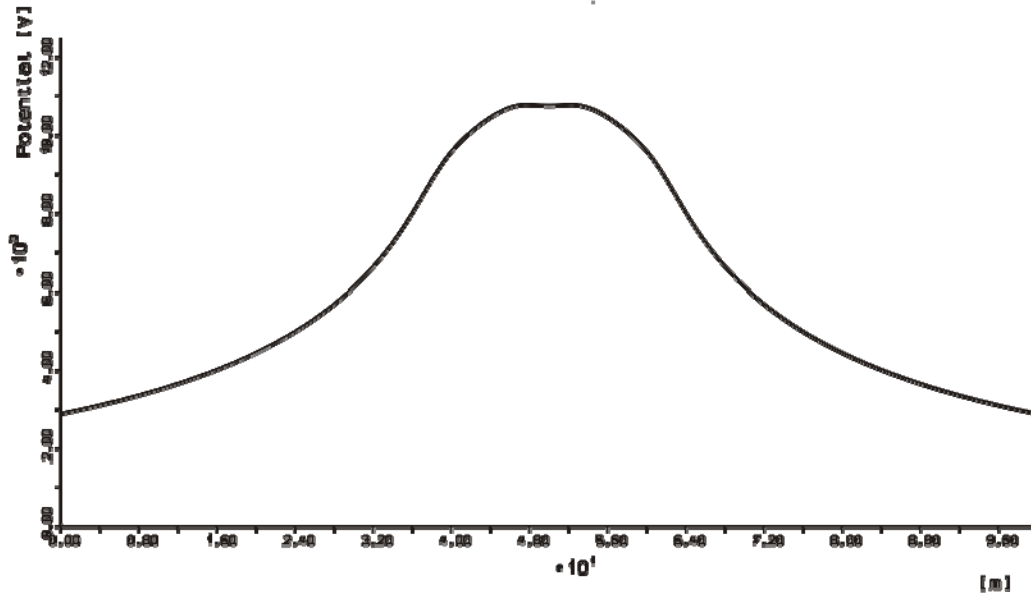


Figure 2-25: Potential Curve with Multilayered Soil $\rho = 100\Omega\text{m}$ & $1000\Omega\text{m}$

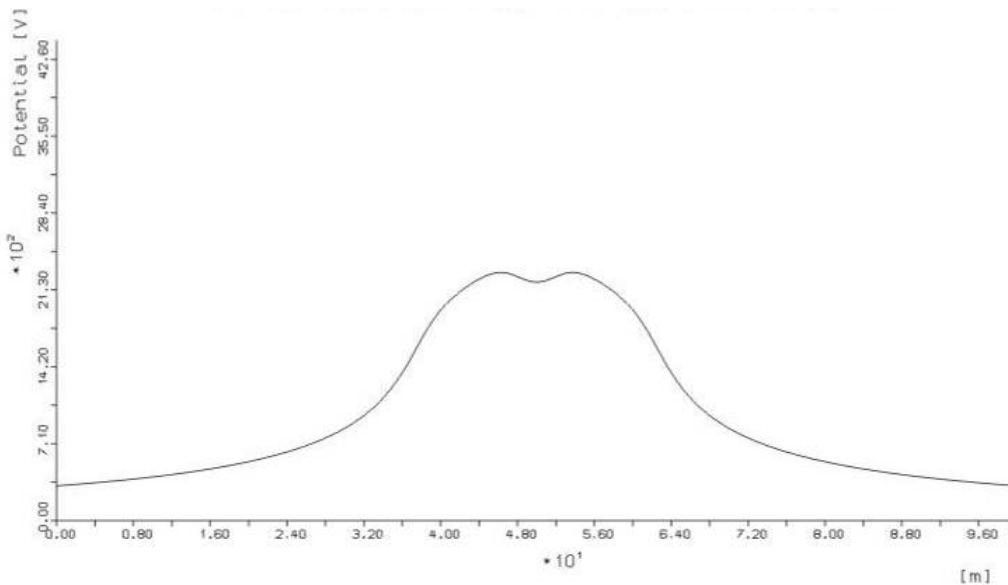


Figure 2-26: Potential Curve without Multilayered Soil $\rho = 100\Omega\text{m}$

3 Ground Currents and Earth Wire Currents

3.1 General Information

In order to assess which data concerning the current in the earth wire or in the ground wire of a pylon may result from a symmetrical current load, a model has been established using MATLAB and a Simulink-Simpower-Systems-Toolbox. This model includes all phase and coupling impedances as well as all ground/earth and coupling capacities. As it works with distributed parameters the exact physical size of the phase wire (material, diameter, bundling, wire sag etc.) and electrical phenomena such as the skin effect have been taken into consideration. In the simulations the power line model has been loaded with a total current of 100A (19MVA at 110kV). As all couplings are linear it is possible to apply the data resulting from the simulation to any other load currents.

3.2 Description of Simulation Model

The simulation is based on the following software:

- MATLAB, version 7.3.0.267 (R2006b) including:
 - Simulink, version 6.5 (R2006b)
 - SimPowerSystems, version 4.3 (R2006b)

With the help of elements contained in the libraries of Simulink and SimPower Systems standardized systems (blocks) have been established, which made it possible to simulate power lines with different physical sizes and different types of wires with six phase wires and one earth wire. By cascading several blocks the required number of spans including pylons can be created (see Figure 3-2). Transposition intervals, sources and loads can simply be integrated, as is shown in Figure 3-1.

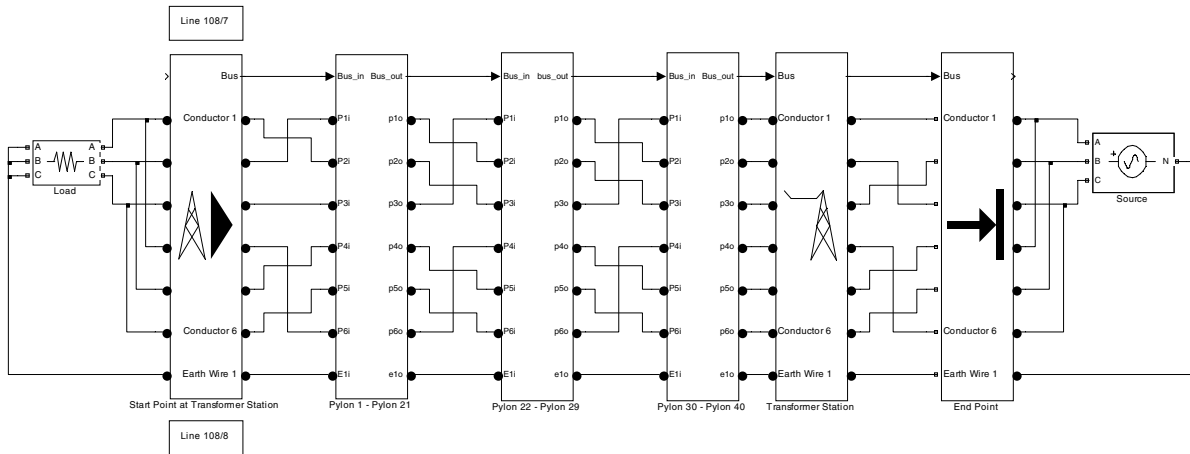
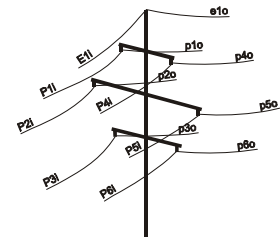


Figure 3-1: Overall View of Model in Simulink (Upper Level)

Caption:

- P1i...P3i incoming phase wire system 1
- P4i...P6i incoming phase wire system 2
- p1o...p3o outgoing phase wire system 1
- p4o...p6o outgoing phase wire system 2
- E1i incoming earth wire
- e1o outgoing earth wire



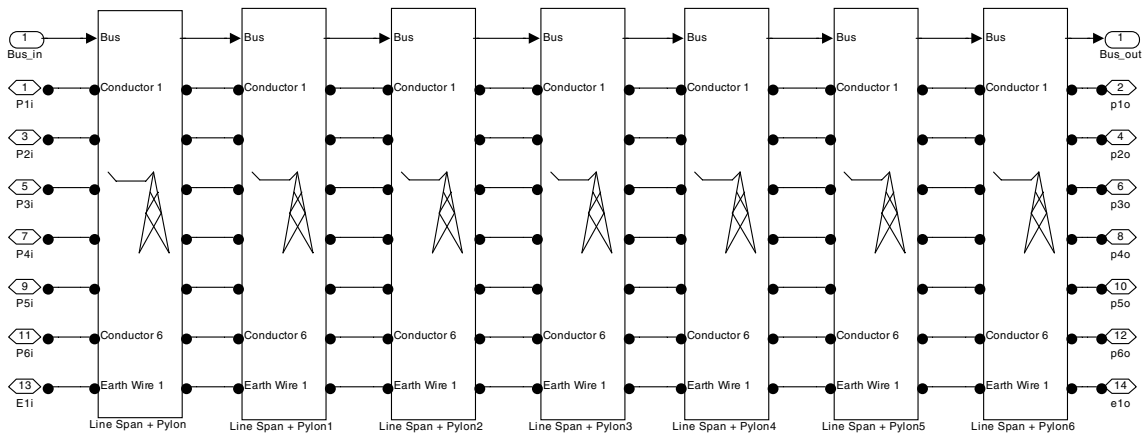


Figure 3-2: Line Section Pylon 22 to Pylon 29 (Including 7 Spans)

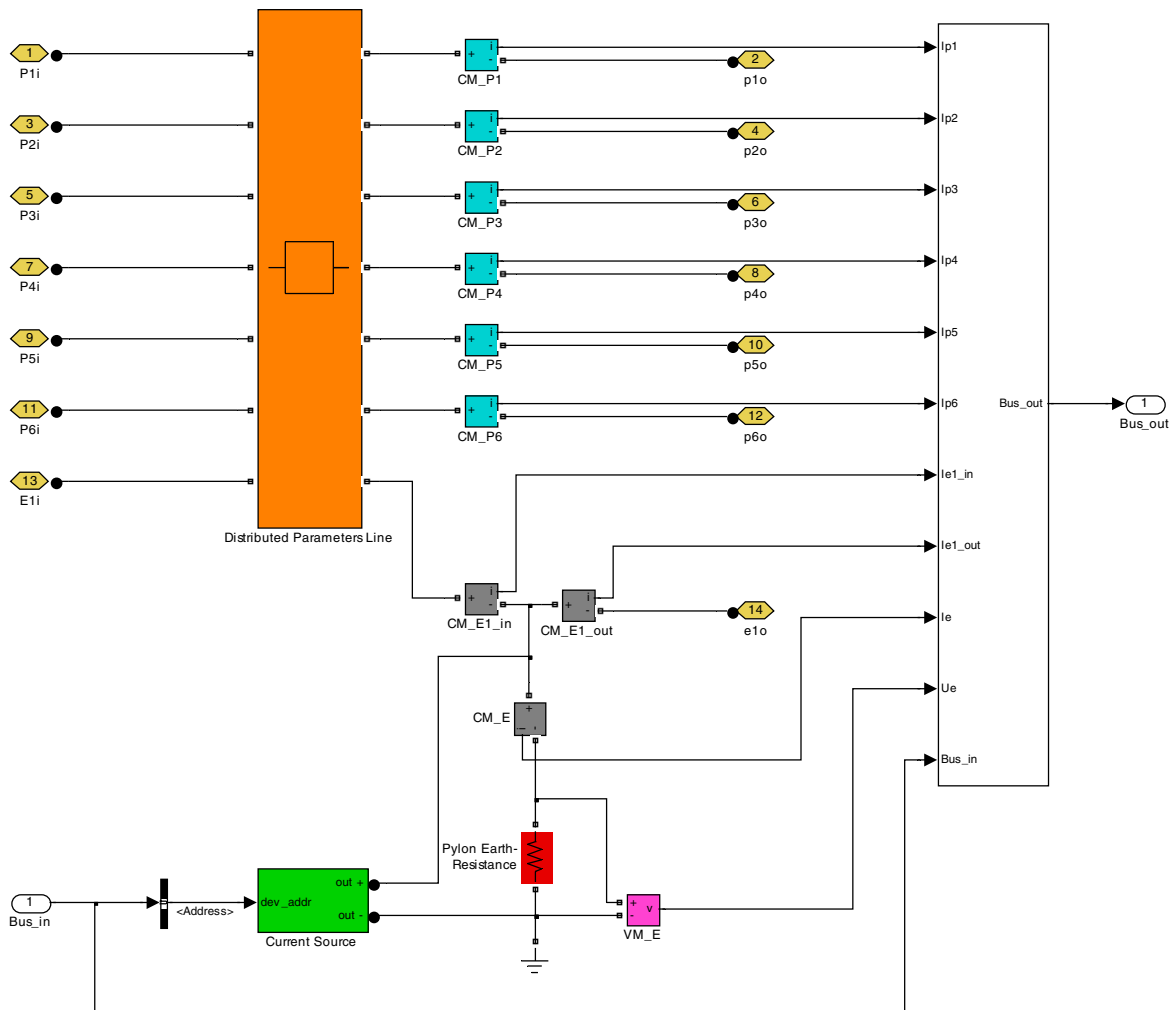


Figure 3-3: Internal Construction of Block 'Span + Pylon'

In the Simulink-model the phase wires reach the system span + pylon via IO-Ports (yellow). There they go through the block 'Distributed Parameters Line' (orange), which models the span and its couplings. After measuring the current (blue), the six phase wires are led towards the end of the system. Before that, however, the earth wire is connected with neutral earth (earth

symbol) using the pylon grounding system resistance (red). Three current measuring blocks in the path of the earth wire (grey) measure exactly the way the earth wire current is split up at the pylon into an incoming earth wire current, an outgoing earth wire current and a current which flows into the earth. A voltage measuring block (magenta) measures the pylon potential towards neutral earth. For the calculation of the ladder network impedance a current source (green) is used to inject frequency-variable currents into the pylon.

3.3 Power Line Model

The following theoretical research is based on the 110kV power line 108/7 and 108/8 near Vienna, which connects transformer station (TS) Wien SO with transformer station Wiener Neudorf. This power line has the following parameters:

Wire designation:

Wien SO – Wr. Neudorf (108/7 108/8)

Phase wire type:

2x3x2x560/50 STALU

Earth wire type:

LWL BRR 24E9 108/37

Soil resistivity:

single-layered $\rho = 35\Omega\text{m}$

Standard span length:

300m

Wire sag:

10m

Transposition pylons at pylons no.:

21, 29

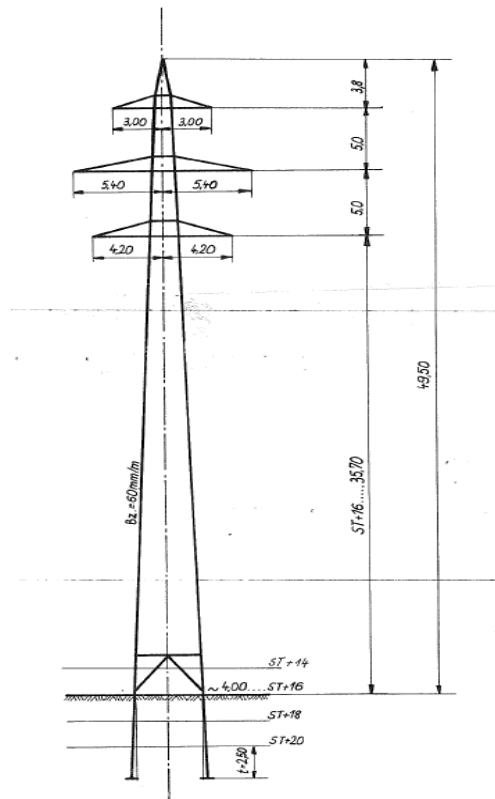


Figure 3-4: Head of Pylon of Simulated Line

The data concerning the grounding system resistance of all pylons of this Power Line have been provided by Wienstrom. As the grounding system resistance has a strong impact on the intensity of the ground current, the grounding system resistance as well as the soil resistivity at first have been kept at a constant level during the general part of the investigation in chapter 3.4. Only for the measurements in chapter 3.5 the actual grounding system resistances and a soil resistivity of $35\Omega\text{m}$ have been used.

As the ground current may be quite small compared to the earth wire current, the pylon potential (blue) and the grounding system resistance (green) are represented in all following Figures.

Thus the ground current can be calculated using the formula
$$I_E = \frac{U_E}{R_A}$$

3.4 General Observations

3.4.1 Method

For the general part of this study the model described above has been simulated using the following configuration:

- Physical size of power line (types and numbers of pylons, arrangement of conductors etc.) corresponding to the actual power line 'Wien-Südost' – 'Wiener Neudorf'
- Grounding system resistance $R_A = 10\Omega$ for all pylons
- Grounding system resistance $R_A = 0.2\Omega$ for both TS ground/earth systems
- Source voltage at TS Wien-Südost: $U_N = 110kV$
- Total load current $I_B \approx 100A$ (using a 3-phase load resistance with $R = \frac{110kV/\sqrt{3}}{100A} \approx 635\Omega$)

The simulation has been carried out in different ways, varying the following parameters:

- Transposing of phase wires:
 - according to the actual situation
 - no transposing
- Systems
 - both systems active (standard operation)
 - only one system active
 - inactive system short-circuited & earthed on both terminals
 - inactive system open on both terminals
- Doubling of system length

In the following Figures the pylon numbers 0 to 41 correspond to the respective electric transformer stations, whereas the pylon numbers 1 to 40 correspond to the pylon numbers from Wiener Neudorf to Wien SO.

3.4.2 Untransposed System - 2 Systems Active

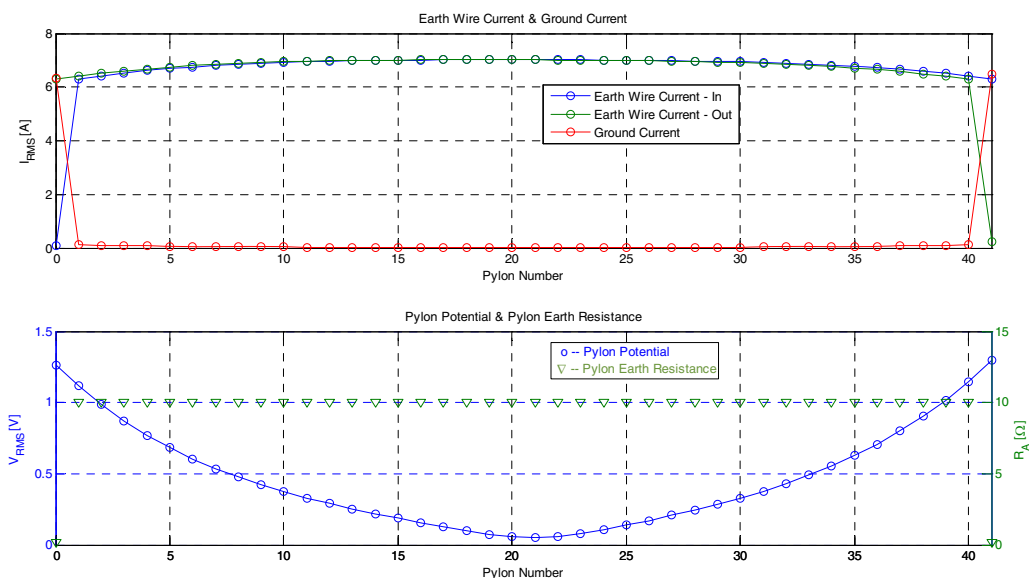


Figure 3-5: General – Untransposed System – 2 Systems Active

3.4.3 Transposed System - 2 Systems Active

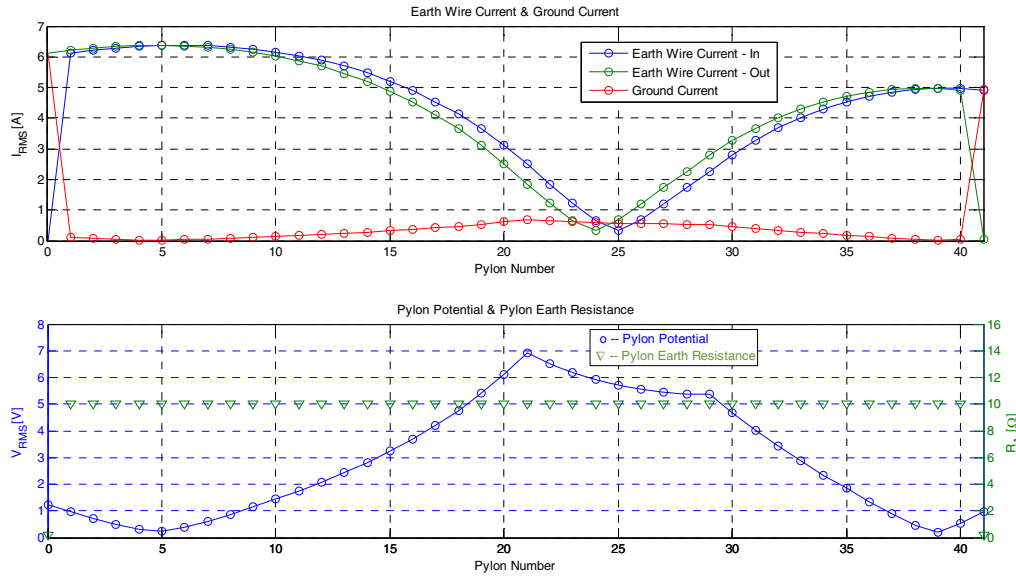


Figure 3-6: General – Transposed System – 2 Systems Active

Chapter 3.4.3 and 3.4.2 shows that transposed systems have higher ground currents than untransposed systems. It also becomes obvious that if untransposed systems are used, ground currents only occur near the transformer station, whereas ground currents rise around the transposition pylons when transposed systems are used.

3.4.4 Transposed System - 2nd System Inactive

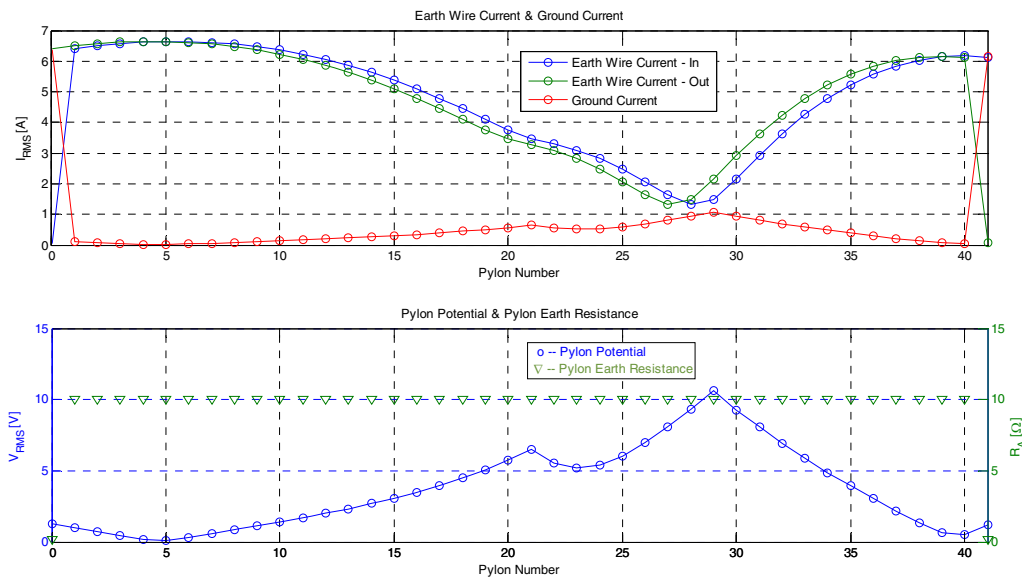


Figure 3-7: General - 1 System Active (2nd System Inactive)

In case only one system is active, untransposed systems show similar effects as transposed systems.

3.4.5 Transposed System - 2nd System Short-Circuited

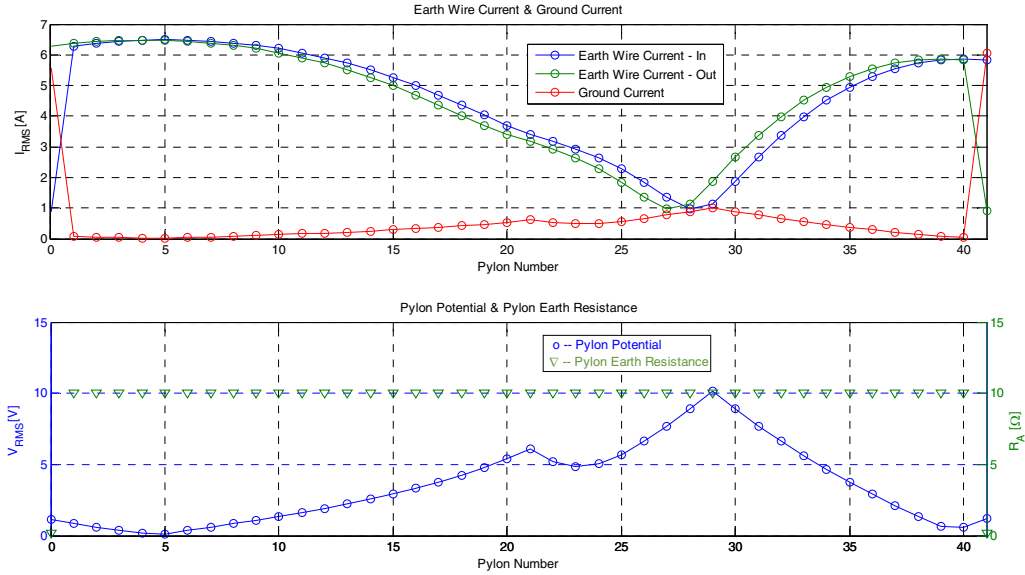


Figure 3-8: General - Transposed System - 1 System Active (2nd System Short-Circuited)

If the inactive system is short-circuited and earthed at both transformer stations, it acts as another earth wire system, which, however, is only earthed at the transformer stations. This is the reason that ground and earth wire currents are slightly lower than in 3.4.4.

3.4.6 Untransposed System - 2nd System Inactive

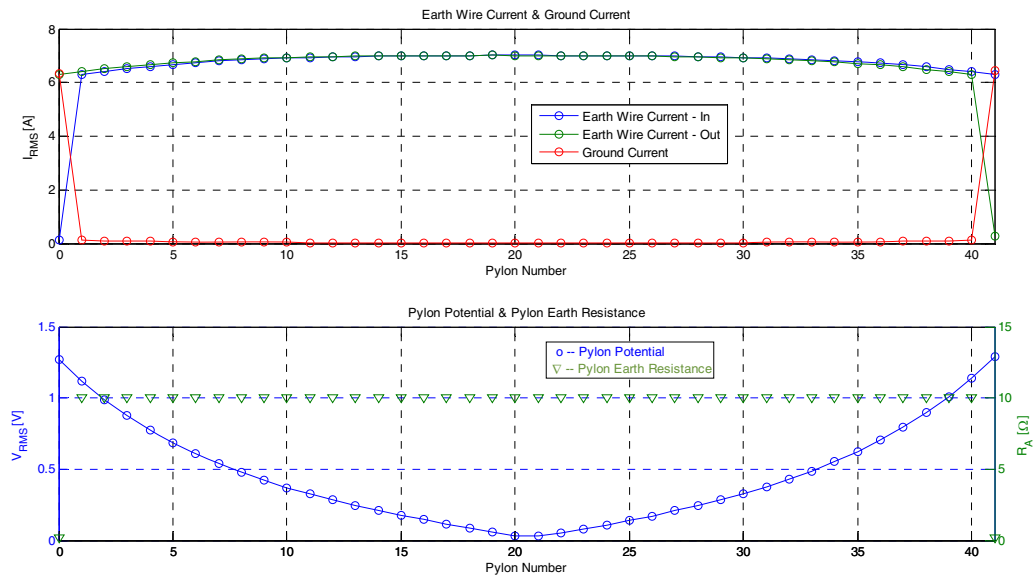


Figure 3-9: General - Untransposed System - 1 System Active (2nd System Inactive)

3.4.7 Untransposed System - 2nd System Inactive and Short-Circuited

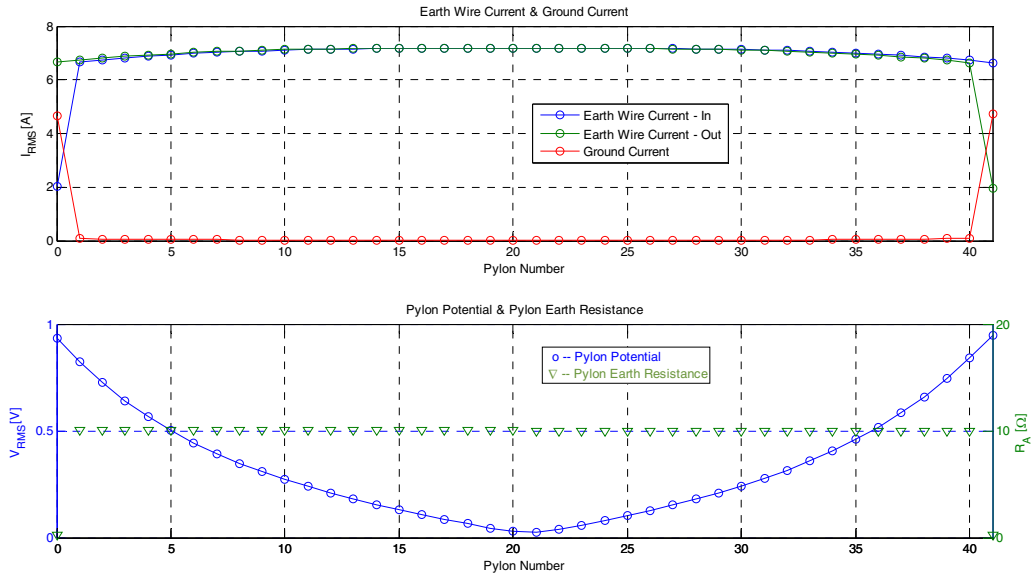


Figure 3-10: General - Untransposed System - 1 System Active (2nd System Short-Circuited)

In case only one system is active, untransposed systems show similar effects as transposed systems.

3.4.8 Doubling Length of Power Line by Doubling Spans and Numbers of Pylons

In order to find out how the predicted earth wire and ground currents are affected by an extension of the power line system, the number of spans between the transformer stations and transposition pylons has been doubled without changing the length of the spans. The difference between Figure 3-11 and Figure 3-6 shows that earth wire currents increase slightly with the length of the power line. The reasons for this rise are capacitance currents. In contrast to this ground currents decrease as they can now branch out to more pylon ground/earths.

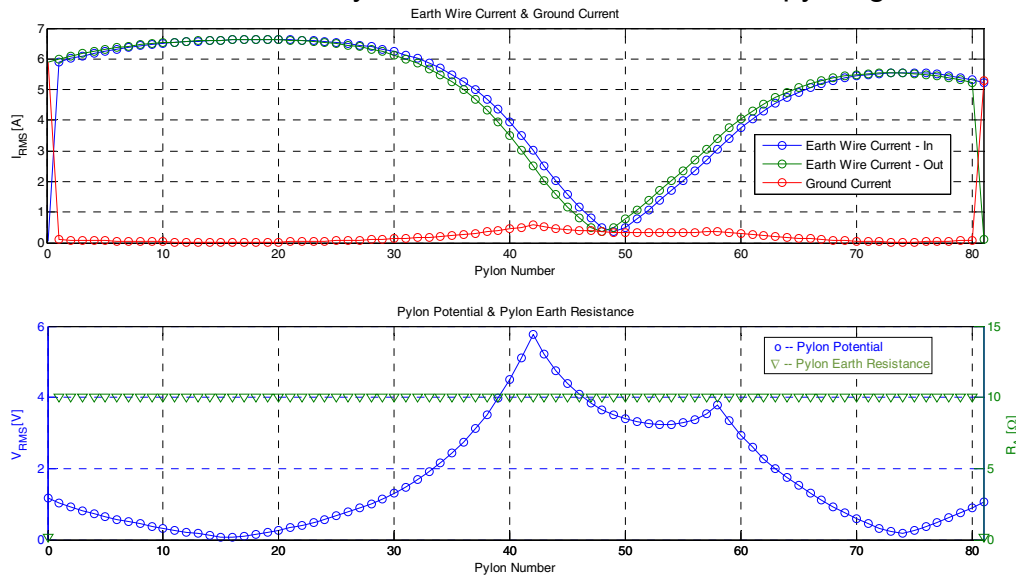


Figure 3-11: General - Doubling of Pylons - Transposed System - 2 Systems Active

3.4.9 Results of General Observations

Earth wire currents are higher in untransposed than in transposed systems. This confirms the observation that untransposed systems have a higher phase wire inductance. If one system of a double system is inactive and the line which is switched off is not short-circuited and earthed, the ground currents are higher than in the case that the system is short-circuited and earthed. Pylon ground currents at transposition pylons and their neighboring pylons are considerably higher than at the remaining pylons. Untransposed systems show the highest ground currents at pylons which are situated in the immediate surrounding of the transformer stations. The length of a power line system does not bear any significant influence on the intensity of earth wire and ground currents.

The strongest influence on earth wire currents and ground currents is due to the operating current (linear dependency), the grounding system resistances of the pylons and the transformer stations, the phase configuration, and the physical size of the pylon (head of pylon).

Transposing		transposed			untransposed		
Number of active systems		2	1	1	2	1	1
2nd system short-circuited and earthed		-	no	yes	-	no	yes
Maximum earth wire current [% I_B in total]	TS	6.00	6.40	6.28	6.29	6.40	6.65
	pylon	6.40	6.61	6.52	7.00	7.00	7.20
Maximum ground current [% I_B in total]	TS	6.00	6.40	6.07	6.29	6.49	4.74
	pylon	0.69	1.09	1.02	0.12	0.11	0.08

Table 3-1: Summary of General Observation

3.5 110kV Power Line Wr. Neudorf 108/7 and 108/8

3.5.1 Introduction

The simulations have been carried out under the same conditions as in chapter 3.4., yet instead of assuming a constant level of the grounding system resistances R_A of the pylons, actual data concerning the grounding system resistances gathered by the network provider have been used, whereas the grounding system resistances R_A of the transformer stations have been kept at 0.2Ω .

For this reason, higher ground currents may occur than in the general simulations.

3.5.2 Transposed System – 2 Systems active

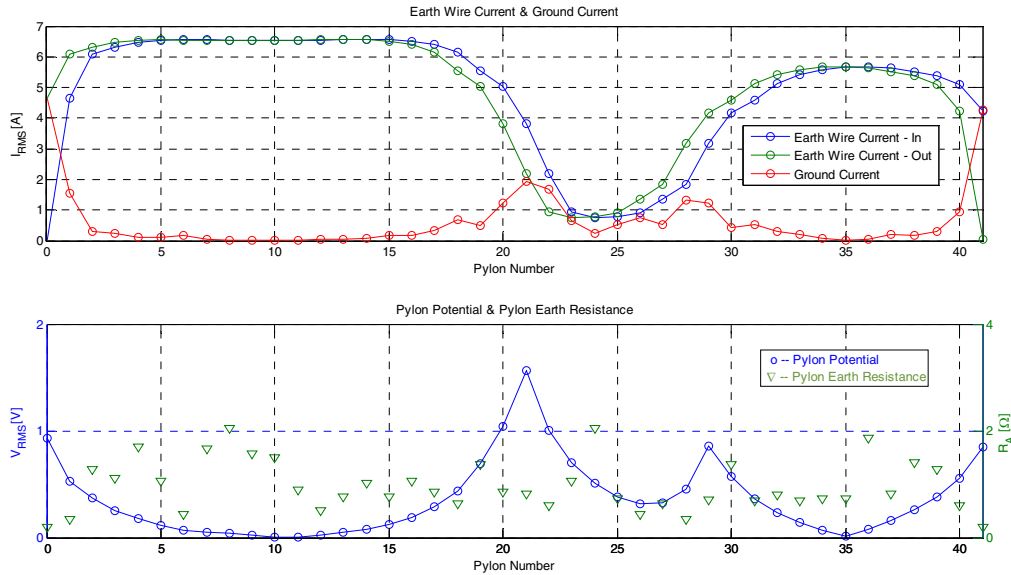


Figure 3-12: – Transposed System – 2 Systems Active

A comparison between Figure 3-12 and Figure 3-6 shows that for grounding system resistances, in reality, the highest ground currents occur in the vicinity of transposition pylons. The intensity of the ground currents increases as the grounding system resistance decreases. If a pylon next to a transposition pylon has a lower resistance than the transposition pylon itself, ground currents at this pylon may be higher than at the transposition pylon, as is the case at pylon 28.

In the authentic case, which is dealt with here, the ground currents of the pylon are higher than in the general simulations due to lower grounding system resistances. For that reason, ground currents near the transformer stations decrease. The maximum earth wire currents, however, basically stay the same.

In the authentic case the highest ground currents of the pylon, which are to be expected occur even if one system is inactive and not earthed. This may add up to 4% of the operating current for the real simulated grid as is shown in Figure 3-14.

3.5.3 Transposed System - 2nd System Short-Circuited

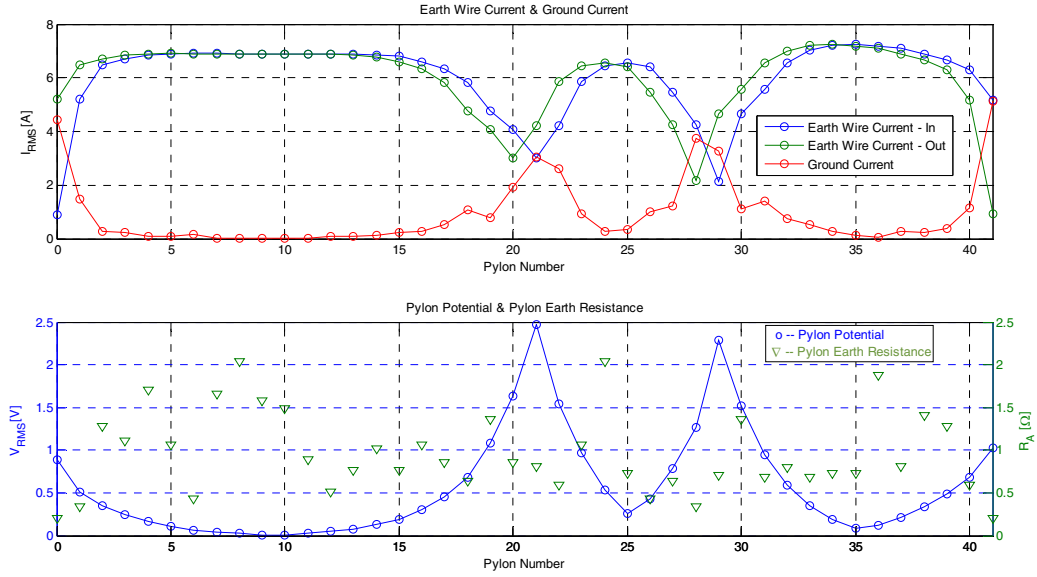


Figure 3-13: Wr. Neudorf – Transposed System - 2nd System Short-Circuited

3.5.4 Transposed System - 2nd System inactive

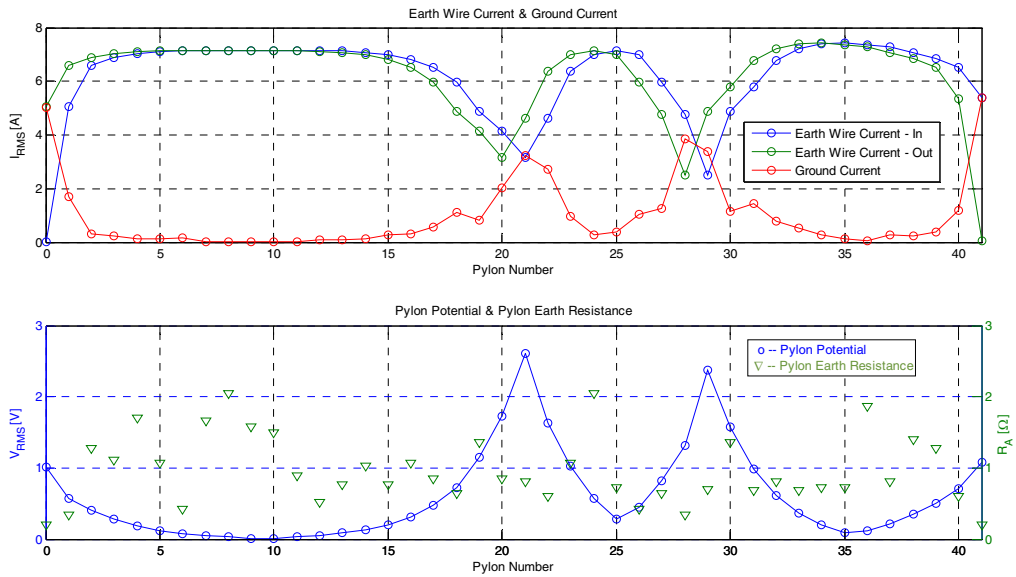


Figure 3-14: Wr. Neudorf – Transposed System - 2nd System Inactive

3.6 Comparison of Simulations and Measurements

In study of the comparative measurements, which are explained in detail in chapter 5.3, the ground currents I_{RA} at three pylons of the 110kV power line in Wr. Neudorf have been measured. Table 3-2 compares the results of measurements with the results of these simulations.

	Simulation	Measurement			Annotation
	I_{RA} Sim.	I_{RA}	I_B	I_{RA}	
	% I_B	A	A	% I_B	
Pylon 28	1.31	9.04	853	1.06	2 systems active
Pylon 29	1.22	17.02	850	2.00	2 systems active
Pylon 32	0.29	1.31	840	0.15	2 systems active
Pylon 32	0.77	2.88	760	0.38	1 system active

Table 3-2: Comparison Simulation - Measurement

At pylon 28 the results of the simulations and the results of the measurement correspond quite well, at pylon 29 the simulation shows a result which is 1.7-fold higher than that of the measurement. At pylon 32 the simulation results in a ground current which is about twice as high as the actual ground current which has been measured on-site. The reason for these deviations may be the values for the pylon grounding system resistances which have been applied for the simulation, as they are based on measurements which were carried out by Wienstrom some time ago. As is also confirmed by comparative measurements explained in chapter 5.3 there are deviations between the actual pylon grounding system resistances and those measured by Wienstrom some time ago.

4 Ladder Network Impedances

4.1 Principle

A power line may be seen as a ladder network consisting of several identical elements (spans and pylons) which results in a chain of repetitive links. This physical phenomenon can also be applied for an analysis of the electrical characteristics of the system. Figure 4-1 shows the ground/earth system of a power line from an electrical perspective. The horizontally arranged resistances and inductances (earth wire impedance) represent the electrical characteristics of the earth wire, whereas vertically arranged resistances reflect the grounding system resistance of the ground/earth system of the pylon. It is obvious that this kind of a ground/earth system in fact is a parallel connection of several units consisting of earth wire impedance including the respective ground/earth system of the pylon.

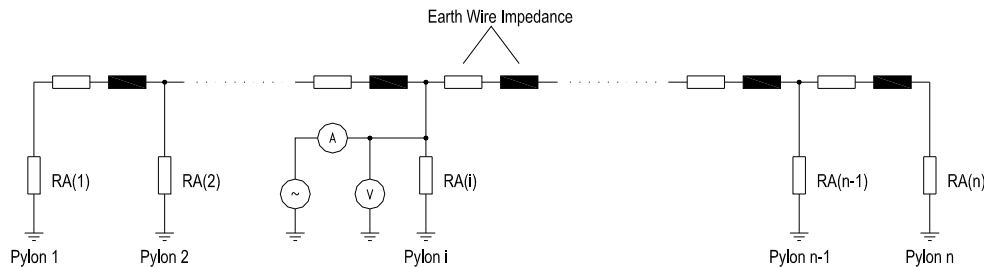


Figure 4-1: Constellation and Measuring of Ladder Network Impedance

If – as shown in Figure 4-1 – a current source is connected to the pylon i and the voltage of the current is measured, the ladder network impedance can be determined with the help of Ohm's law. Its result depends on the frequency and varies from pylon to pylon. Thus each pylon has specific ladder network impedance as well as a specific earth resistance.

4.2 General Information

In order to simulate ladder network impedances the same Simulink model as in chapter 3 has been applied and configured accordingly:

- Physical size of power line (types and numbers of pylons, phase configuration, transposition etc.) according to the existing power line 'TS Wien-Südost' – 'Wiener Neudorf'
- Grounding system resistance $R_A = 0.2\Omega$ for the ground/earth systems of both transformer stations

As the operating currents of the phase wires are of no importance for this research, the high voltage source at the end terminal has been removed from the model and the phase wires have been short-circuited (see Figure 4-2).

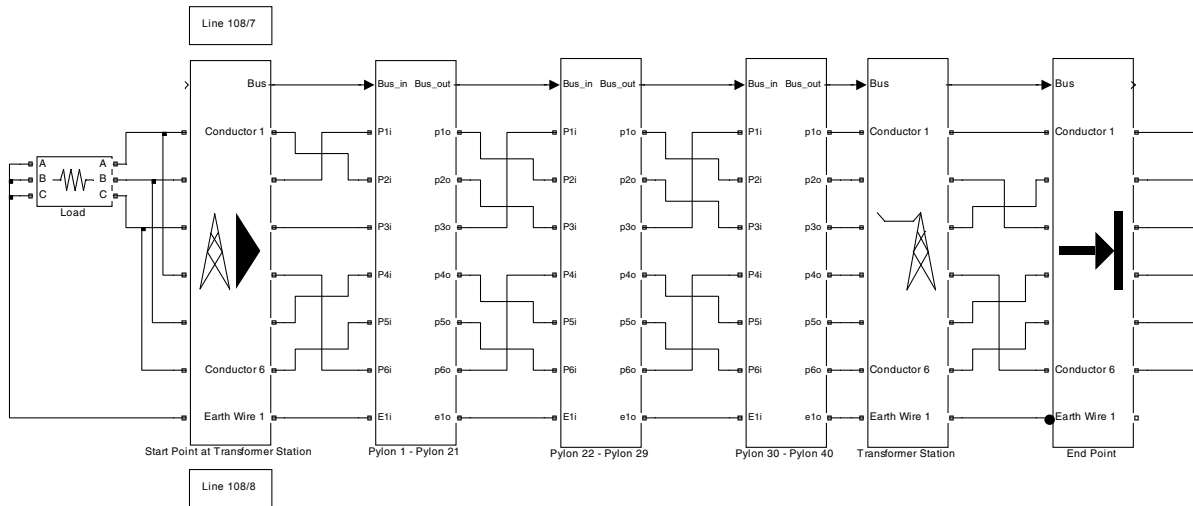


Figure 4-2: Simulink Model for Ladder Network Impedances

At the pylon at which the frequency-dependent ladder network impedance is to be found, a current source with the following configuration is activated:

- Fundamental frequency $f_g = 50\text{Hz}$
- Range: 1st harmonic (50Hz) to 100th harmonic (5000Hz)
- Root-mean-square value of the fundamental harmonic and every single harmonic: 1A

With the help of this method, the ladder network impedance and its frequency-dependence can be established in just one simulation procedure. This is done by applying the fast Fourier transform (FFT) for the respective pylon potential. As each harmonic, which is injected through the current source, has a root-mean-square value of 1A, the root-mean-square values of the pylon potential correspond exactly to those of the ladder network impedance.

$$Z_K(f_i) = \frac{U(f_i)}{I(f_i)} = \frac{U(f_i)}{1A} \quad 4-1$$

The simulation has been carried out several times, during which the following parameters have been varied:

- Pylon at which the current source is applied:
 - pylon 29
 - pylon 32
- Soil resistivity ρ_{soil} :
 - 100Ωm
 - 35Ωm
- Grounding system resistances R_A at each pylon:
 - 1Ω
 - according to the specific conditions in reality
 - R_A of pylon 29 = 0.7Ω
 - R_A of pylon 32 = 0.8Ω

4.3 Results of the Simulations and Comparison with the Results of the Measurements

The following Figures compare the results of the simulations ('Simulink') with the results of the measurements of the Model 6472. Furthermore the ladder network impedance has been determined with the help of a simplified method of calculation using a MATLAB script and is shown as curve 'MATLAB' in the Figures below. This MATLAB script establishes the frequency-dependent admittance matrix of the system. The inverse admittance matrix results in the impedance matrix whose principal diagonal contains the ladder network impedances of all pylons.

4.3.1 Ladder Network Impedances of Pylon 29 of Power Line 108/7 and 108/8

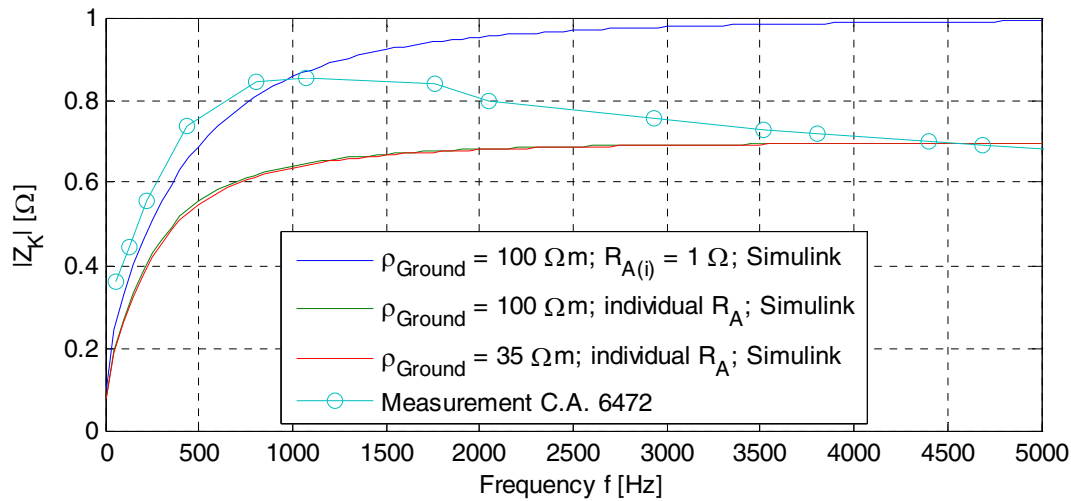


Figure 4-3: Wr. Neudorf - Pylon 29 – Comparison Simulink / Model 6472

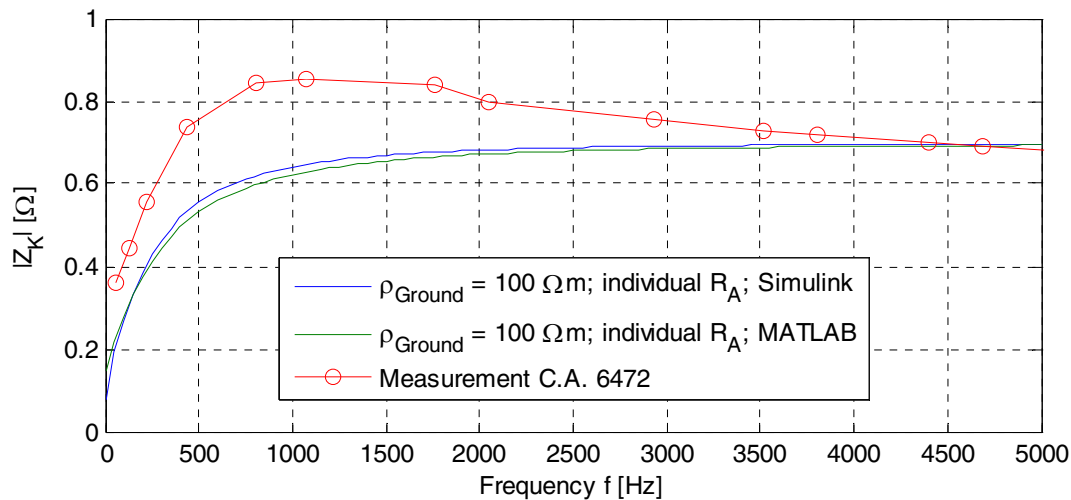


Figure 4-4: Wr. Neudorf - Pylon 29 – Comparison Simulink / Simplified Calculation /Model 6472

4.3.2 Ladder Network Impedance of Pylon 32 of Power Line 108/7 and 108/8

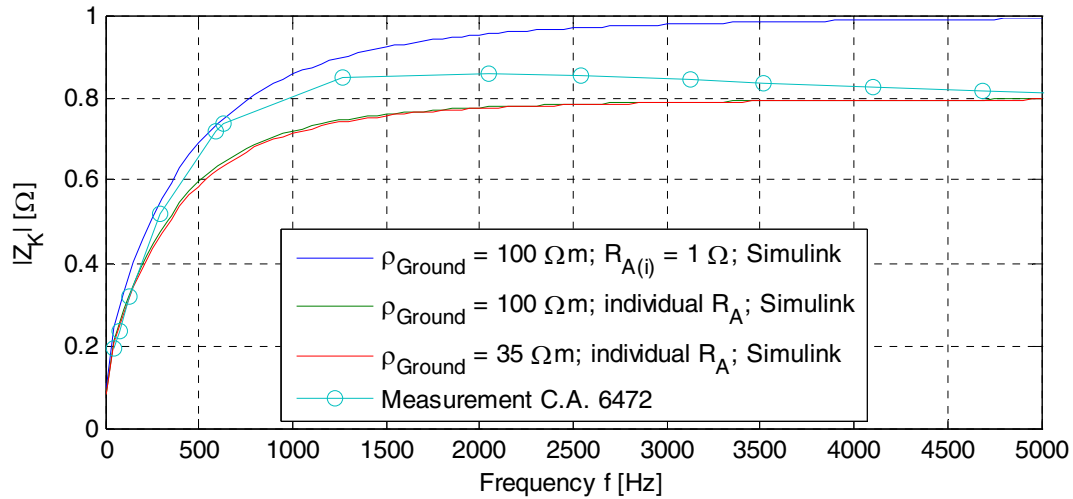


Figure 4-5: Wr. Neudorf – Pylon 32 – Comparison Simulink / Model 6472

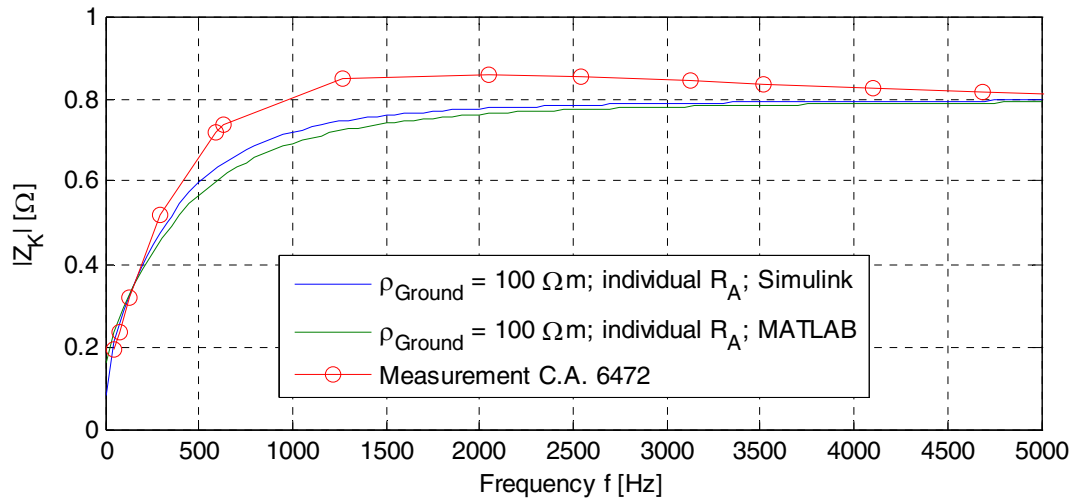


Figure 4-6: Wr. Neudorf – Pylon 32 – Comparison Simulink / Simplified Calculation / Model 6472

The curves of both pylons show clearly how the ladder network impedance – starting from $Z_K = 0.2\Omega$ at 50Hz – converges with increasing frequency towards the value of the grounding system resistance R_A of the pylon. This is due to the inductance of the earth wire which impairs the current flow through the earth wire with increasing frequency. The main part of the injected current takes its way through the pylon ground/earth. A change in the soil resistivity ρ_{soil} is of no importance as the almost identical red and green curves in Figure 4-3 and Figure 4-5 show. In this context it has to be considered that the ground resistance of the pylon has been kept at a constant level. This means that a change in the soil resistivity only results in a change in the coupling impedance of the earth wire. Moreover, it has been proved that the simplified calculation with the help of the admittance matrix already leads to realistic results.

5 Comparative Measurements

In order to compare the results of the measurements of the Model 6472 with the results of other measuring systems, measurements at 110kV power lines on unimproved meadows have been carried out in Wr. Neudorf and in Lieboch near Graz. The ladder network resistance and the grounding system resistance have been measured with the following methods and measuring systems:

5.1 Measuring Methods and Measuring Systems

5.1.1 Soil Resistivity

Based on the Wenner method, the soil resistivity has been measured using the Model 6472 and – in order to be able to compare different results - with the Unilap GEO X.

5.1.2 Ladder Network Impedance

The ladder network impedance equals the grounding system resistance of the pylon in parallel connection with all pylons of the power line system which are connected through the earth wire impedance (see chapter 4).

With the help of the Model 6472, a 4-pole measurement has been carried out in Sweep mode in order to establish the ladder network impedance (see Figure 5-1).

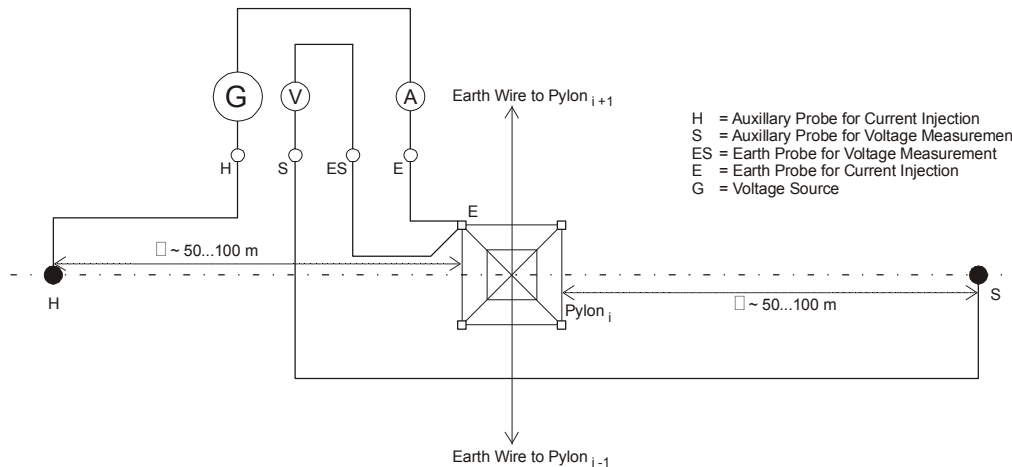


Figure 5-1: Probe Configuration of the 4-Pole Measurement

It remains to be clarified whether the intensity of the testing current influences the results of the measurements. For this purpose, the primary testing system Omicron CPC CU1 has been used for a comparative measurement, as it is able to generate testing currents which are considerably higher than those generated by the Model 6472. With the help of the current and voltage measuring inputs of the CPC, the CPC is able to perform an internal calculation of value and angle of the ladder network impedance at a certain frequency. In order to reach higher frequencies the secondary testing system Omicron CMC has been applied for the range from 400Hz to 1000Hz, which, however, has generated slightly lower currents. In order to cover the range from 1000Hz to 5000Hz as well, square-wave signals have been injected with the help of the Omicron CMC, and the results for each harmonic have been analyzed. The curves of the pylon potentials and of the testing currents of the CPC, as well as those of the CMC have been recorded with a Fluke 199 Scope and a Dewetron 3010. Based on these curves, network ladder impedances can be computed using the FFT.

5.1.3 Grounding System Resistance

The grounding system resistance is the ground resistance of the ground/earth system of a pylon. Thanks to the new procedure of the Model 6472, this can be measured without removing the earth wire or without disconnecting the ground/earth strips from the pylon. Basically there are two different measuring methods: an active measurement and a passive measurement using Rogowski coils (GroundFlex™ Sensors).

5.1.3.1 Passive Measurement

For the passive measurement it is not necessary to generate a measuring signal, as the grounding system resistance can be calculated with the help of the results of the measurement of the pylon potential and the ground current of the pylon which is induced in normal operation (see chapter 3). In that case the pylon ground current is measured with the help of four Rogowski coils which are attached to the pylon footings. The pylon potential is measured between the pylon and a point in a distance of about 50m to 100m perpendicular to the route of the power line.

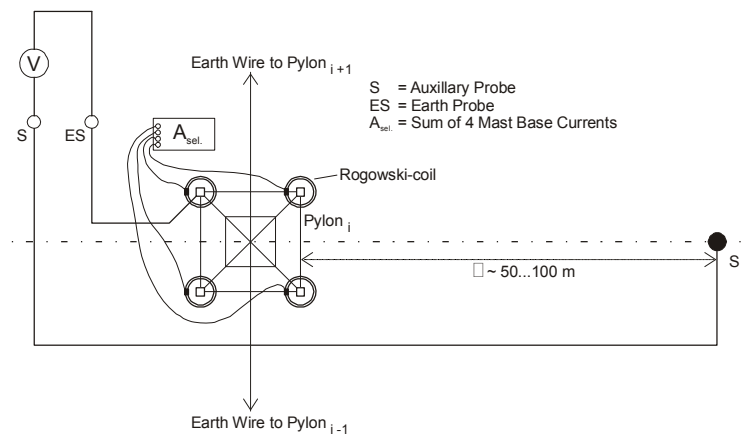


Figure 5-2: Probe Configuration of the Passive Measurement

For this purpose the Model 6472 has been applied in combination with the GroundFlex™ Adapter Model 6474 in order to carry out a GroundFlex™ measurement in which the value of the grounding system resistance resulting from the passive measurement is stored inside the Model 6472.

For the comparative measurement, four LEM-Flex RR3020 Rogowski coils have been used. The curve of the signals of the ground current of the pylon as well as the pylon potential have been recorded with a Fluke 199 Scope and a Dewetron 3010. Based on the curves of these signals the earth resistance of the pylons can be calculated for the fundamental harmonic and some other harmonics using the FFT.

5.1.3.2 Active Measurement (GroundFlex™ Measurement)

In contrast to the passive measurement, the active measurement generates a signal and thus requires an auxiliary ground/earth rod H, at which the measuring signal can be injected (Figure 5-3). This measuring signal is generated within the Model 6472 and can range from 40Hz to 5000Hz. In this case the ground current, which is selectively measured with the help of four Rogowski coils (GroundFlex™ Sensors), is amplified by the GroundFlex™ Adapter Model 6474 and led to the Model 6472. Thus it is possible to measure the grounding system resistance without removing the earth wire.

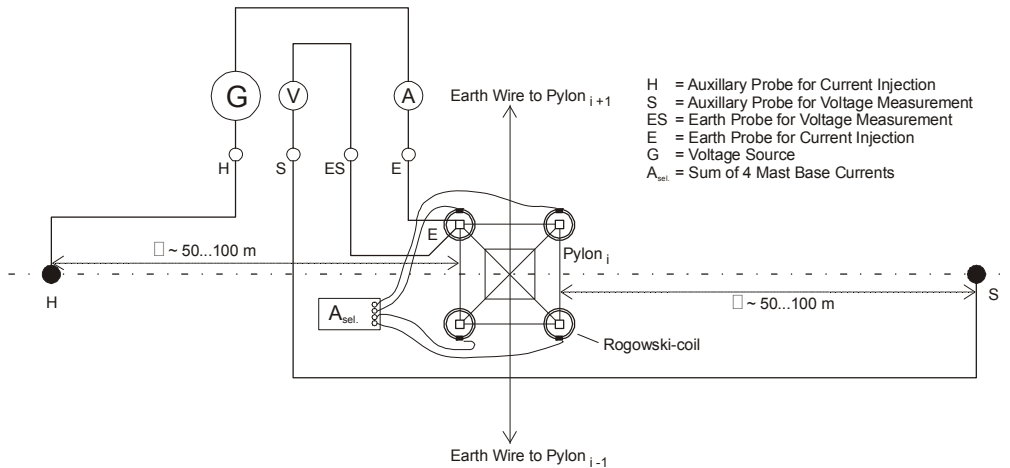


Figure 5-3: Probe Configuration of the GroundFlex™ Measurement

For the comparative measurement, the same systems have been used as for measuring ladder network impedances. For this purpose, however, the current has been measured selectively with the help of four LEM-Flex RR3020 Rogowski coils which have been attached to the footings of the pylon. The series connection of the output signals of all four Rogowski coils equals an addition of the current vectors of all four pylon footing currents, whereas the total amount of this addition equals the ground current.

5.1.4 Relative Errors of Measuring Systems using Rogowski coils

Before the start of the measurements, the relative errors of the GroundFlex™ Adapter with the Model 6472 and those of the Dewetron with the LEM-Flex RR3020 were calculated under laboratory conditions. For this purpose 1A and 0.2A, respectively, were generated at a frequency ranging from 128Hz and 317Hz with the help of a Yokogawa referential source. Each of these currents was led through four Rogowski coils, and the total amount of the addition of the respective four Rogowski coils was analysed. The results are shown in Table 5-1, with the relative error relating to the desired value (I_{Soll}) of 4A or 0.8A.

I_{Soll}	f	Dewetron & LEM-Flex	Model 6472 with Model 6474
		rel. error	rel. error
A	Hz	%	%
4	128	-0.75	-0.32
0.8	128	-0.88	-0.75
4	317	-0.72	-0.50
0.8	317	-1.00	-0.75

Table 5-1: Measurement Errors of Measuring Systems with Rogowski Coils

5.2 Measurements in Lieboch Concerning Power Line 130/7 and 130/8B

5.2.1 Soil Resistivity ρ

In order to be able to recalculate the results of the measurements at pylon 37 in Lieboch, the stratification of the soil resistivity in the vicinity of the pylon has been measured.

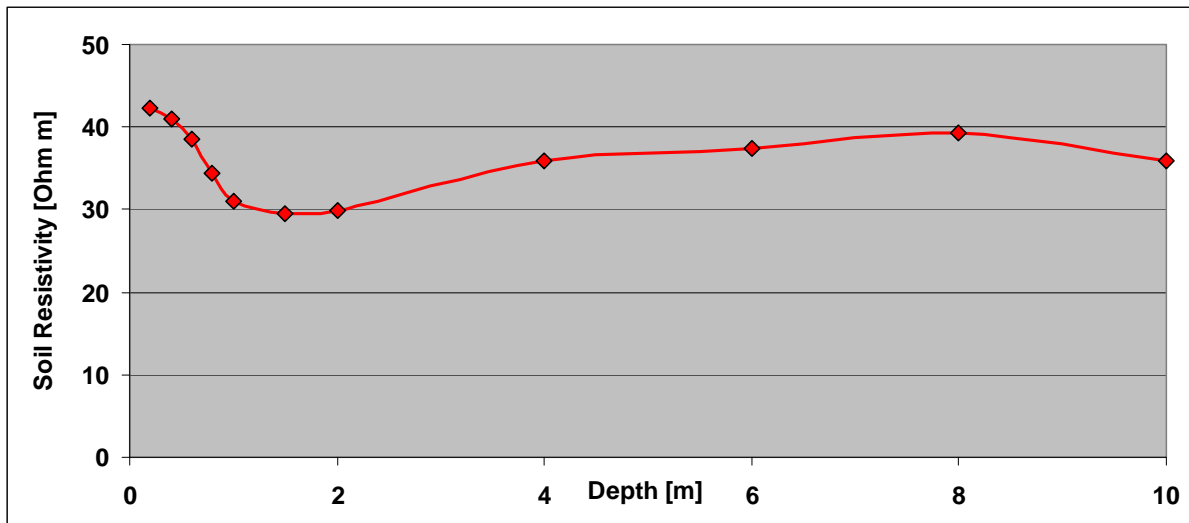


Figure 5-4: Soil Resistivity at Pylon 37 of the 110kV Power Line in Lieboch

5.2.2 Grounding System Resistance R_A Determined by Active Measurement

In order to find out whether the intensity of the testing current influences the result of the measurement, and whether different measuring systems lead to the same results, comparative measurements have been carried out at a 110kV pylon using testing currents up to 2.5A. This comparative measurement of the grounding system resistance R_A has been carried out with the help of a frequency-selective measurement using different measuring systems and sources:

- (1) GroundFlex™ measurement with the Models 6472 & 6474
- (2) Source Model 6472 and measuring system Dewetron 3010
- (3) Source Omicron CPC CU1 & CMC and measuring system Dewetron 3010
- (4) Source Omicron CPC CU1 & CMC and measuring system Fluke 199 Scope

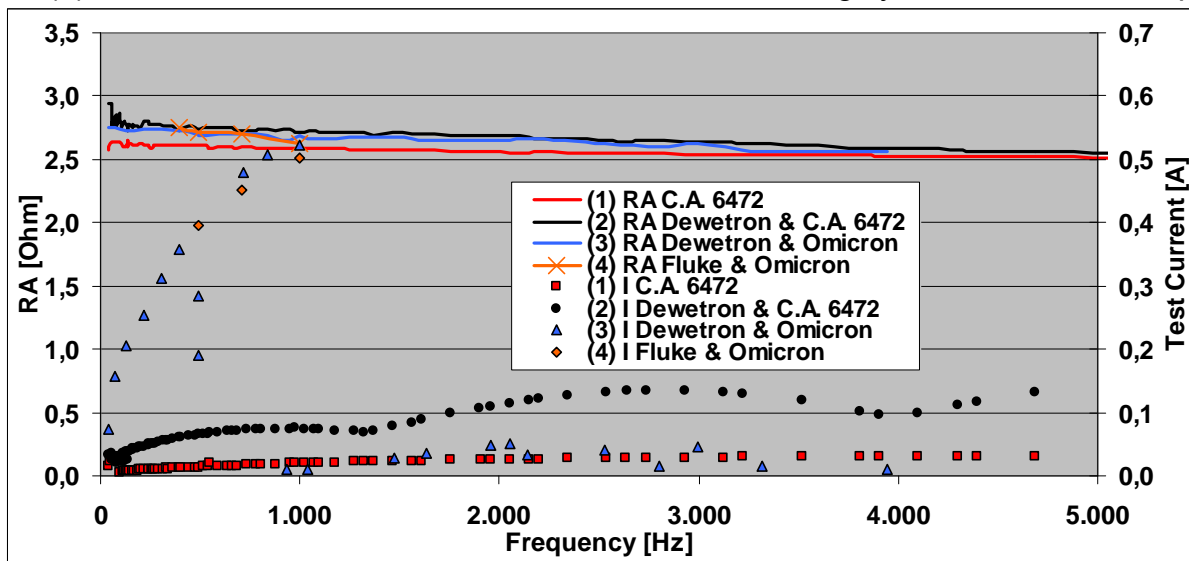


Figure 5-5: Grounding System Resistance and Testing Currents at Pylon 37 in Lieboch

The curves in Figure 5-5, which indicate the frequency-dependent course of the grounding system resistance R_A , show that all measuring systems lead to similar results. The deviations of the measurements in the lower frequency range (40Hz to 350Hz) are due to an interference of the power line grid. The most significant deviations occur close to 50Hz and the first 7 harmonics of 50Hz.

Thus it becomes obvious that the amplitude of the testing current (see points in Figure 5-5) does not influence the result of the measurement. The selected frequencies, however, should not be too close to 50Hz and its harmonics, whereas the pre-selected frequencies of {61, 180, 220, 439, 806, 1074, 1758, 2051, 2930, 3516, 3809, 4395, 4688, and 5078} Hz of the Model 6472 have been very helpful in this respect.

5.2.3 Grounding System Resistance R_A Determined by Passive Measuring

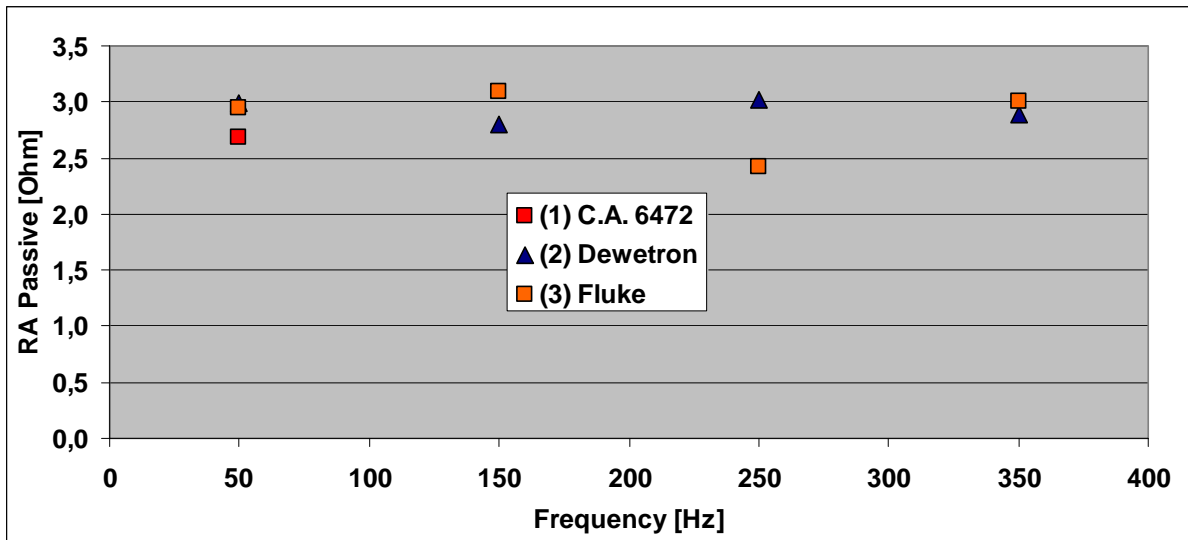


Figure 5-6: R_A Determined by Passive Measurement at Pylon 37 in Lieboch

For the passive measurement, the Model 6472 selects the current with the highest frequency which occurs in the range from 40Hz to 450Hz and calculates the passive resistance in this frequency range. For this measurement, the dominant frequency of course was the fundamental frequency of the power line of 50Hz, so that a result can only be found within this range. In study of the comparative measurements, the resistance in a narrow frequency band around the fundamental harmonic and the first three odd harmonics have been analyzed. The results of these measurements also match quite well.

The calculation with OBEIN for homogenous soil and a soil resistivity of $35\Omega\text{m}$ resulted in a grounding system resistance of 2.42Ω . The result of this calculation also comes close to the grounding system resistances which have been actually measured.

5.2.4 Ladder Network Impedance

For the comparative measurement of the ladder network impedance Z_K the following measuring systems have been applied:

- (1) 4-pole measurement with Model 6472
- (2) Impedance measurement with Omicron CPC CU1
- (3) Source Omicron CPC CU1 & CMC and measuring system Dewetron 3010

The Model 6472 has used a testing current of 0.19A. For measurement (2) and measurement (3) a testing current of 5A has been used for the frequency range from 40Hz to 400Hz, whereas a testing current of 1A has been applied for the frequency range from 400Hz to 1000Hz. In the range from 1000Hz to 4000Hz, harmonics of square-wave signals with a fundamental harmonic which is about 1000Hz and with amplitude of about 0.4A have been analyzed with the help of FFT.

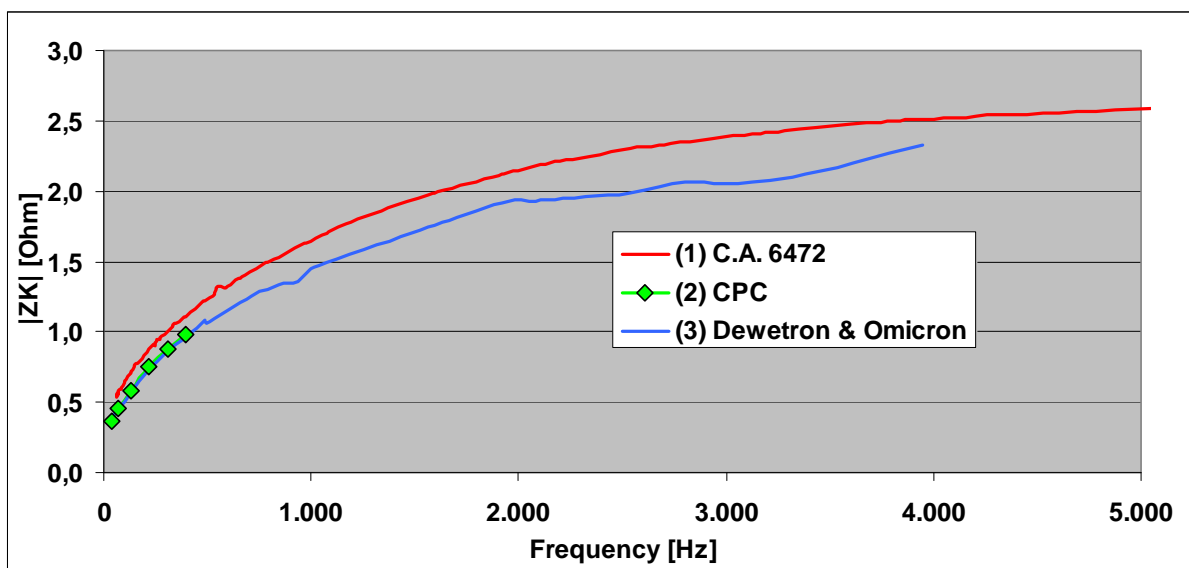


Figure 5-7: Ladder Network Impedance at Pylon 37 in Lieboch

The results of the measurements performed with the Model 6472 (1) show values which are slightly higher than those which have been determined with the help of Omicron CPC (2) and Dewetron (3). The reason for these differences could not be found. Still, the results of the Model 6472 concerning the evaluation of ground/earth systems can be considered safe.

5.2.5 Grounding System Resistance and Ladder Network Impedance

In Figure 5-8, the grounding system resistance R_A and the ladder network impedance Z_K are shown in dependence on the frequency. Thus, it becomes obvious that it is possible to determine the grounding system resistance in a higher frequency range with the help of a 4-pole measurement. It shows that the impedance of the earth wire (overhead ground conductor), which connects the neighboring pylon ground/earth systems in parallel to the earth resistance of the pylon which is to be determined, gets so high-resistance for higher frequencies that it does not influence the measurement result.

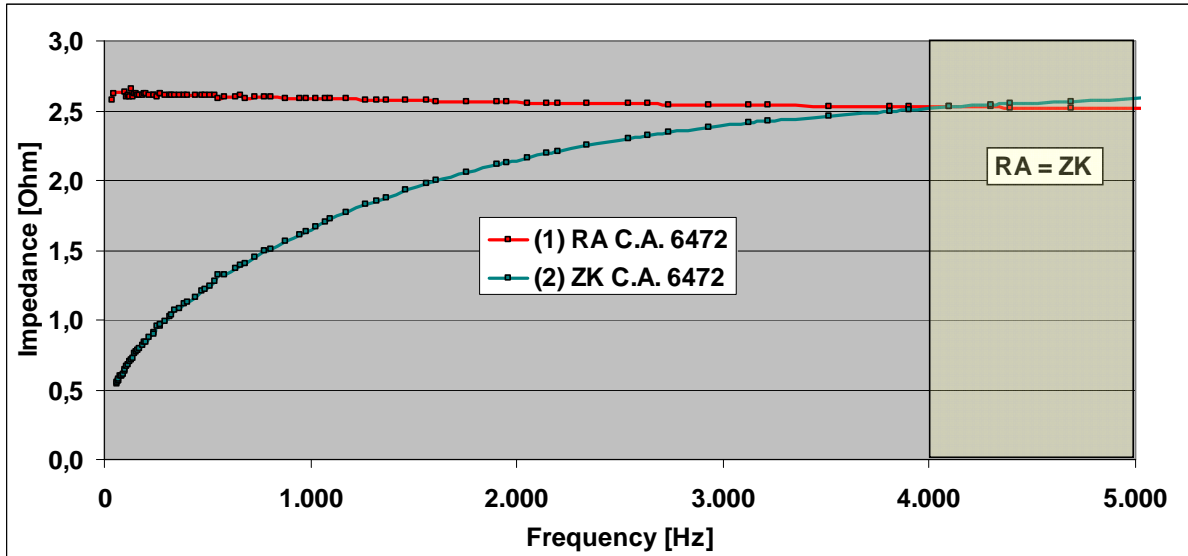


Figure 5-8: Comparison of RA and ZK at Pylon 37 in Lieboch

The fact that the ladder network impedance equals the grounding system resistance of the pylon at high frequencies means that in case of lightning strike – which has to be considered as high-resistance – only the grounding system resistance of the pylon contributes to the percentage of the current of the lightning which flows towards earth.

5.2.6 Grounding System Resistances of Several Pylons (Active Measurement)

During the comparative measurements at pylon 37 in Lieboch, the grounding system resistances of several neighboring pylons have been determined by active and passive measurements with the Model 6472.

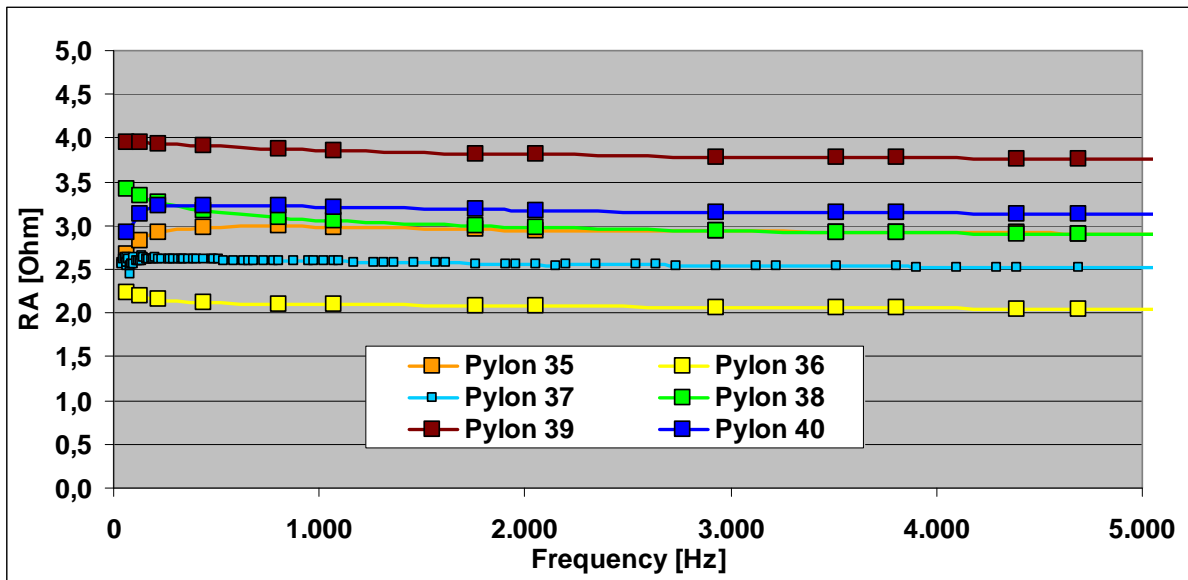


Figure 5-9: Grounding System Resistance at Pylons 35 to 40 in Lieboch

The most striking results are the varying frequency-dependences in the lower frequency range. The exact causes of this phenomenon, however, have not been found out yet. A possible reason for the frequency-dependent increase of the grounding system resistances at pylon 35 and pylon 40 could be the fact that the probes did not reach neutral earth, and that the difference in measuring frequencies caused a difference in the penetration depth of the testing current so that the stratification of the soil also has to be considered.

5.2.7 Grounding System Resistance of Several Pylons (Passive Measurement)

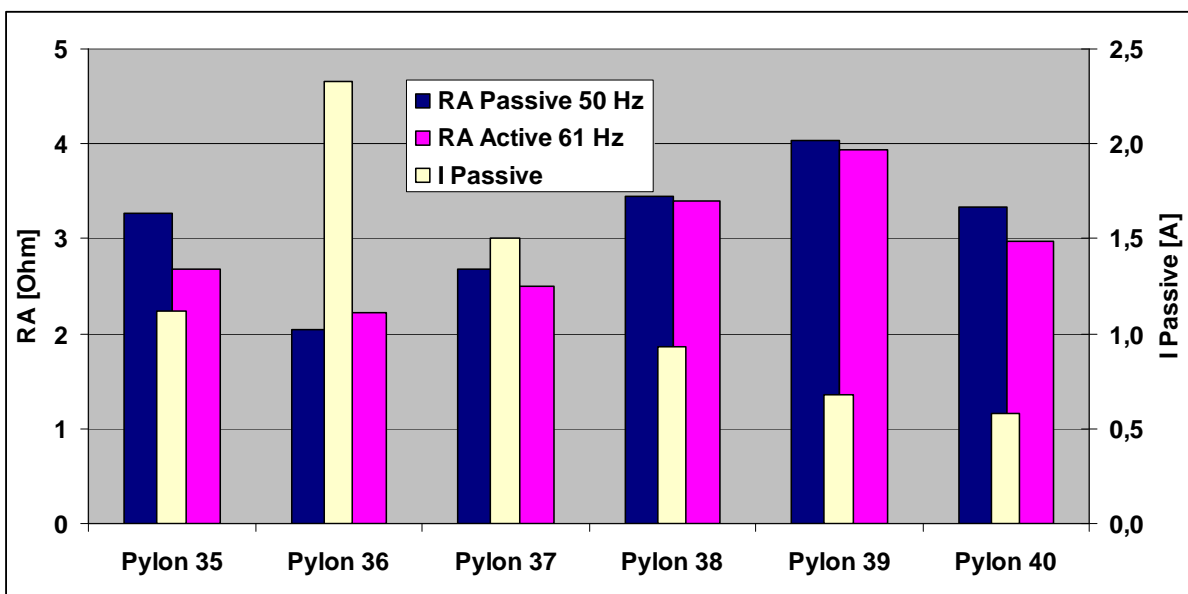


Figure 5-10: Grounding System Resistance and Passive Ground Currents in Lieboch

5.2.8 Pictures Illustrating the Measuring Setup at Pylon 40

The following two pictures illustrate the measuring setup for the measurement at pylon 40 as it is explained in 5.2.6 and 5.2.7.



Figure 5-11: Alignment of the Four GroundFlex™ Sensors



Figure 5-12: A GroundFlex™ Sensor around a Pylon Footing (Multiple Turns)

5.3 Measurements in Wr. Neudorf

In Figure 5-13 and Figure 5-14 all measurements concerning the 110kV power line 108/7 and 108/8 in Wr. Neudorf are compared. It can be seen that the results of the measurements are largely in accordance.

Only the values which were measured by the network provider some time ago differ slightly from the present results. This could be due to a difference in soil humidity at the time when the respective measurements were carried out. As explained in 5.2.5, it shows again that the influence of the earth wire can be neglected for higher frequencies. The results of the selective GroundFlex™ measurement (R_A), and those of the 4-pole measurement (Z_K) are almost identical starting from about 2kHz. The earth wire inductance is about 0.5mH to 1mH for most of the spans. That is why the frequency at which the value of the grounding system resistance approaches that of the ladder network impedance depends on the amount of the grounding system resistance. For higher values of the grounding system resistance it takes higher frequencies to make the influence of the earth wire negligible.

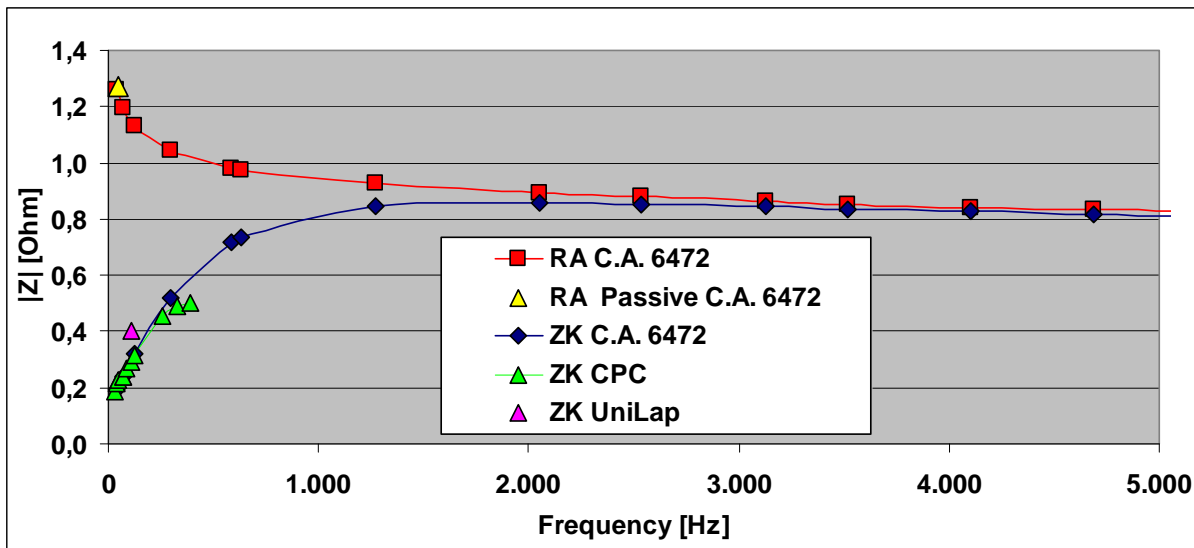


Figure 5-13: Measurements at Pylon 32 in Wr. Neudorf

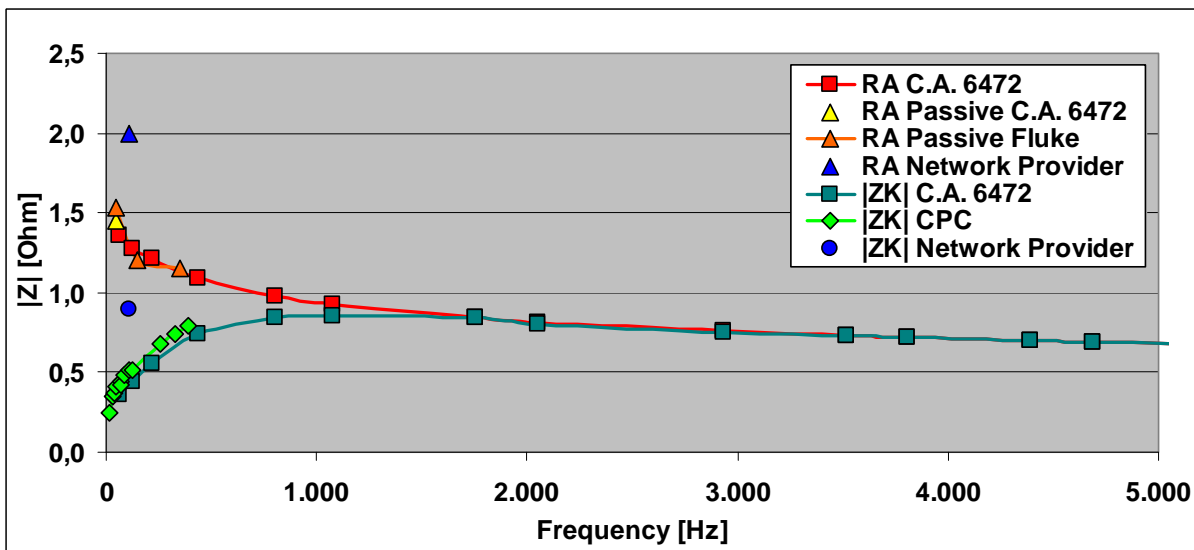


Figure 5-14: Measurements at Pylon 29 Wr. Neudorf

5.3 Measurements in an Unimproved Meadow

As the measurements at pylons have shown unusual frequency-dependences of the grounding system resistance, more experiments have been carried out in unimproved meadows with different soil structures.

5.3.1 Measurements in Highly Conductive Soil

In an unimproved meadow, 25 ground/earth rods have been driven into the soil at a depth of about 30cm and have been connected in a highly conductive way as shown in Figure 5-15.

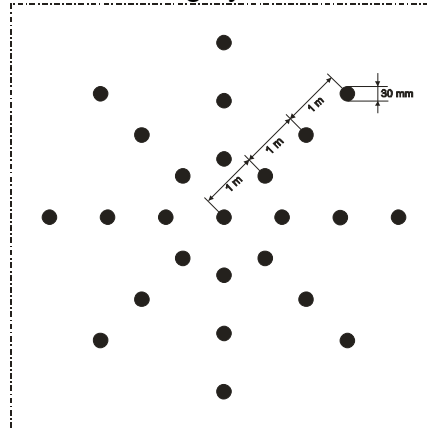


Figure 5-15: Physical Size of the Ground/Earth System

5.3.1.1 Soil Resistivity ρ

In order to carry out a comparative measurement with OBEIN, the soil resistivity has been measured with the Model 6472 as well. For this measurement, an additional comparative measurement has been carried out using a Norma Unilap GEO X. As can be seen in Figure 5-16, both measurements produced almost identical results.

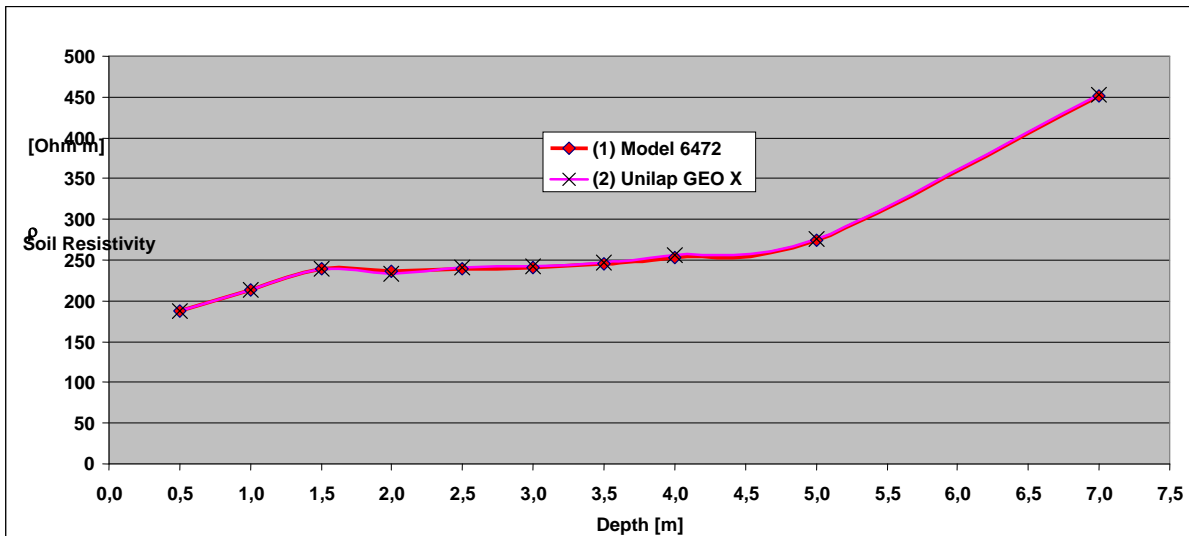


Figure 5-16: Soil Resistivity ρ of a Highly Conductive Soil

Based on this soil structure, the grounding system resistance has been calculated with OBEIN in 2-layered soil. For the first layer, a soil resistivity ρ of 250 Ohm·m has been chosen up to a depth of 7m, whereas a soil resistivity ρ of 500 Ohm·m has been assumed for the deeper layers. The calculation with OBEIN resulted in a soil resistivity of 42.4 Ohm.

5.3.1.2 Grounding System Resistance

The grounding system resistance of the ground/earth system shown in Figure 5-15 has been determined by two different measuring systems. For measurement (1) and (3), a 4-pole measurement with the Model 6472 has been carried out, whereas for measurement (2) the Omicron CPC CU1 has been applied. It can easily be seen that the measurement in this unimproved meadow does not show any frequency-dependence. In order to find out whether the amount of the testing current influences the contact resistance of the newly applied ground/earth rods, a first measurement has been carried out with the Model 6472 and a testing current of 0.2A, followed by a second measurement with the Omicron and a testing current of 2A to 4.5A and a final measurement again with the Model 6472 and a testing current of 0.2A. As Figure 5-17 shows in none of these measurements has the respective result been influenced by the amount of the testing current.

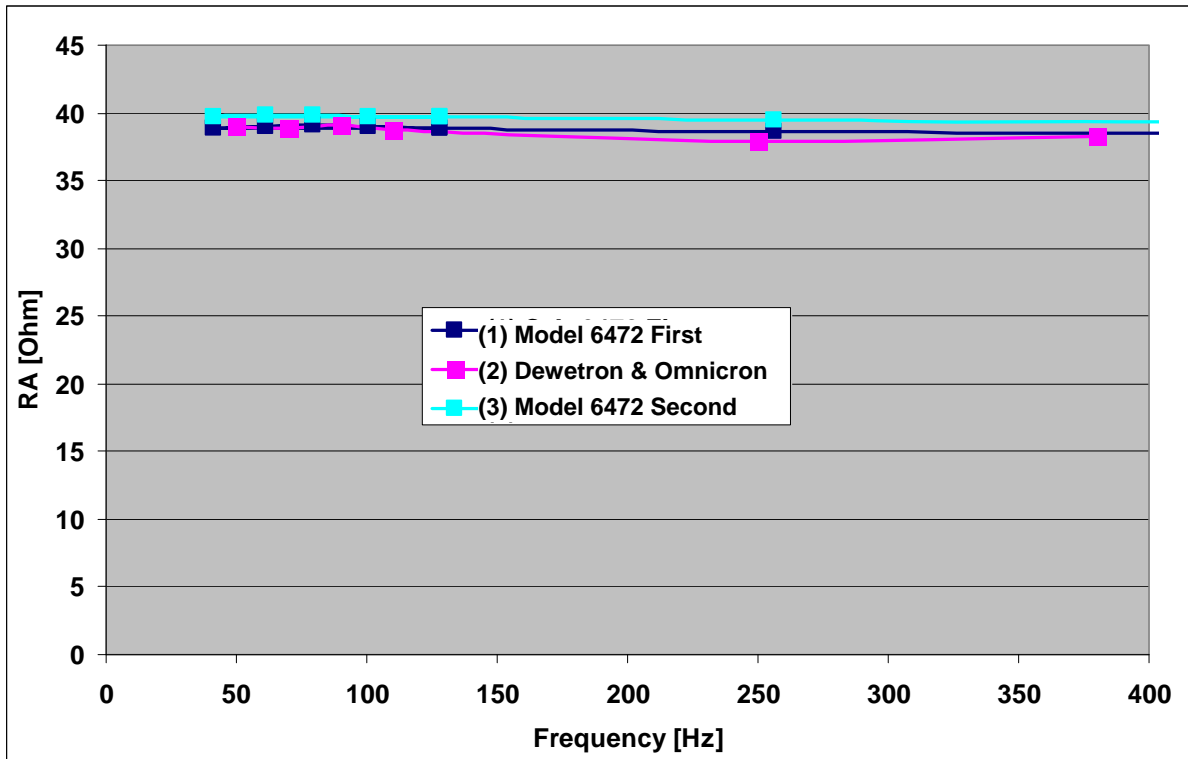


Figure 5-17: Grounding System Resistances of the Ground/Earth System in Highly Conductive Soil

The results of all measurements again are almost identical and are also very close to the result of the OBEIN calculation, which has resulted in a grounding system resistance of 42.4Ω.

5.3.2 Measurements in Low Conductive Soil

In an unimproved meadow with low conductivity, four ground/earth rods have been driven into the soil at a depth of about 30cm and have been connected in a highly conductive way as shown in Figure 5-18.

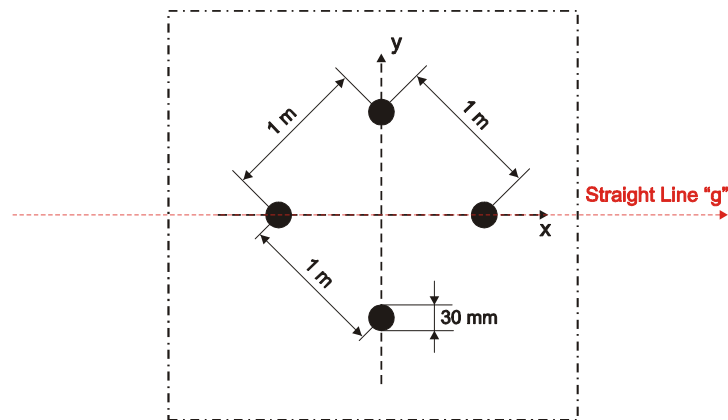


Figure 5-18: Physical Size of the Ground/Earth System

5.3.2.1 Soil Resistivity ρ

The soil resistivity, which is shown in Figure 5-19, has been determined with the Model 6472 according to the Wenner method. This Figure shows that in this case the soil is definitely less conductive than that in chapter 5.3.1.

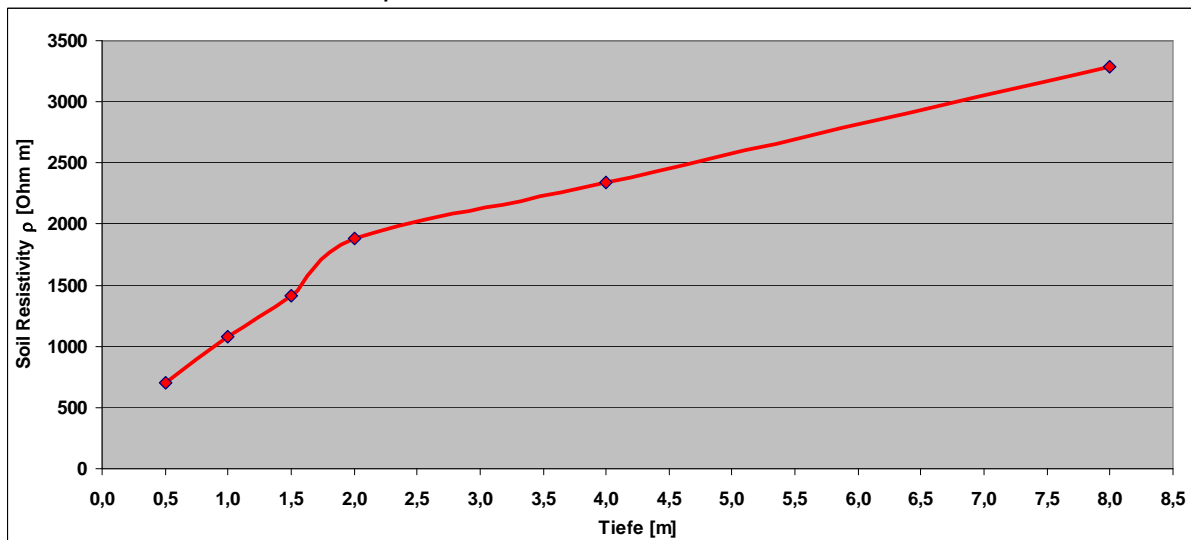


Figure 5-19: Soil Resistivity ρ of Lowly Conductive Soil

As the OBEIN calculation concerning the ground/earth system can only be applied for two different layers, the following soil resistivities have been used: Up to a depth of 2 meters, the soil resistivity has been considered to be $1000\Omega\text{m}$ and beyond that depth $3000\Omega\text{m}$. Due to these assumptions, the calculation with OBEIN results in a grounding system resistance R_A of 630Ω .

5.3.2.2 Grounding System Resistance

The study of the grounding system resistance shown in Figure 5-20 has been measured with the Model 6472. The values which have been measured for the grounding system resistance correspond to those which have been produced by the OBEIN calculation.

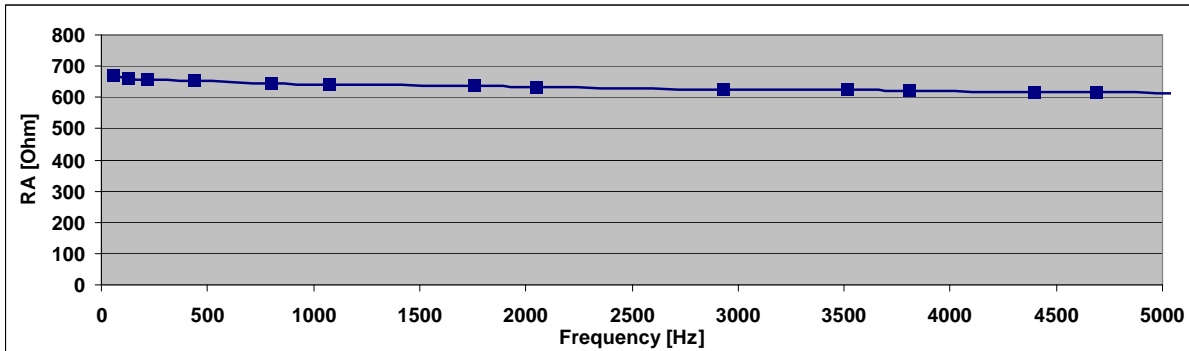


Figure 5-20: Grounding System Resistance of the Ground/Earth System in Lowly Conductive Soil

Even if the ground/earth system is applied in lowly conductive soil there is hardly any frequency-dependence of the grounding system resistance R_A in the frequency range of 50Hz to 5000Hz.

5.3.2.3 Comparison of the Results of Measurements and Calculations of the Ground Potential Rise

As OBEIN can also show the curve of the ground potential rise, the ground potential rise at this ground/earth system has been measured with the Model 6472, and contrasted with the values resulting from the OBEIN calculation as shown in Figure 5-21.

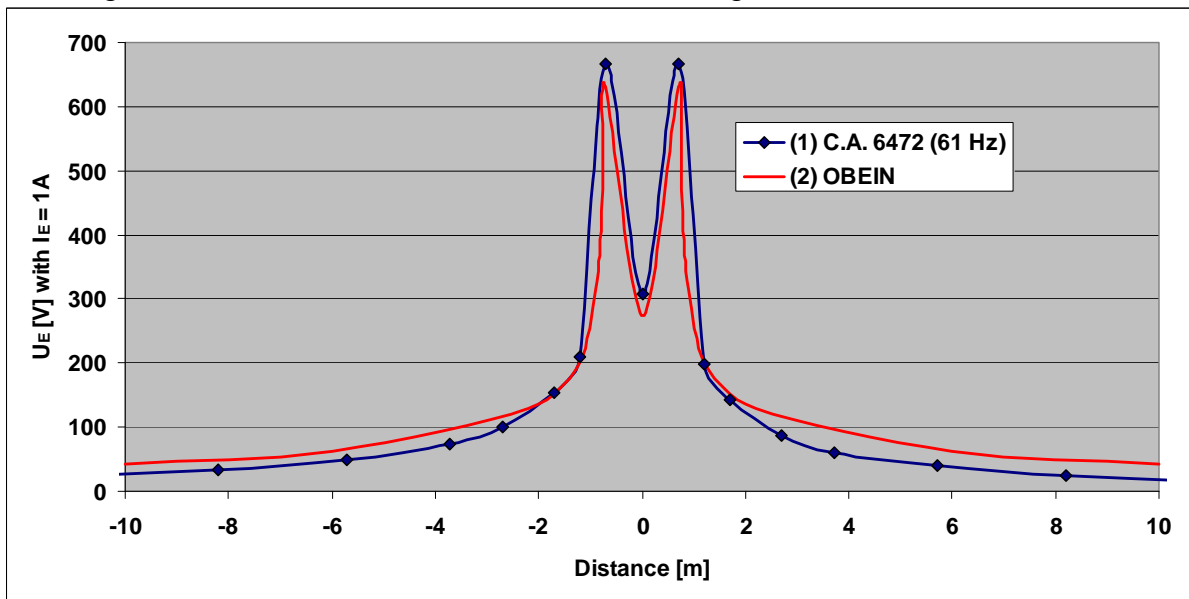


Figure 5-21: Measurement and Calculation of Ground Potential Rise along the Straight Line g

The earth potential U_E occurs between the points along the straight line g (Figure 5-18) and neutral earth, if a current of exactly 1A flows into the ground/earth system. As can be seen here, the results of the measurements and the calculation of the ground potential rise are almost identical.

6 Influences on Rogowski Coils

Measuring the impedance at ground/earth systems of power lines can be carried out as a current and voltage measurement. If the current is measured with the help of Rogowski coils (GroundFlex™ Sensors), the results may be influenced by magnetic fields of current-carrying conductors (e.g. phase wires, earth wires, the steel lattice of the pylon etc.) in the immediate vicinity. This may result in measuring errors which could cause mismeasurements. One purpose of this research has been to find out how the interfering fields mentioned above influence the measuring of currents with Rogowski coils.

Suggestions for further analyses, as well as for possible solutions of the respective problems are contained in the following chapter.

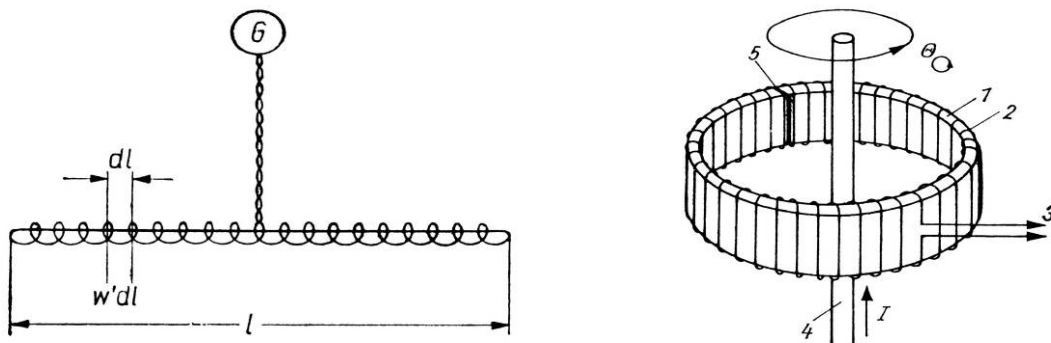
6.1 Basics

6.1.1 Construction

The Rogowski coil (GroundFlex™ Sensor) is a testing coil whose winding is wrapped around a long and flexible core. The diameter of the respective windings is comparatively small in contrast to the length of the coil.

Usually the coil can be opened so that it can be placed around a current-carrying conductor. This way the current in a conductor can be measured without any interruption.

In order to make sure that the measurements will not influence the respective magnetic field which is to be measured, the core consists of non-magnetic material like plastic or rubber.



a) Open Coil (according to equation 6-1) b) Closed Coil (acc. to equation 6-2)

Figure 6-1: Rogowski Coil - Construction

Legend to Figure 6-1 (b):

- 1..... core (flexible)
- 2..... winding
- 3..... terminal points
- 4..... current-carrying conductor
- 5..... end of coil (butt joint)

Further information concerning the alignment of the winding (on the core) and its physical size can be found in the respective technical literature [7].

6.1.2 Mode of Operation

The original way of applying Rogowski coils was to measure magnetomotive force between two user-defined points within a magnetic field, i.e. the line integral of the magnetic field strength (see Figure 6-2 and Figure 6-1a). For this reason, Rogowski coils are also referred to as magnetomotive force meters.

For all of the line integral applies:

$$\int_1^2 \vec{H} \circ d\vec{l} = U_{m_{12}} \tag{6-1}$$

6-1

\vec{H} Magnetic field strength

$d\vec{l}$ differential line element

$U_{m_{12}}$ Magnetomotive force between (points) 1 and 2

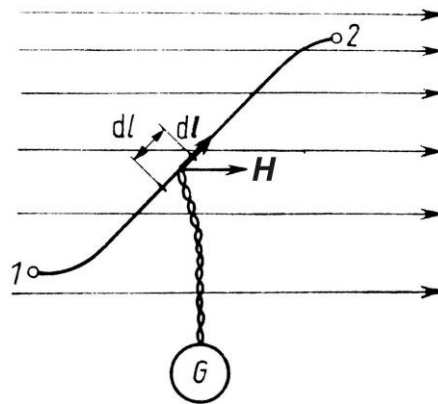


Figure 6-2: Determination of the Line Integral (according to equation 6-2)

In case that both (points) 1 and 2 coincide and thus produce a closed line integral (See 6-1 as well as Figure 6-1 b), the following equation applies:

$$\int_1^2 \vec{H} \circ d\vec{l} = U_{m_{12}} = \oint \vec{H} \circ d\vec{l} = \Theta = \sum_n I_n \tag{6-2}$$

6-2

Θ magnetomotive force of the closed line integral
 (= magnetomotive force along the closed circuit)

I_n All electrical currents linked with the closed line integral
 (For the summation the direction of the current has to be taken into consideration)

Equation 6-2 is also referred to as Ampere's law.

Equation 6-2 also shows that the Rogowski coil can be used to measure currents without interrupting the current-carrying conductor.

The electrical measuring signal at the terminals of the Rogowski coil is the voltage which is induced into the coil.

Considering the 2nd Maxwell equation (2nd field equation, see 6-3) and applying Stokes's theorem for the voltage $u_q(t)$, which is induced into a single winding, the following equation applies, provided that the Rogowski coil is not moved in the magnetic field:

$$\text{rot } \vec{E} = -\frac{\partial \vec{B}}{\partial t} \tag{6-3}$$

\vec{E} Electrical field strength

\vec{B} Magnetic flux density

t..... Time

$$\iint_A \text{rot } \vec{E} \circ d\vec{A} = -\iint_A \frac{\partial \vec{B}}{\partial t} \circ d\vec{A} = -\frac{\partial}{\partial t} \left(\iint_A \vec{B} \circ d\vec{A} \right) = -\frac{\partial \Phi}{\partial t} = \oint_L \vec{E} \circ d\vec{s} = u_q(t) \tag{6-4}$$

A Plane penetrated by magnetic flux
 (= cross sectional area of the winding)

Φ Magnetic flux interlinked with the winding

L..... Marginal curve of plane A (= marginal curve of the winding)

$u_q(t)$ Voltage induced into the winding

According to equation 6-4 the flux of the magnetic induction Φ can be expressed like that:

$$\Phi = \iint_A \vec{B} \circ d\vec{A} = \iint_A |\vec{B}| \cdot |d\vec{A}| \cdot \cos \alpha = \cos \alpha \cdot \iint_A B \cdot dA \tag{6-5}$$

\vec{B} Vector of the magnetic flux density

$d\vec{A}$ Vector of the differential planar element (perpendicular to plane A)

α Angle between the vectors \vec{B} and $d\vec{A}$ ($0 \leq \alpha \leq \pi$)

If – as mentioned above (see chapter 6.1.1) - the diameters and consequently the cross sectional areas of the windings are very small, the plane penetrated by the magnetic flux density can be defined as:

$$B = |\vec{B}| = \text{const.} \tag{6-6}$$

Thus the equation 6-5 is simplified as:

$$\Phi = B \cdot A \cdot \cos \alpha \tag{6-7}$$

For the induced voltage per winding (see equation 6-4) this means:

$$u_q(t) = -\frac{\partial \Phi(t)}{\partial t} = -\frac{\partial B(t)}{\partial t} \cdot A \cdot \cos \alpha \quad 6-8$$

For homogeneous magnetic fields, equation 6-8 represents the exact solution. For inhomogeneous magnetic fields, it is a more or less close approximation, depending on the degree of their inhomogeneity.

Equation 6-8 can also be expressed like that:

$$u_q(t) = -A \cdot \frac{\partial (B(t) \cdot \cos \alpha)}{\partial t} = -A \cdot \frac{\partial B_N(t)}{\partial t} = -A \cdot \frac{dB_N(t)}{dt} \quad 6-9$$

In this case, $B_N(t)$ is the part of the magnetic flux density \vec{B} , which penetrates plane A in a perpendicular way ($\alpha = 0^\circ$), and can also be referred to as effective flux density.

Another way of expressing equation 6-8 is:

$$u_q(t) = -A \cdot \cos \alpha \cdot \frac{\partial B(t)}{\partial t} = -A_N \cdot \frac{\partial B(t)}{\partial t} = -A_N \cdot \frac{dB(t)}{dt} \quad 6-10$$

with A_N being the so-called effective plane.

6.2 Current Measuring

6.2.1 Principle

In the vicinity of current-carrying conductors there is a quantitative relationship between the current in the conductor (as a cause for the interlinked magnetic field) and the magnetic flux density (as a consequence of the interlinked current).

When analyzing, for example, a very (infinitely) long straight conductor, the following applies for the total amount of the magnetic flux density in its vicinity:

$$B = |\vec{B}| = \mu \cdot |\vec{H}| = \mu \cdot H = \mu_0 \cdot \mu_r \cdot H = \mu_0 \cdot \mu_r \cdot \frac{I}{2\pi \cdot r} \quad 6-11$$

B total amount of the magnetic flux density \vec{B}

H total amount of the magnetic field strength \vec{H}

μ absolute permeability

μ_0 permeability of the vacuum (magnetic field constant, induction constant)

μ_r relative permeability (permeability number)

I current in the conductor

r distance from the centre of the conductor

If the result of equation 6-11 is substituted into equation 6-8, this results in:

$$u_q(t) = -\frac{\partial \Phi(t)}{\partial t} = -\frac{\mu_0 \cdot \mu_r \cdot A \cdot \cos \alpha}{2\pi \cdot r} \cdot \frac{\partial i(t)}{\partial t} = k \cdot \frac{\partial i(t)}{\partial t} = k \cdot \frac{di(t)}{dt} \quad 6-12$$

k constant (for 1 winding)

For measuring electrical currents in conductors this means:

According to equation 6-12, the induced voltage at the clamps of the Rogowski coil depends on the temporal course of the current $i(t)$ in the conductor.

If the winding of the Rogowski coil consists of a total of N windings, the total of the induced voltage $u_{q-ges}(t)$ can be expressed as:

$$u_{q-ges}(t) = N \cdot k \cdot \frac{di(t)}{dt} = K \cdot \frac{di(t)}{dt} = M \cdot \frac{di(t)}{dt} \quad 6-13$$

N number of windings ($N \in \mathbb{N}$)

K coil constant (see also [5] and [6])

M mutual inductance between conductor and Rogowski coil ($M = K$!)

Thus the current $i(t)$ can be calculated as follows:

$$i(t) = \frac{1}{K} \cdot \int u_{q-ges}(t) \cdot dt \quad 6-14$$

The integration in equation 6-14 can be performed with the help of analogue computation. This is done with the help of so-called integrators like e.g. an operational amplifier which is wired-up as reverse integrator (see Figure 6-3).

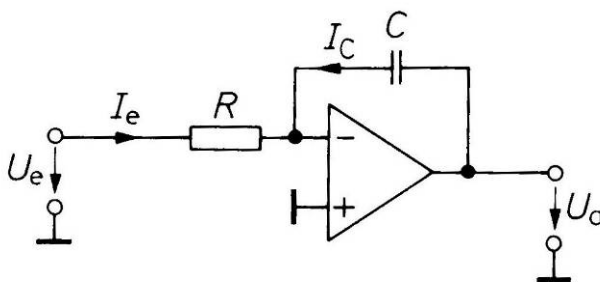


Figure 6-3: Reverse Integrator (according to [9])

According to [9] the output voltage of the reverse integrator (Figure 6-3) can be described as:

$$u_a(T) = -\frac{1}{R \cdot C} \cdot \int_0^T u_e(t) \cdot dt + u_a(0) = -\frac{1}{\tau} \cdot \int_0^T u_e(t) \cdot dt + u_a(0) \quad 6-15$$

τ integration time constant ($\tau = R \cdot C$)

T integration time

With $u_a(0) = 0$ and equation 6-13 (with $u_{q-ges}(t) = u_e(t)$, see also equation 6-14) this results in:

$$u_a(T) = -\frac{1}{\tau} \cdot \int_0^T K \cdot \frac{di(t)}{dt} \cdot dt = -\frac{K}{\tau} \cdot \int_0^T di(t) = -\frac{K}{\tau} \cdot i(T) \quad 6-16$$

provided $i(0) = 0$

Equation 6-16 shows that the output voltage of the integrator equals the current in the conductor.

Practical experience has shown that the current which is measured does neither depend on the shape of the individual windings, nor on the physical size of the closed Rogowski coil, nor on the relative position of the coil to the conductor which is surrounded by it as long as the respective cross sectional areas remain unchanged. How can this be proved mathematically?

The magnetic flux densities which are linked with the individual windings of the Rogowski coil can also be calculated, depending on to the physical size of the coil and its individual windings, respectively. In this way it can be shown that average of the interlinked flux densities and thus the induced total voltage $u_{q-ges}(t)$ stay the same (see equation 6-13 as well as equations 6-8 to 6-12).

6.2.2 Disturbing Interference

If the magnetic fields in the vicinity of a Rogowski coil are not exclusively caused by the current which is to be measured, i.e. there are additional external magnetic fields (e.g. caused by neighboring current-carrying wires), this can influence the induced coil voltage (the basis for the measured value of the current in the conductor, see equations 6-13 to 6-16) by falsifying the measured values of the current.

In case that several magnet interference fields coexist simultaneously, the interference voltage induced into the Rogowski coil can be calculated according to the following two variants (provided there is a linear system, which usually is the case anyway).

Variant 1: As each winding of the coil – due to its spatial expansion - is in another place, the respective interlinked vector of the resulting interference flux density must be computed with the help of the geometrical addition of its individual components. Moreover, it is necessary to calculate the respective normal component of the flux density mentioned above for each winding separately (see equations 6-8 and 6-9). This can be complicated considerably by complex geometrical shapes (e.g. contorted cross sectional areas). The induced interference voltage $u_{q-s}(t)$, which can be measured at the terminals of the coil, results from the total amount of the individual voltages caused by all of the windings. (In that case it is important to pay attention to the algebraic signs)

In mathematical terms this can be expressed like that:

$$u_{q-s}(t) = \sum_{j=1}^N \left\{ - \frac{\partial \Phi_{s-j}(t)}{\partial t} \right\} = \sum_{j=1}^N \left\{ - \frac{\partial \vec{B}_{s-j}(t)}{\partial t} \cdot \vec{A}_j \cdot \cos \alpha_j \right\} =$$

$$= \sum_{j=1}^N \left\{ - \frac{\partial}{\partial t} \left(\left| \sum_{i=1}^n \vec{B}_{s-ij}(t) \right| \right) \cdot A_j \cdot \cos \alpha_j \right\}$$
6-17

$\Phi_{s-j}(t)$ Magnetic flux interlinked with winding j

N Number of windings ($N \in \mathbb{N}$)

$\vec{B}_{s-ij}(t)$ Component of the resulting interference flux density $\vec{B}_{s-j}(t)$ interlinked with winding j

A_j Cross sectional area of the winding j

α_j Angle between the vectors $\vec{B}_{s-j}(t)$ and \vec{A}_j ($0 \leq \alpha \leq \pi$)

Variant 2: Analogical to variant 1 for each individual interference field $\vec{B}_{s-ij}(t)$ a resulting partial interference voltage $u_{q-s-i}(t)$ is calculated for the whole coil. Thus, the total of the induced interference voltage $u_{q-s}(t)$ which can be measured at the terminals of the Rogowski coil (consisting of N windings), result from the total amount of all

partial interference voltages $u_{q-s-i}(t)$. (Again, the algebraic signs have to be paid attention to.)

In mathematical terms this means:

$$u_{q-s}(t) = \sum_{i=1}^n u_{q-s-i}(t) = \sum_{i=1}^n \left\{ \sum_{j=1}^N \left(-\frac{\partial \Phi_{s-ij}(t)}{\partial t} \right) \right\} = \sum_{i=1}^n \left\{ \sum_{j=1}^N \left(-\frac{\partial B_{s-ij}(t)}{\partial t} \cdot A_j \cdot \cos \alpha_{ij} \right) \right\} \quad \text{6-18}$$

$\Phi_{s-ij}(t)$ Magnetic flux (of the flux density $\vec{B}_{s-ij}(t)$ interlinked with winding j)

α_{ij} Angle between the vectors $\vec{B}_{s-ij}(t)$ and \vec{A}_j ($0 \leq \alpha \leq \pi$)

The following equation applies:

$$u_{q-1-s}(t) = u_{q-2-s}(t) \quad \text{6-19}$$

As a consequence of the plane encircled by the Rogowski coil A_{SP} , interference fields may occur so that the additional interference voltage $u_{q-SP-s}(t)$ has to be added to the interference voltages $u_{q-1-s}(t)$ or $u_{q-2-s}(t)$ which have already been calculated (serial connection).

This results in:

$$u_{q-SP-s}(t) = -\frac{\partial \Phi_s(t)}{\partial t} = -\frac{\partial B_s(t)}{\partial t} \cdot A_{SP} \cdot \cos \beta = -\frac{\partial}{\partial t} \left(\left| \sum_{i=1}^n \vec{B}_{s-i}(t) \right| \right) \cdot A_{SP} \cdot \cos \beta \quad \text{6-20}$$

$\Phi_s(t)$ Magnetic flux interlinked with the cross sectional area of the coil \vec{A}_{SP}

$\vec{B}_{s-i}(t)$ Component i of the resulting flux density $\vec{B}_s(t)$

A_{SP} Plane encircled by the Rogowski coil

β Angle between vectors $\vec{B}_s(t)$ and \vec{A}_{SP} ($0 \leq \alpha \leq \pi$)

For the interference voltage $u_{q-s}(t)$, which can be measured at the clamps of the Rogowski coil, this results in:

$$u_{q-s}(t) = u_{q-1-s}(t) + u_{q-SP-s}(t) = u_{q-2-s}(t) + u_{q-SP-s}(t) \quad \text{6-21}$$

In order to compensate for the possible interference voltage $u_{q-SP-s}(t)$, a return conductor with a counter-rotating winding may be attached to the carrier. In that case the plane encircled by the return conductor must be identical with the plane encircled by the coil \vec{A}_{SP} . A further advantage of the serial connection of the winding with the return conductor is that both terminals of the Rogowski coil are at the same end.

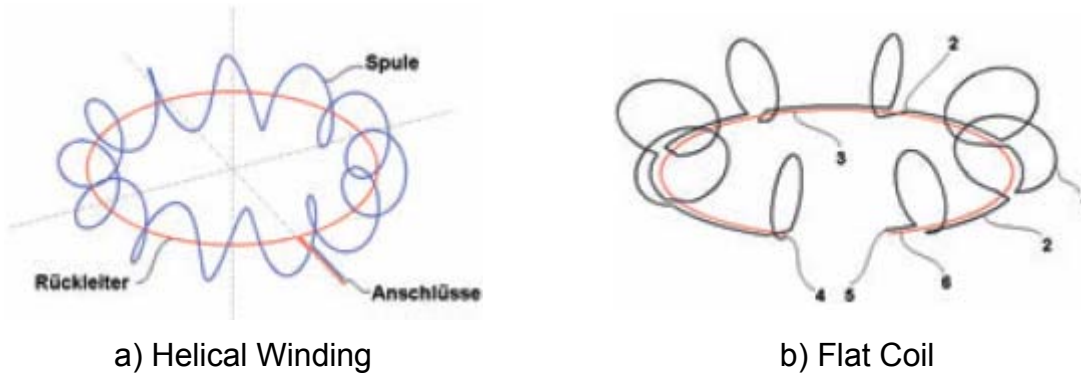


Figure 6-4: Rogowski Coils with Return Conductors (according to [7])

The exact calculation according to the equations 6-17, 6-18, 6-20 and 6-21 is rather laborious. This is due to the fact that computing the interference fields (external magnetic fields) which are interlinked with the individual windings of the Rogowski coil in most cases is quite complex. Thus, it is advisable to develop an approximation method.

6.3 Magnetic Fields as Sources of Interference

6.3.1 Calculation of Interference Currents

Implementing the formulas which have been established for the induced interference voltage into the Rogowski coil (see equations 6-17 and 6-18) with the help of MS-Excel[®], cannot be recommended as it is extremely complex. Developing an approximation method (see 6.2.2) or applying already existing software is more advisable.

The vectors, as well as the normal components of the magnetic flux densities of the interference fields, are established with the help of numeric field calculation programmes. If the necessary information concerning the physical size of the Rogowski coil is available, an already existing MS-Excel[®] program (see [8]) can be modified and upgraded in a way that the total amount of the induced interference voltages can be calculated according to the equations 6-17 and 6-18.

The following examples require that:

- (1) All j windings ($1 \leq j \leq N$) of the Rogowski have a circular cross sectional area.
- (2) The Rogowski coil is placed in the x - y -plane. Thus for all of the windings applies: $A_{j-z} = 0$.
- (3) For the cross sectional area A_j of all j windings ($1 \leq j \leq N$) of the Rogowski coil applies: $A_j = |\vec{A}_j| = A = \text{const.}$ and $d_j = d = \text{const.}$ (d_j : diameter of the winding).
- (4) There is only 1 magnetic interference field $\vec{B}_{s-j}(t)$, e.g. $i = 1$ (see equation 6-17 and equation 6-18).
- (5) All j windings ($1 \leq j \leq N$) of the Rogowski coil are interlinked with the (homogeneous) magnetic interference field (interference flux densities): $\vec{B}_{s-j}(t) = \vec{B}_s(t)$.
- (6) The magnetic interference flux $\vec{B}_s(t)$ follows a sinusoidal temporal course. Thus, the following equation applies:

$$\vec{B}_s(t) = \vec{B}_s \cdot \sin(\omega t) = \sqrt{2} \cdot \vec{B}_{s\text{-eff}} \cdot \sin(\omega t)$$

6-22

For the induced interference voltage $u_{q-s}(t)$, according to Figure 6-4, the conditions (1) to (6) results in:

$$u_{q-s}(t) = \sum_{j=1}^N - \frac{\partial}{\partial t} (B_{s-i_j-x}(t) \cdot A_{j-x} + B_{s-i_j-y}(t) \cdot A_{j-y} + B_{s-i_j-z}(t) \cdot A_{j-z}) =$$

$$= -A \cdot \sum_{j=1}^N \frac{\partial}{\partial t} (B_{s-x}(t) \cdot \cos \gamma_j + B_{s-y}(t) \cdot \sin \gamma_j)$$

6-23

$B_{s-x}(t)$ X-component of the magnetic flux density $\vec{B}_s(t)$

$B_{s-y}(t)$ Y-component of the magnetic flux density $\vec{B}_s(t)$

A Cross sectional area of the windings

γ Angle \vec{A} (see **Figure 6-5**)

N Number of the windings ($N \in \mathbb{N}$)

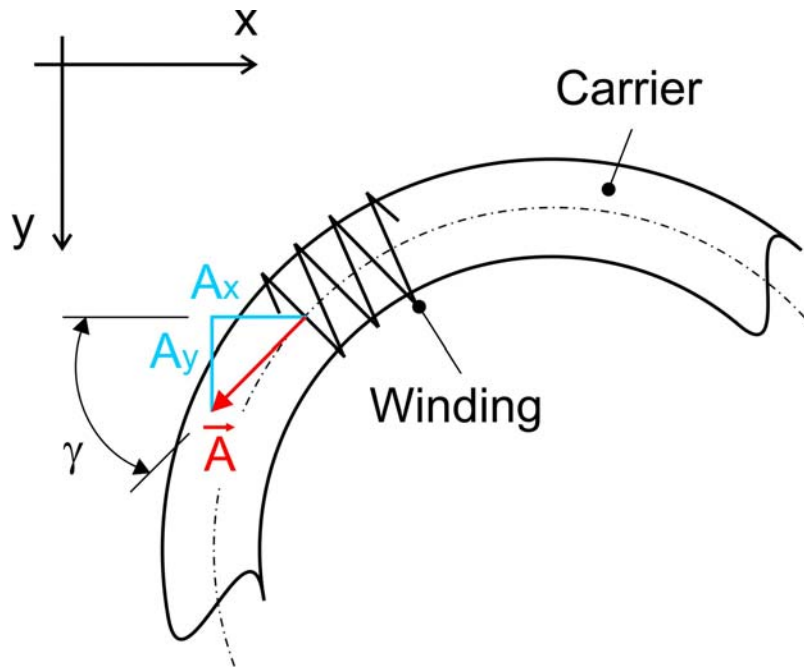


Figure 6-5: Rogowski Coil Spatial Vectors of the Windings

If the temporal function of the magnetic flux density (see equation 6-22) is implemented in equation 6-23, this results in the following equation for the interference voltage which is induced into the Rogowski coil:

$$u_{q-s}(t) = -8,886 \cdot A \cdot f \cdot \sum_{j=1}^N (B_{s-x-eff} \cdot \cos \gamma_j + B_{s-y-eff} \cdot \sin \gamma_j) \cdot \cos(2\pi \cdot f \cdot t) =$$

$$= -6,979 \cdot d^2 \cdot f \cdot \sum_{j=1}^N (B_{s-x-eff} \cdot \cos \gamma_j + B_{s-y-eff} \cdot \sin \gamma_j) \cdot \cos(2\pi \cdot f \cdot t) =$$

6-24

$B_{s-x-eff}$ X-component of the root-mean-square value of the magnetic flux density $\bar{B}_s(t)$

$B_{s-y-eff}$ Y-component of the root-mean-square value of the magnetic flux density $\bar{B}_s(t)$

d diameter of the winding

f frequency

For a given Rogowski coil with the following characteristics (specification according to Chauvin Arnoux®)

Output voltage: 47µV/A (at 50Hz)

Diameter of the winding wire: 0.32mm

Twist of the winding: 0.35mm/winding → 2857 winding/m

Diameter of the winding: 7.32mm → $A = 42\text{mm}^2$ (cross sectional area)

It would be necessary to calculate with $\Delta\gamma = 360^\circ/2857 = 0.13^\circ$ for each single winding (see Figure 6-5). In order to facilitate the process, the calculation is performed for 24 groups of windings with $N_G = 119$ windings each ($N = N_G \cdot 199 = 2856$, e.g. very good approximation) with $\Delta\gamma = 360^\circ/24 = 15^\circ$.

This leads to the following result for the spatial vectors (see Figure 6-5):

$$\gamma_j = j \cdot \Delta\gamma = j \cdot 15^\circ \quad \text{for } 1 \leq j \leq 24$$

6-25

When implemented in equation 6-24 this results in:

$$u_{q-s}(t) = -0,019 \cdot \sum_{j=1}^{24} [B_{s-x-eff} \cdot \cos(j \cdot 15^\circ) + B_{s-y-eff} \cdot \sin(j \cdot 15^\circ)] \cdot \cos(314,16 \cdot t)$$

6-26

$B_{s-x-eff}$ X-component of the root-mean-square value of the magnetic flux density in T

$B_{s-y-eff}$ Y-component of the root-mean-square value of the magnetic flux density in T

t Time in s

$u_{q-s}(t)$ Induced interference voltage (temporal value) in V

In general for all $n \in \mathbf{N}$ applies:

$$\sum_{k=1}^n \cos\left(k \cdot \frac{360^\circ}{n}\right) = \sum_{k=1}^n \sin\left(k \cdot \frac{360^\circ}{n}\right) = 0$$

6-27

This is also true for the example below:

$$\sum_{j=1}^{24} \cos(j \cdot 15^\circ) = \sum_{j=1}^{24} \sin(j \cdot 15^\circ) = 0$$

6-28

Thus, the induced interference voltage $u_{q-s}(t)$ results in:

$$u_{q-s}(t) = -0,019 \cdot \left\{ B_{s-x-eff} \cdot \sum_{j=1}^{24} \cos(j \cdot 15^\circ) + B_{s-y-eff} \cdot \sum_{j=1}^{24} \sin(j \cdot 15^\circ) \right\} \cdot \cos(314,16 \cdot t) =$$

$$= -0,019 \cdot \{ B_{s-x-eff} \cdot 0 + B_{s-y-eff} \cdot 0 \} \cdot \cos(314,16 \cdot t) = 0$$
6-29

From the equations 6-27 to 6-29 the following statements can be deduced:

- (1) If a closed Rogowski coil is situated in a homogeneous, as well as isotropic magnetic interference field (i.e. the total amount as well as the direction of the vector of the magnetic flux density are completely identical in all space coordinates), this interference field does neither influence the induced clamp voltage $u_{q-s}(t)$ (measuring signal) nor the measured value of the current.
- (2) An unwanted influence on the measured values can only occur if:
 - The Rogowski coil is not closed completely (both terminals are not connected properly, see equations 6-1 and 6-2).
 - The magnetic field caused by the current which is to be measured is highly inhomogeneous and/or anisotropic (e.g. in case of a field distortion caused by the presence of highly permeable materials).
 - The already existing magnetic interference fields are highly inhomogeneous and/or anisotropic (see above).
 - There are errors concerning the physical size and the geometrical construction of the Rogowski coil (e.g. diameter of the carrier, diameter of the windings, and position of the return conductor as well as the plane which is encircled by it).

In point (2) of the requirements for the calculations (see above), a user-defined local coordinate system for the position of the Rogowski coil has been introduced (see also Figure 6-5). This coordinate system can only be used for the remaining calculation if, at the same time, all relevant magnetic fields are also transformed into said coordinate system, provided that the original relative position of the spatial vectors of the windings to the magnetic interference fields remains unchanged.

A reduction of measuring errors can be achieved by either finding the best possible way of aligning the Rogowski coil in the magnetic interference field (Try to find the right position by rotating the coil) or by minimizing the plane encircled by the coil (by wrapping the Rogowski coil several times around the current-carrying conductor and subsequently correcting the measured values).

6.3.2 Measurements in a Homogeneous Magnetic Field

In order to determine the influence of external magnetic fields, the measured current of the Model 6474 has been analyzed, while the GroundFlex™ sensors were placed in a homogeneous magnetic field. This is the current I_f , which is read by the Model 6472, if a GroundFlex™ sensor is influenced by an external magnetic field. The field has been positioned in either an x-, y-, or z-direction, and the field strength as well as the frequency have been varied. The GroundFlex™ sensor has always been placed in the x-z-plane, with its lock pointing in z-direction (see Figure 6-6).

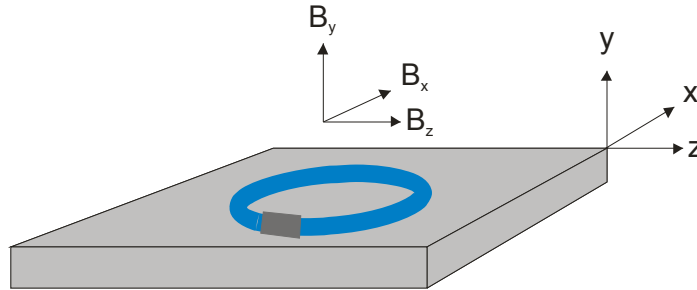


Figure 6-6: Position of the GroundFlex™ Sensor

Figure 6-7 shows the frequency dependence of the interference, with the GroundFlex™-sensors wrapped in three and four turns. Obviously, the interference decreases with the number of the turns, as the plane encircled by the coil gets smaller. In y-direction there is hardly any frequency dependence, as can be expected according to theory. In x- and z-direction, however, certain frequency dependence can be noted. Yet, as the most significant interferences occur in y-direction, interferences in x- and z-direction can be neglected.

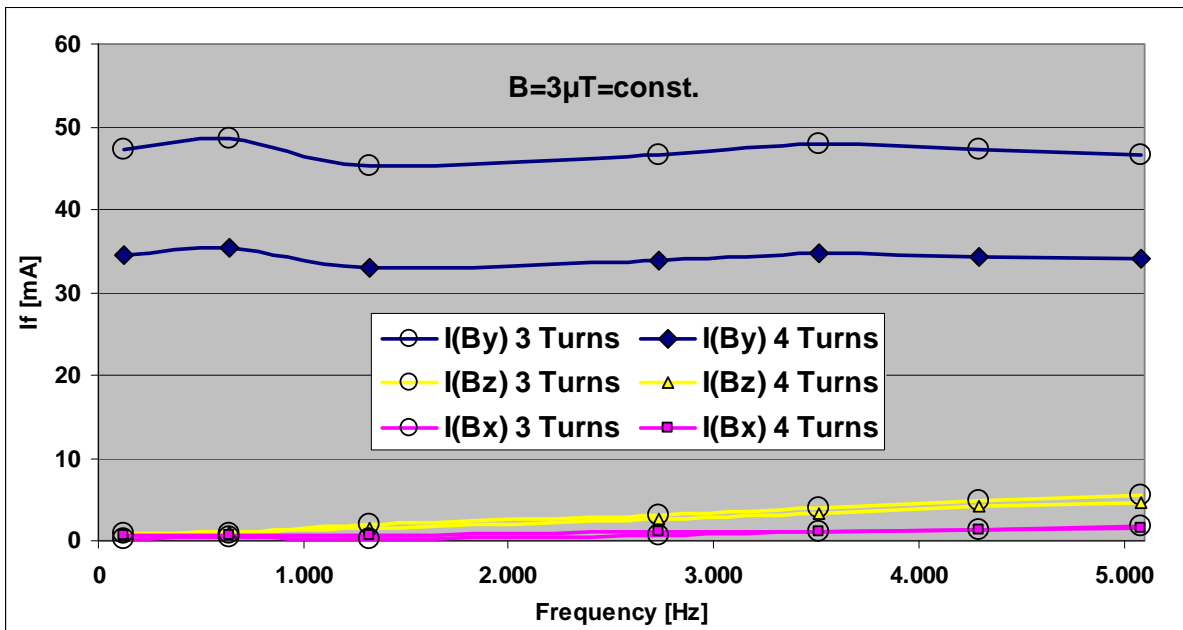


Figure 6-7: Frequency Dependence of the Interferences (x, y, z)

Figure 6-8 shows the currents measured by a GroundFlex™ sensor at varying flux densities. In this case the GroundFlex™ sensors were wrapped in 4 turns.

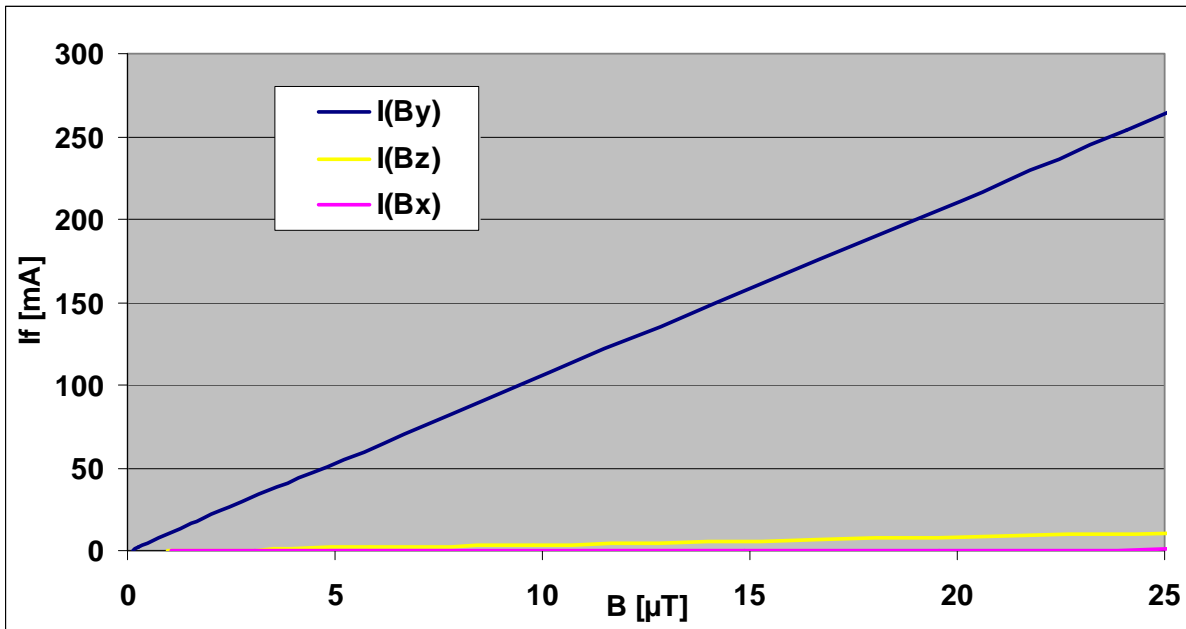


Figure 6-8: Field Dependence of the Interferences (x, y, z)

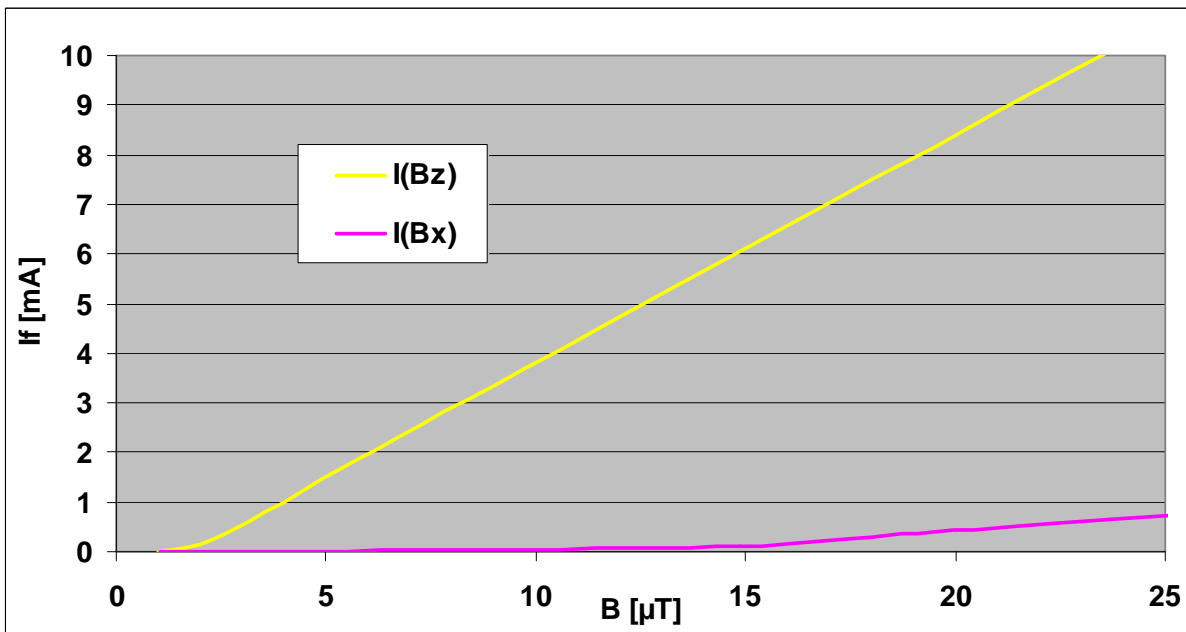


Figure 6-9: Field Dependence of the Interferences (x, z)

Obviously, the highest interference is caused by magnetic fields in y-direction. This is also confirmed by the theoretical approach in chapter 6.3. The tests have resulted in an interference of about 10.5mA/μT in y-direction.

According to theory fields, x- and z-direction do not produce any measuring results. Yet Figure 6-8 already shows that also in this case, values have been measured. In order to illustrate this phenomenon, Figure 6-9 only shows the results in x- and z-direction. Fields in z-direction, i.e. those pointing towards the lock of the GroundFlex™ sensor, cause higher interferences than fields in x-direction. Up to a certain flux density no interference can be detected (1μT in z-

direction, $14\mu\text{T}$ in x-direction). From this flux density on, interferences occur. These induced interferences result in about $0.445\text{mA}/\mu\text{T}$ in z-direction and $0.049\text{mA}/\mu\text{T}$ in x-direction.

For measurements at pylons during which the GroundFlex™ sensor, which has been wrapped around a pylon footing, is lying at the pylon foundation this means: As the highest interferences occur vertically to the GroundFlex™ sensor lying at the pylon foundation, it seems advisable for measurements at pylon footings to attach the GroundFlex™ sensors to the pylon in a way that the planes encircled by the coils point into the direction of the route (see Figure 6-11), as magnetic flux densities are lowest in this direction. The following reflections, however, are based on the assumption that the GroundFlex™ sensors are lying at the pylon foundation (as in Figure 6-10).

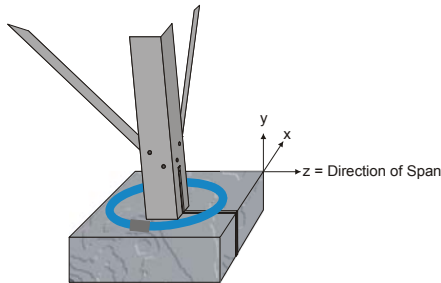


Figure 6-10:

Pylon footing with Lying GroundFlex™

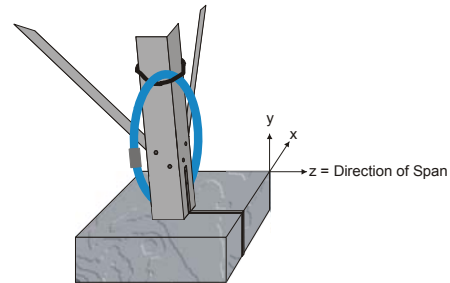


Figure 6-11:

Pylon Footing with Hanging GroundFlex™

6.3.3 Calculation of the Magnetic Flux Density at the Footing of a Pylon

In order to determine interferences which occur when measuring currents at pylons, it is necessary to determine the flux density in the vicinity of the pylon. For this purpose an Excel program has been developed at the Institute of Electrical Power Systems of the Graz University of Technology which is able to determine vectors of the flux density for any space coordinate with the help of Biot-Savart equations. These are calculated for a specific physical size of the pylon as well as a specific phase configuration of the wires with a given symmetrical phase current. Influences caused by currents which are induced into the pylon are neglected. The phase wires are assumed to be infinitely long, straight and parallel to the ground, which means that there are no magnetic flux densities in the z-direction. The coordinate system is assumed to be placed at the middle section of a pylon, with the y-direction being vertical, the z-direction positioned in the direction of the span and the x-direction transverse at right angle to the direction of the span (see Figure 6-13).

As basis for the configuration of the pylon in Figure 6-12, data of the standard pylon of the power line 108/7 and 108/8 in Wiener Neudorf have been used. The characteristic distances of the footings of this pylon measure up to about 4 to 8 meters depending on the height of the pylon.

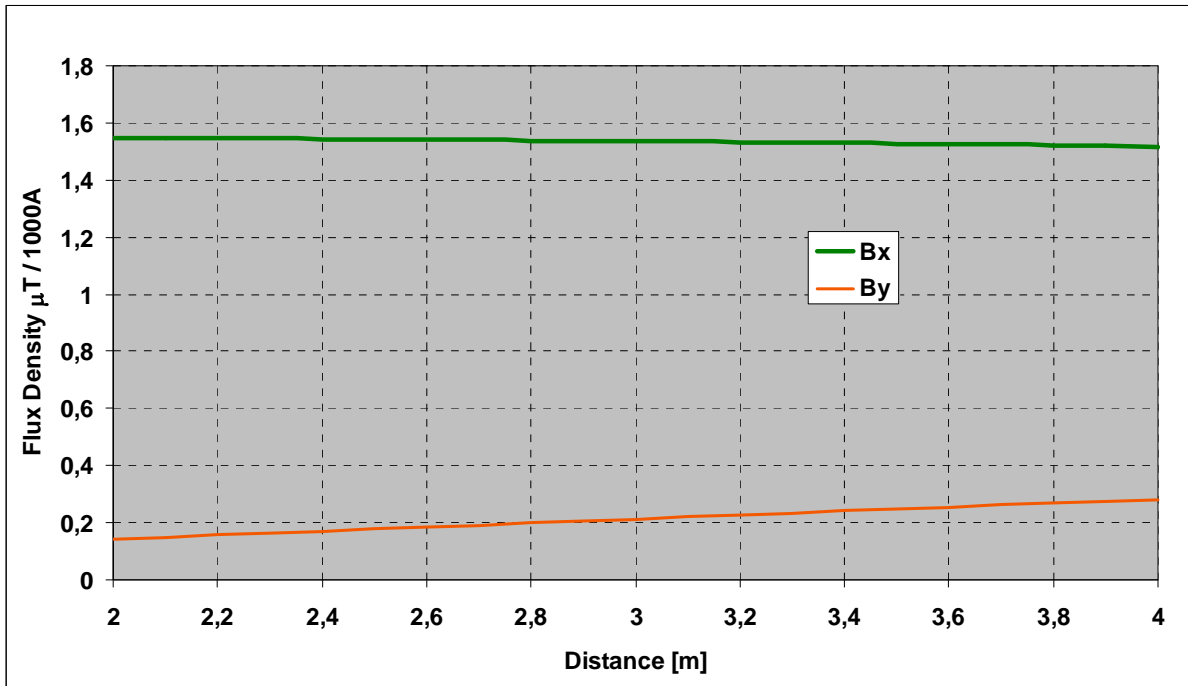


Figure 6-12: Flux Density in the Vicinity of the Pylon Footing

The flux density in the vicinity of the pylon footing at $x = 2$ to 4 meters and $y = 0$ meter on the surface of the soil is shown in Figure 6-12. In case the diameter of the GroundFlex™ sensors is about 32cm (with 4 turns), the flux density in x- and y-direction can be assumed to be homogeneous.

In chapter 6.3.4 measured values which are influenced by external magnetic fields (caused by phase currents) will be investigated with the help of the interfering factors which have been dealt with in chapter 6.3.2.

6.3.4 Assessment of Additionally Induced Errors

The additionally induced errors are only relevant for the passive measurement as they can only occur as the nominal frequency of 50Hz and its harmonics. For the active measurement, however, only frequencies beyond this range are used, so that additionally induced errors do not occur.

The following section focuses on the errors which may occur when performing a passive measurement (50Hz) with the GroundFlex™ measurement.

It has to be ensured that the interference fields in x- and y-direction, and those at the respective pylon footings, are not cophasal. Thus, it is necessary to add the interferences geometrically.

Depending on the phase configuration of the system, different kind of influences may occur.

Some errors may sum up; others may even cancel each other out. The Figure 6-13 shows the additionally induced error for some phase configurations and a distance of the pylon footing of 4m.

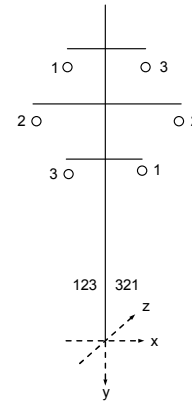
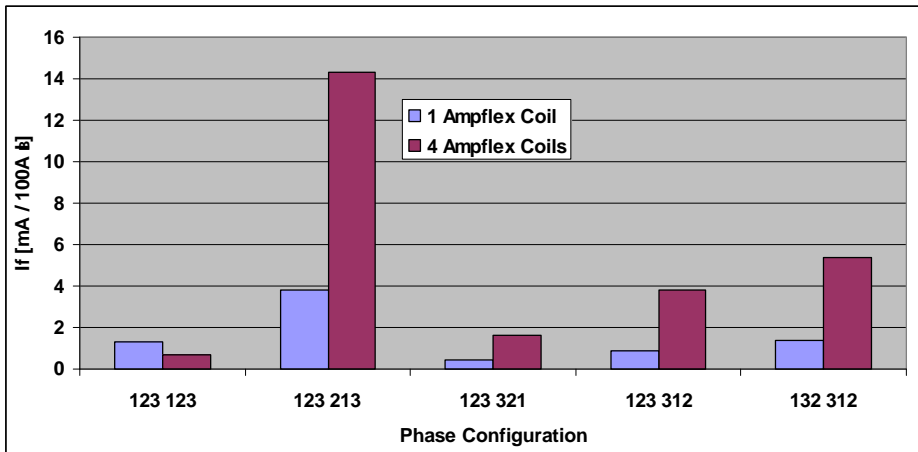


Figure 6-13: Additionally Induced Error

The cumulative errors shown in Figure 6-13 have a certain phase position to the actual measured quantity, the ground current of the pylon. This means that mostly this error does not take full effect and is only fully summed up or subtracted in worst cases.

It also becomes obvious that many different parameters contribute to the interferences of the magnetic field caused by phase and earth wires which might ultimately impair the measuring of the ground current with the help of GroundFlex™ sensors. If the GroundFlex™ measurement was applied at an insulating pylon (where there is no ground current), the Model 6472 would read a current of about 14mA/1000A operating current in the worst case (phase configuration 123-321).

The ground current of the pylon which is to be measured, as well as the induced error, are linearly dependent on the operating current. Thus, the relative measurement error is constant for a given pylon. For pylons which carry higher ground currents independent of the operating current, the error gets smaller, whereas it gets bigger for pylons with lower ground currents. For a standard pylon ground current of about 0.1% of the operating current (at 1000A about 1A), the worst relative error caused by the GroundFlex™ measurement with 4 GroundFlex™ turns with the most disadvantageous phase configuration may mount up to a maximum of ±1.4 %. This means that, in this case, the grounding system resistance of the pylon which has been determined by passive measurement may result in an additional error of ±1.4 %.

7 Summary

The theoretical calculations of the grounding system resistance of ground/earth systems based on the physical size of the pylon ground/earth are almost identical with the comparative measurements. The model which has been established for the exact computation of ground currents and earth wire currents of power line systems shows how ground currents are distributed to the individual pylons in a power line system. Apart from the linear influence of the operating current, the ground current is mainly influenced by the phase configuration and the physical size of the head of the pylon as well as the nearness of the pylon to transformer stations or transposition pylons. The highest ground currents always occur in transformer stations and at transposition pylons. Pylons in the vicinity of transformer stations or transposition pylons also have higher ground currents.

At transposition pylons or at pylons with comparatively low-resistance grounding system resistances, ground currents ranging from 1 to 7% can be expected. At other pylons, the ground currents range from 0 to 1% of the operating current. Transformer stations and pylons in their vicinity can carry ground currents of the same intensity as the earth wire current, which in a power line system may amount up to 10% of the operating current. With the help of this simulation model ladder network, impedances at pylons can also be computed. The results of these simulations, which also include capacitive couplings, are very similar to those achieved by simpler calculation methods, which only concentrate on earth wire impedances and earth resistances. The comparative measurements with the Model 6472 which were carried out during the study have led to the following results:

- Testing the soil resistivity with the help of the Model 6472 showed exactly the same results as the Norma Unilap GEO X.
- Contrasting the 4-pole measurement of the ladder network impedance with various other methods again showed a high degree of accordance in all cases. Even measuring methods with significantly higher testing currents led to similar results as the Model 6472.
- The active measurements of the grounding system resistance with the help of selective current measurement using GroundFlex™ sensors and the Model 6474 did not show any significant differences to other measuring methods during which considerably higher testing currents were applied. This confirms that the intensity of the testing current does not influence the result of the measurement. Tests with a newly installed ground/earth system led to the same result.
- The passive measurement of the grounding system resistance turned out to be in rather good accordance with other measuring systems as well. The error which occurs during the passive measurement with GroundFlex™ sensors is induced by the magnetic field of the phase current decreases with the amplitude of the ground current of the pylon which on its part depends on the operating current. For pylons at which these ground currents are very low, this error can be quite big (e.g. for a pylon ground current of 0.1% of the operating current, the relative error amounts to 1.4% in the worst case).

In general, it can be stated that the frequency-dependent measurement of grounding system resistances and ladder network impedances is a quick and very valid method to evaluate ground/earth systems.

8 Applied Devices

8.1 Measurement Devices and Sources

Earth and resistivity tester Model 6472
Primary testing system Omicron CPC
Omicron extension CU1
Secondary testing system Omicron CMC 256/6
Yokogawa reference source

8.2 Measurement Devices

Dewetron 3010
Fluke 199 Scopemeter
Norma Unilap GEO X

8.3 Current Probes

GroundFlex™ with GroundFlex™ Adapter Model 6474
LEM-Flex RR3020
AC Current Probe Model E3N (SL261)

9 Bibliography

- [1] Richter, W.: Elektrische Messtechnik – Grundlagen. 3., bearbeitete Auflage. Berlin: Verlag Technik; Berlin, Offenbach: vde-Verlag. (1994).
- [2] Philippow, E.: Grundlagen der Elektrotechnik. 8., bearbeitete Auflage. Heidelberg: Hüthig. (1988).
- [3] Frohne, H.: Elektrische und magnetische Felder (Leitfaden der Elektrotechnik). Stuttgart: Teubner. (1994).
- [4] Bronstein, I.N.; Semendjajew, K.A.: Taschenbuch der Mathematik. 23.Auflage. Moskau: Nauka. Leipzig: BSB B.G. Teubner Verlagsgesellschaft. (1987).
- [5] Labuhn, F.; Weinhardt, K.: Strommessungen an Impulsentladungen mit Rogowski-Spulen. Messtechnik 6/71. S.128-133.
- [6] Ward, D.A.; Exon, J. La T.: Using Rogowski coils for transient current measurements. Engineering science and education journal. (June 1993). pp.105-113.
- [7] Zumbrunn, W.: Wenn Stromwandler am Anschlag sind. Mit sättigungsfreien Spulen große Wechselströme messen. Bulletin SEV/VSE 24/25 04. S.11-14.
- [8] Frei, J.: Technischer Bericht: ÖBB – Schleife für Herzschrittmacher. (IFEA-Nr.: 2006-28). Graz: Technische Universität – Institut für Elektrische Anlagen. (Oktober 2006).
- [9] Tietze, U.; Schenk, Ch.: Halbleiter-Schaltungstechnik. Neunte, neu bearbeitete und erweiterte Auflage. Berlin, Heidelberg, New York, London, Paris, Tokyo: Springer. (1989).
- [10] Iskra R.; Schmutzger E.: Digitale Berechnung niederfrequenter ohmscher Beeinflussung von Erdungsanlagen (IFEA 1990)

NOTES:



Chauvin Arnoux®, Inc. d.b.a. AEMC® Instruments
(603) 749-6434 • (800) 343-1391